4. EXPERIMENTAL RESULTS

4.1 Full-scale experiments

4.1.1 Hydrodynamic study of full-scale APs

Flow, wind direction, pH and temperature. Tables 4.1 and 4.2 summarise all the data taken on-site during the tracer experiments. Daily maximum and minimum water-column temperatures were measured during the experiments in Toro and in the last two experiments at Ginebra.

Table 4.1 Wastewater flows and wind data taken on-site.

Parameters / Experiments	Flow (l/s)		Wind direction and velocity related to inlet-outlet line		
	n	Mean / σ / *CV**	*n*	Predominant direction**	Mean velocity (km/h)***
Ginebra 1 (53% sludge)	39	19.1 / 4.1 / 0.2	20	Against (95%)	5.61
Ginebra 2 (30% sludge)	48	18.4 / 1.9 / 0.1	47	Against (53%)	5.51
Ginebra 3 (20% sludge)	44	10.2 / 0.7 / 0.1	47	Against (45%)	5.42
Toro 1 (adjacent inlet-outlet)	41	14.6 / 1.9 / 0.1	41	Against (56%)	6.43
Toro 2 (diag. opp. in-out)	40	22.9 / 3.1 / 0.1	40	Against (48%)	5.83

* *CV* = Coefficient of variation
** Frequency of wind blowing in opposite direction to the main flow path in the pond
*** Historical records from the nearby local meteorological station (Cenicaña, 2000).

Table 4.2 Temperature and pH data taken on-site.

Parameters / Experiments	Temperature range in influent and effluent (°C)			pH range in influent and effluent		
	n	T_i	T_e	*n*	pH_i	pH_e
Ginebra 1 (53% sludge)	39	23.2-27.1	23.7-27.9	39	6.53-7.17	6.20-7.01
Ginebra 2 (30% sludge)	50	21.9-28.3	22.9-28.5	50	7.02-7.66	6.77-7.58
Ginebra 3 (20% sludge)	52	21.2-26.4	22.1-28.8	52	6.15-7.12	6.00-7.10
Toro 1 (adjacent inlet-outlet)	41	24.9-27.3	25.6-29.3	41	7.32-7.82	7.16-7.68
Toro 2 (diag. opp. in-out)	40	23.9-27.6	24.6-28.2	40	6.94-7.40	6.78-7.10

Maximum and minimum daily temperatures in the water-column for Toro AP showed a small variation in both experiments (< 3 °C). However, there was a difference of 6 °C observed in the first experiment (T_{max} = 31 °C and T_{min} = 25 °C) on the first sampling day. The same trend was also observed in the second experiment (T_{max} = 32

°C and T_{min} = 26 °C) on the same sampling day. At the Ginebra AP maximum and minimum water-column temperatures were taken during the last two experiments. A difference of only 1 °C was observed during the four days of the second experiment (T_{max} = 25 °C and T_{min} = 24 °C). In the third experiment, however, a difference of 7.4 °C was observed during the four days period (T_{max} = 32.2 °C and T_{min} = 24.8 °C).

Inlet-outlet arrangements and sludge accumulation. The positioning of inlets and outlets as well as three-dimensional sludge profiles in both APs are shown in Figures 4.1, 4.2, 4.3 and 4.4. The total sludge volumes calculated by using the sludge profile data and Surfer 6.01 package (Golden Software Inc.) were: 1805 m^3 (Ginebra 53 percent sludge accumulation), 1033 m^3 (Ginebra 30 percent sludge accumulation), 696 m^3 (Ginebra 20 percent sludge accumulation) and 1373 m^3 (Toro 31 percent sludge accumulation). The positioning of the inlets and outlets in both AP is far from optimal, with the situation in Toro AP being much worse than in Ginebra.

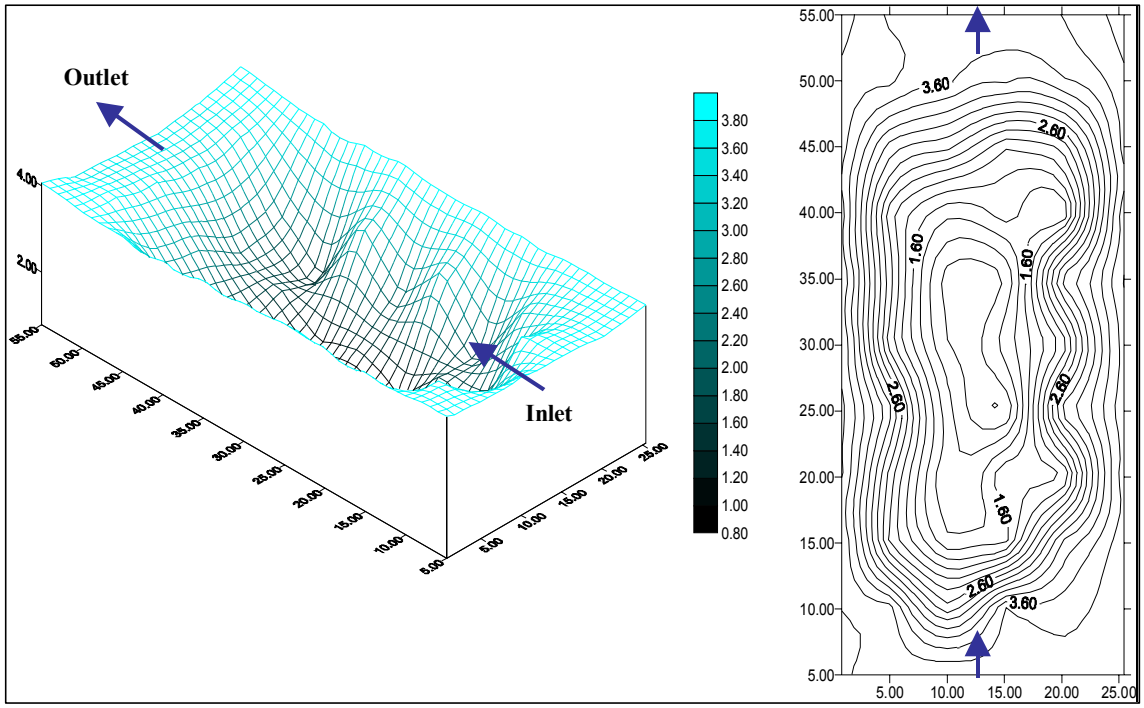

Figure 4.1 Sludge profile at Ginebra's AP for a 53% sludge accumulation.

The sludge volumes accumulated at the time of the first tracer experiments allowed calculation of the average sludge accumulation rates in each AP. The Ginebra AP had been working for five years and the Toro AP for three years. Taking into account the population of each town, the average sludge accumulation rates were 0.040 and 0.055 m^3 per person per year at Ginebra and Toro, respectively. These figures

compare well with the long-term design value of 0.040 m^3 per person per year recommended by Mara (1996).

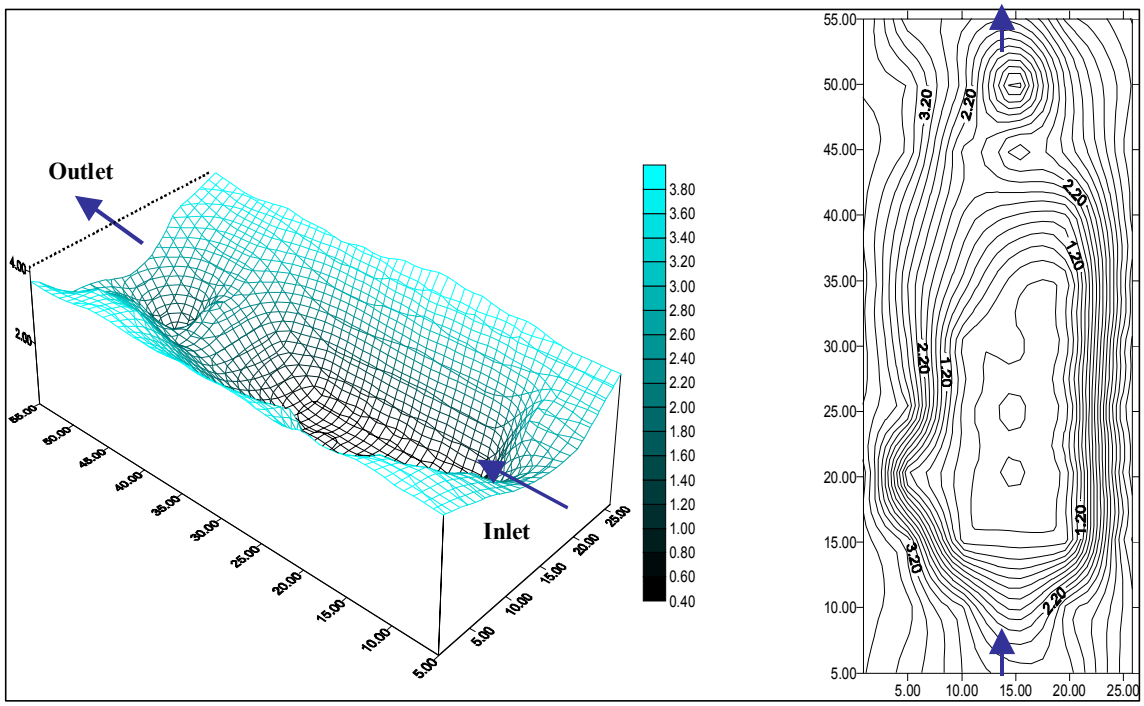

Figure 4.2 Sludge profile at Ginebra's AP for a 30% sludge accumulation.

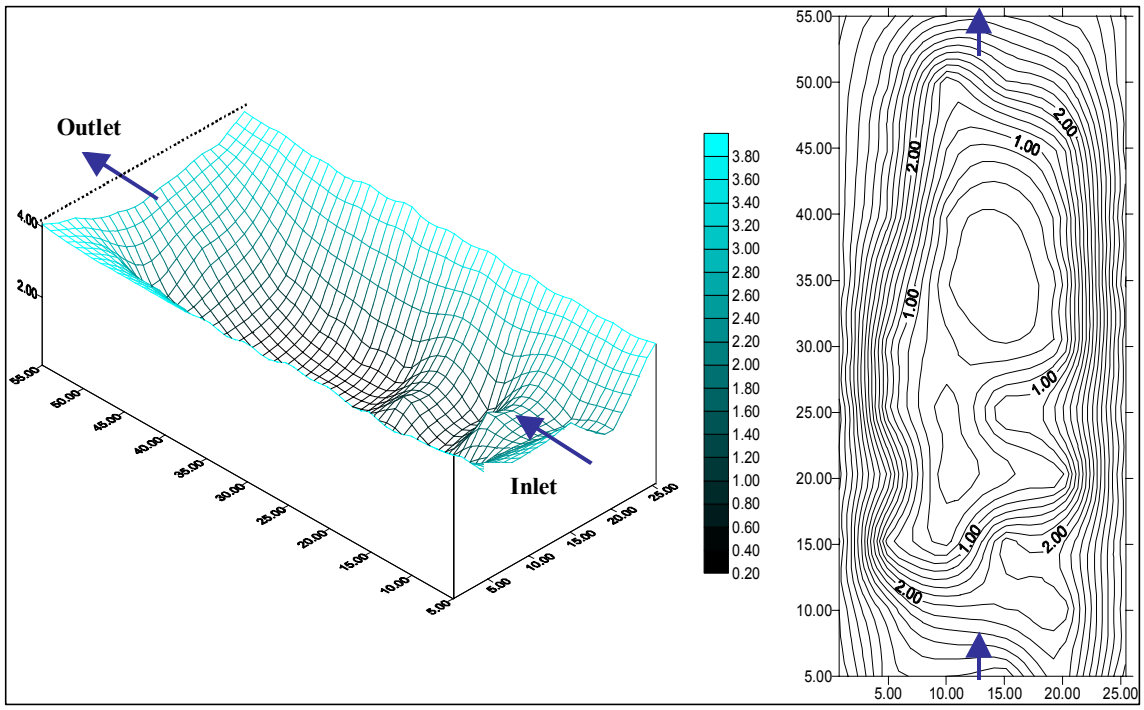

Figure 4.3 Sludge profile at Ginebra's AP for a 20% sludge accumulation.

Figure 4.4 shows the sludge accumulation at Toro AP, the positioning of the existing inlet-outlet and also the modified inlet layout evaluated.

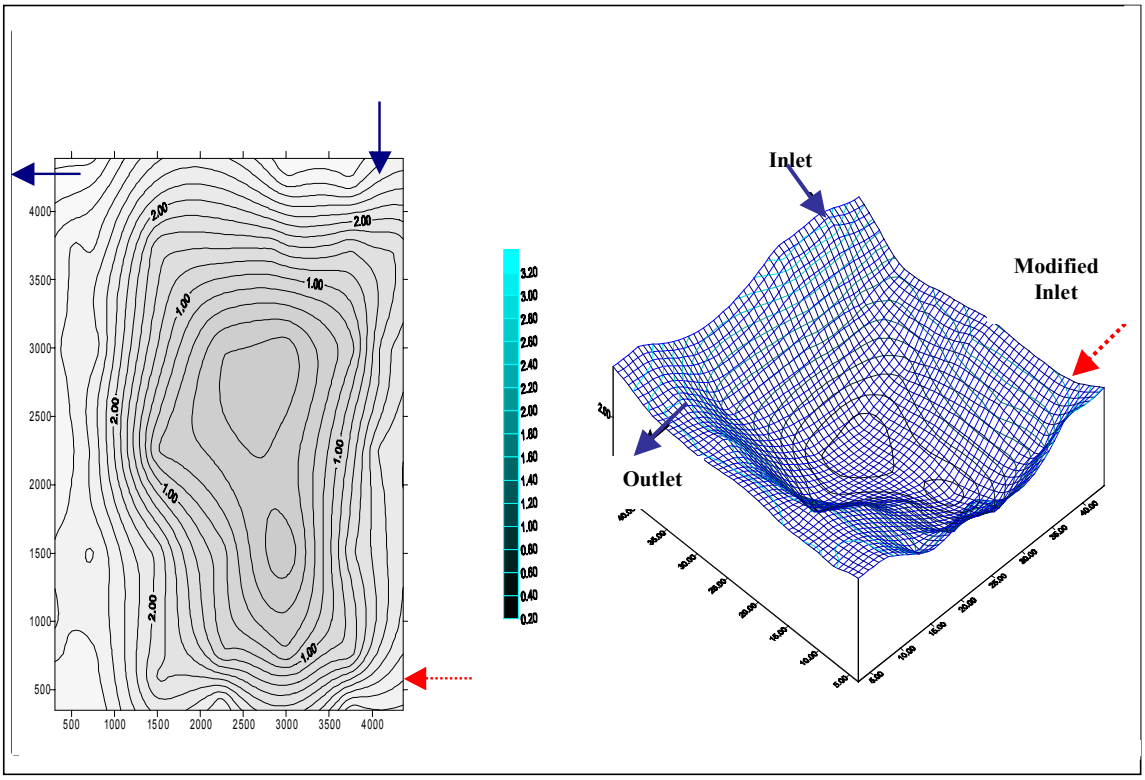

Figure 4.4 Sludge profile at Toro AP (31% sludge accumulation).

Retention time distribution curves (RTD). Figure 4.5 (a) and (b) shows the dimensionless RTD curves obtained in the preliminary tests at both Ginebra and Toro APs respectively. These curves were used to plan the final experiments.

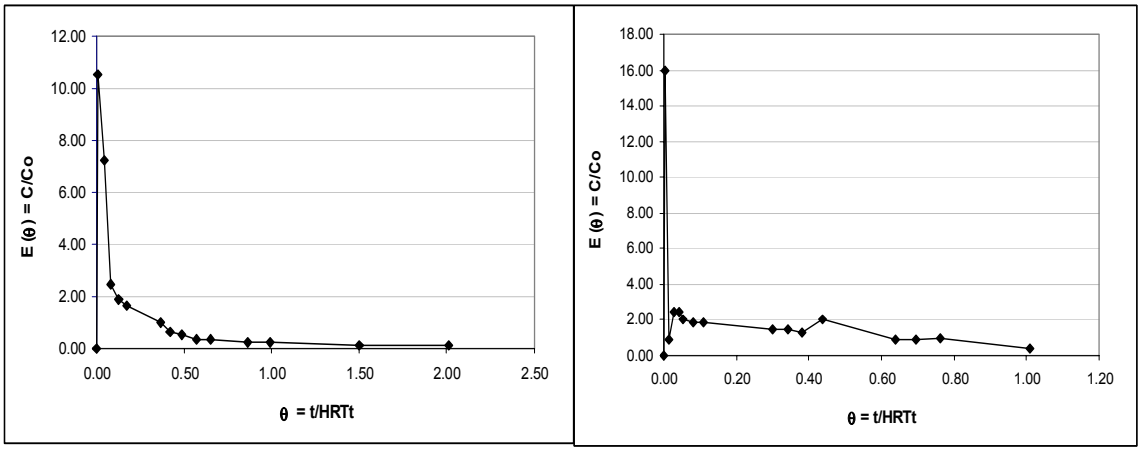

Figure 4.5 (a) Curve obtained at Ginebra AP (b) Curve obtained at Toro AP.

Figure 4.5 shows that Li^+ concentrations reached values around the detection limit of 0.01 mg Li^+/l when the monitoring period surpassed 1.5 times the theoretical HRT value. The tracer sampling periods, frequencies and number of samples in subsequent experiments were defined based on this feature.

The preliminary experiment at Ginebra also comprised sampling in three internal points located along the axis between inlet to outlet. Samples at the surface (0.10 m depth) and at 1.0 m depth were taken and analysed for Li^+ concentration. The differences in Li^+ concentrations found between surface and in-depth samples encouraged additional sampling in internal points of both APs. Figure 4.6 shows the RTD curves for the three runs carried out at Ginebra AP with different sludge accumulations. Meanwhile, Figure 4.7 shows the RTD curves for Toro AP with different inlet-outlet layouts.

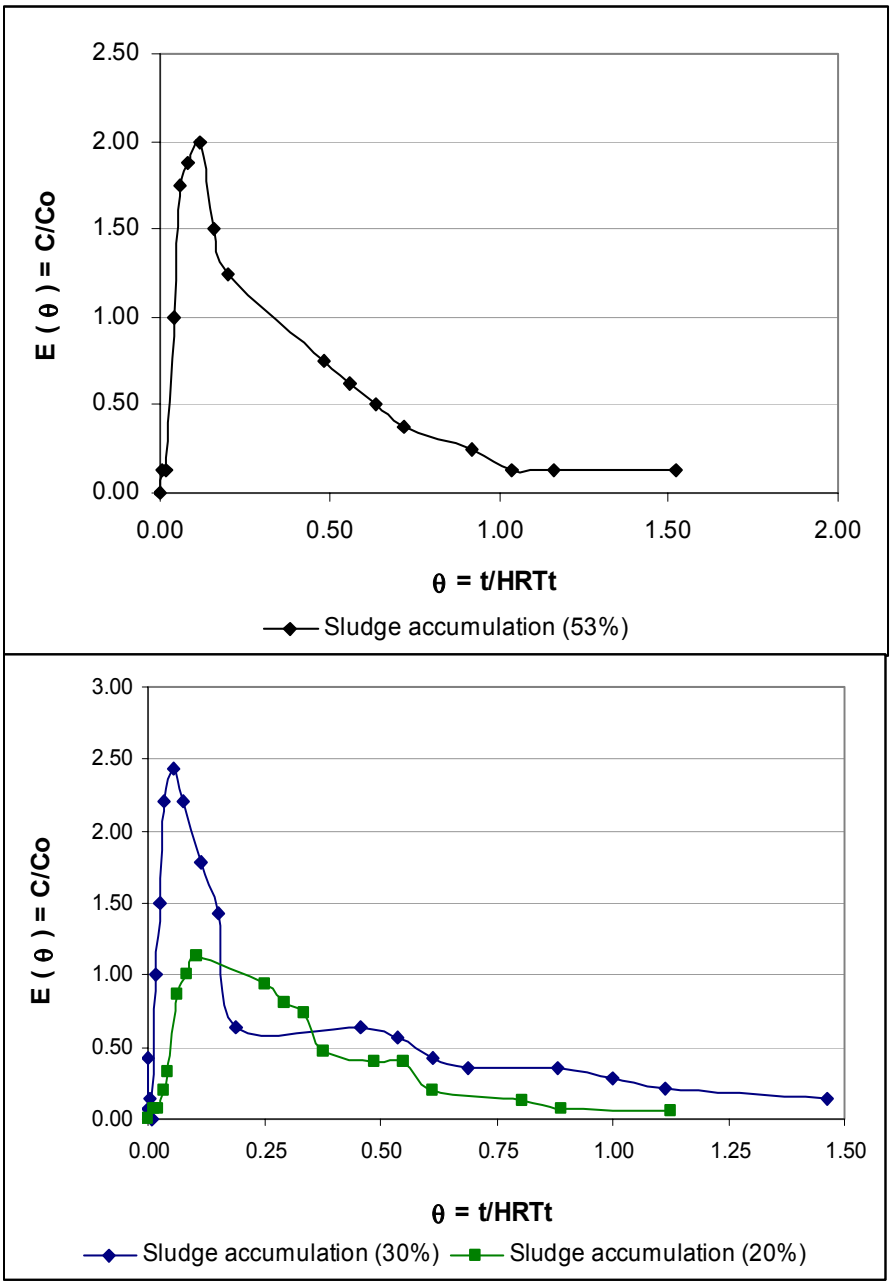

Figure 4.6 RTD curves for different sludge volumes at Ginebra AP.

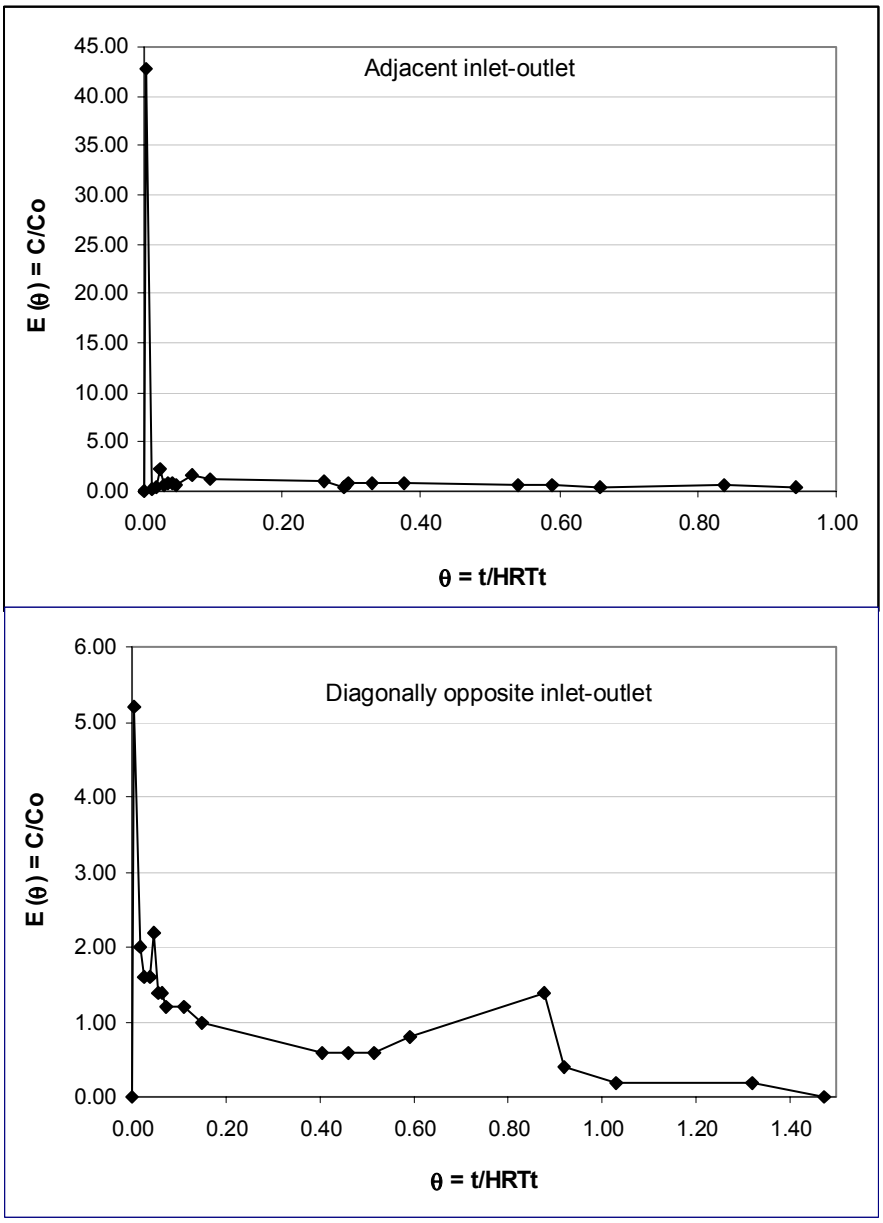

Figure 4.7 RTD curves for different inlet-outlet layouts at Toro AP.

The Figures 1 to 6 in Appendix I show (*C vs. T*) graphs for the internal points at Ginebra's AP in each tracer run. Figures 7 to 10 in the same appendix display (*C vs. T*) charts for the internal points at Toro AP. The analysis of these plots at the internal points allowed checking for preferential flow paths and tracer dispersion evolution within the ponds.

HRT and dispersion number (δ) values. Experimental HRT (HRT_e) and dispersion number *(δ)* values were calculated from the RTD curves shown in Figures 4.6 and 4.7 by applying the dispersion model to discrete data series (Levenspiel, 1999). The effective volume of both APs was calculated by subtracting sludge accumulation from the total APs volume. Thus, HRT values (T_{obs}) based on the effective APs volume

were also calculated for comparison purposes. Table 4.3 presents the figures for these hydrodynamic parameters.

Table 4.3 Summary of HRT and (δ) values for Ginebra and Toro AP.

Experiment	T_d (d)	HRT_t (d)	HRT_e (d)	T_{obs} (d)	σ^2	δ
Preliminary run at Ginebra	2.0	2.0	0.66	0.94	0.1950	0.109
Ginebra 1 (53% sludge accum.)	2.0	2.1	0.88	0.98	0.1129	0.060
Ginebra 2 (30% sludge accum.)	2.0	2.2	0.95	1.50	0.1458	0.079
Ginebra 3 (20% sludge accum.)	2.0	3.9	1.30	3.10	0.0538	0.028
Preliminary run at Toro	2.0	3.1	1.19	2.12	0.0779	0.041
Toro 1 (adjacent inlet-outlet)	2.0	3.5	1.03	2.45	0.0798	0.042
Toro 2 (diagonally opp. in-out)	2.0	2.3	1.15	1.56	0.1243	0.067

T_d: Design hydraulic retention time; HRT_t: Theoretical hydraulic retention time (V/Q)

Process performance. Table 4.4 shows the daily values of the physicochemical parameters along the tracer runs, and Table 4.5 presents the daily removal efficiencies of the APs.

Table 4.4 Daily values of physicochemical parameters in APs influents and effluents.

Parameter (mg/l)	Day	1		2		3		4	
	Experiment	Inf.	Eff.	Inf.	Eff.	Inf.	Eff.	Inf.	Eff.
COD	Ginebra 1	652	216	550	200	556	257	383	160
	Ginebra 2	360	155	274	110	316	145	360	126
	Ginebra 3	447	320	367	312	294	260	447	320
BOD_5	Ginebra 1	490	200	222	118	187	64	325	140
	Ginebra 2	245	70	175	55	185	90	260	76
	Ginebra 3	380	157	240	120	250	140	210	120
Settled BOD_5	Ginebra 1	375		167		140		240	
	Ginebra 2	170		173		165		153	
	Ginebra 3	247		160		170		140	
TSS	Ginebra 1	522	364	473	420	228	51	474	213
	Ginebra 2	180	70	160	50	130	42	140	30
	Ginebra 3	271	130	205	74	138	100	90	81
COD	Toro 1	480	310	474	208	578	152	454	135
	Toro 2	597	209	559	191	581	328	375	181
BOD_5	Toro 1	160	50	280	77	345	87	340	144
	Toro 2	388	90	363	170	378	285	244	163
Settled BOD_5	Toro 1	130		217		204		195	
	Toro 2	245		326		346		214	
TSS	Toro 1	679	381	742	391	769	404	714	409
	Toro 2	135	60	384	42	382	67	179	47

Table 4.5 Daily values of removal efficiencies in the APs.

Parameter	Day / Experiment	1	2	3	4	Mean / σ	*CV*
COD (%)	Ginebra 1	66.9	63.6	53.8	58.2	60.6 / 5.8	0.10
	Ginebra 2	56.9	59.9	54.1	65.0	59.0 / 4.7	0.08
	Ginebra 3	28.4	15.0	11.6	28.4	20.8 / 8.9	0.42
BOD_5 (%)	Ginebra 1	59.2	46.8	65.8	56.9	57.3 / 9.6	0.17
	Ginebra 2	71.4	68.6	51.4	70.8	65.5 / 9.5	0.15
	Ginebra 3	58.7	50.0	44.0	42.9	48.9 / 7.2	0.15
TSS (%)	Ginebra 1	30.3	11.2	77.6	55.1	43.5 / 28.9	0.67
	Ginebra 2	61.1	68.8	67.7	78.6	69.0 / 7.2	0.10
	Ginebra 3	52.0	63.9	27.5	10.0	38.4 / 24.2	0.63
COD (%)	Toro 1	35.4	56.1	73.7	70.3	58.9 / 17.4	0.30
	Toro 2	65.0	65.8	43.5	51.7	56.5 / 10.8	0.19
BOD_5 (%)	Toro 1	68.8	72.5	74.8	57.6	68.4 / 7.6	0.11
	Toro 2	76.8	53.2	24.6	33.2	46.9 / 23.2	0.49
TSS (%)	Toro 1	43.9	47.3	47.5	42.7	45.3 / 2.4	0.05
	Toro 2	55.6	89.1	82.5	73.7	75.2 / 14.5	0.19

The results of these experiments provided the evidence of hydrodynamic behaviour distortions encountered in two full-scale APs. The deficient hydrodynamic performance revealed by the parameters in Table 4.3, may be one of the main factors affecting the removal efficiency of these ponds. These results are further discussed in Chapter 5. The raw experimental data can be seen in electronic format in Appendix II in the FULL-SCALE-EXP\AP-DISPERSION folder.

4.1.2 CFD modelling of anaerobic ponds

The tracer studies carried out in the field and presented earlier were useful to diagnose the distortions of mixing patterns commonly encountered in full-scale anaerobic ponds. Nonetheless, to perform regularly tracer studies in full-scale ponds is a costly and time-consuming activity. Moreover, the replication of dispersion studies results even in the same pond system is not very good, as uncontrollable environmental variables (e.g. wind speed and direction, temperature variations, sunlight intensity and rainfall) seem to affect the outcome of this sort of studies.

Sludge dynamics seems to be another important factor that affects process performance in full-scale AP. Physical phenomena such as sludge settling, cyclical resuspension (due to biogas bubbling and hydrodynamic shear forces), sliding and motion of biosolids along the pond are believed to influence greatly its removal

efficiency (Warren 1998; Paing *et al.,* 2000). Uneven sludge settling patterns commonly found in AP (Saqqar and Pescod, 1995; Nelson and Jimenez, 2000 and Paing *et al.,* 2000) are also related to flow conditions, pond geometry, and relative positioning and type of inlet-outlet devices (Peña *et al.,* 2000). The combined effect of all these factors influences the hydrodynamic efficiency and process performance of AP. As pointed out by Peña *et al.* (2000), the complexity of interrelated biochemical and hydrodynamic phenomena occurring in these reactors should be tackled by integrating field studies and modern research tools such as computational fluid dynamics modelling (CFD).

In this sense, a combination of fieldwork data along with modern modelling techniques based on CFD is currently being promoted as a good approach to understand the hydrodynamic phenomena that occur in waste stabilisation ponds (Wood *et al.* 1995; Wood *et al.* 1998; Shilton, 2000; Salter *et al.* 2000; Baleo *et al.* 2001). Thus, this part of the research presents the results of the hydrodynamic modelling of the AP at Ginebra. Part of the experimental data set was used to calibrate the CFD MIKE 21 model and run several simulations in order to have a better understanding of the mixing pattern deviations. Consequently, likely interventions to improve the hydrodynamic inefficiencies were also evaluated.

Model calibration and verification. Figure 4.8 presents the velocity values measured in different points of the AP by using the procedure described in Section 3.3.2. Figure 4.9 (a) shows the sludge profile obtained from fieldwork and (b) the hydrodynamic velocity field simulated with the MIKE 21 package. Figure 4.10 depicts a 3D view of the sludge profile plus the inlet-outlet boundary conditions.

Point	X (m)	Y (m)	V * x 10^{-3} m/s
A	5	50	3.4
B	20	40	4.9
C	13	35	7.7
D	5	20	1.9
E	15	20	7.6
F	20	10	5.4
G	15	5	2.9

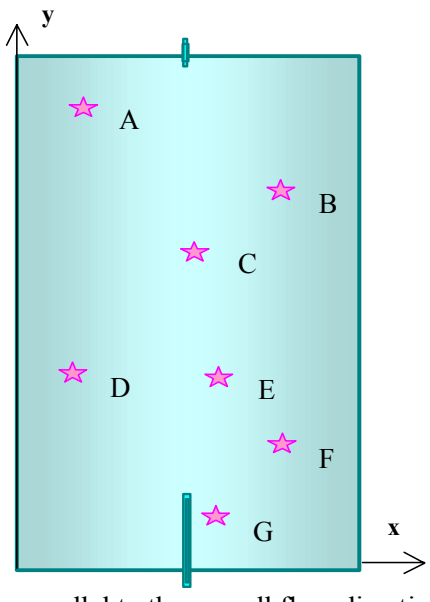

* These values correspond to the component of velocity parallel to the overall flow direction.

Figure 4.8 Internal points location for velocity measurements.

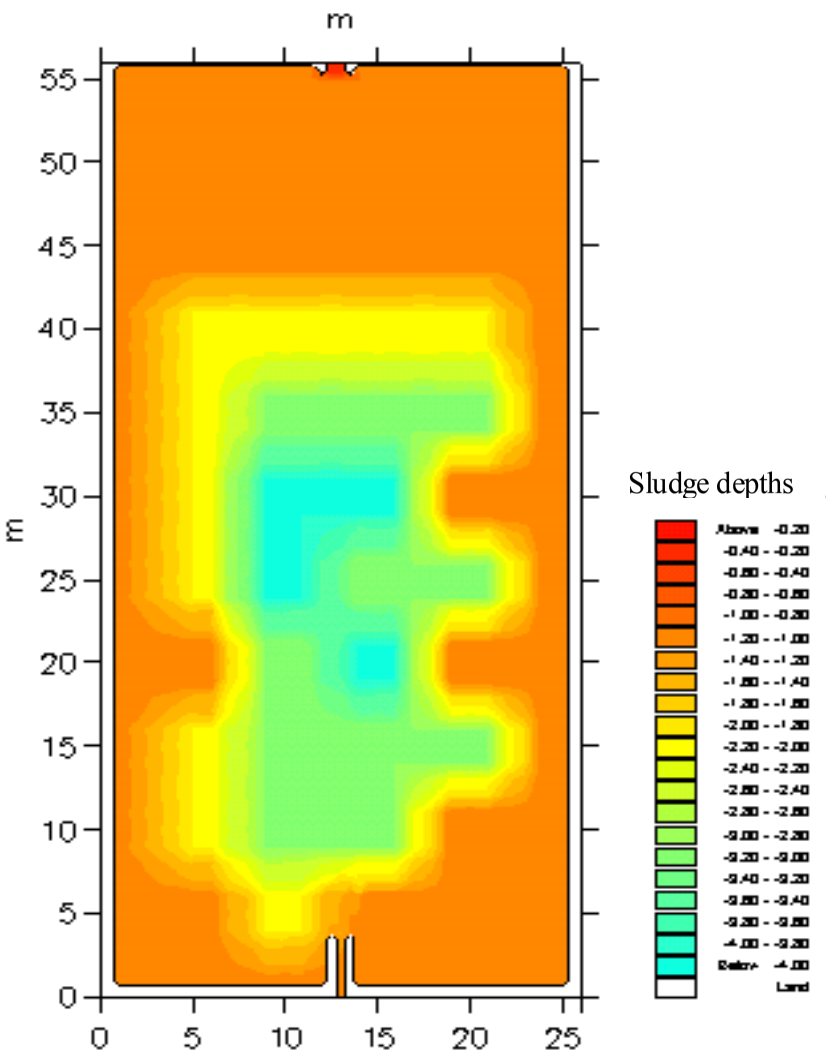

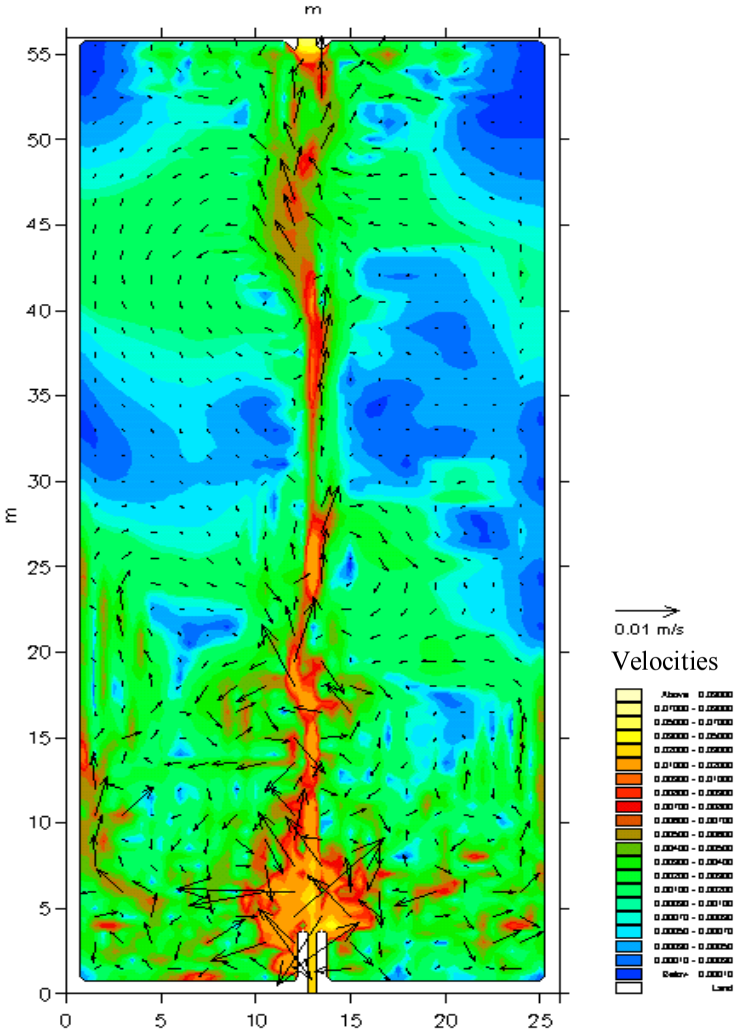

Figure 4.9 (a) Measured sludge profile (50% sludge volume) (b) Velocity field simulated for sludge profile in (a)

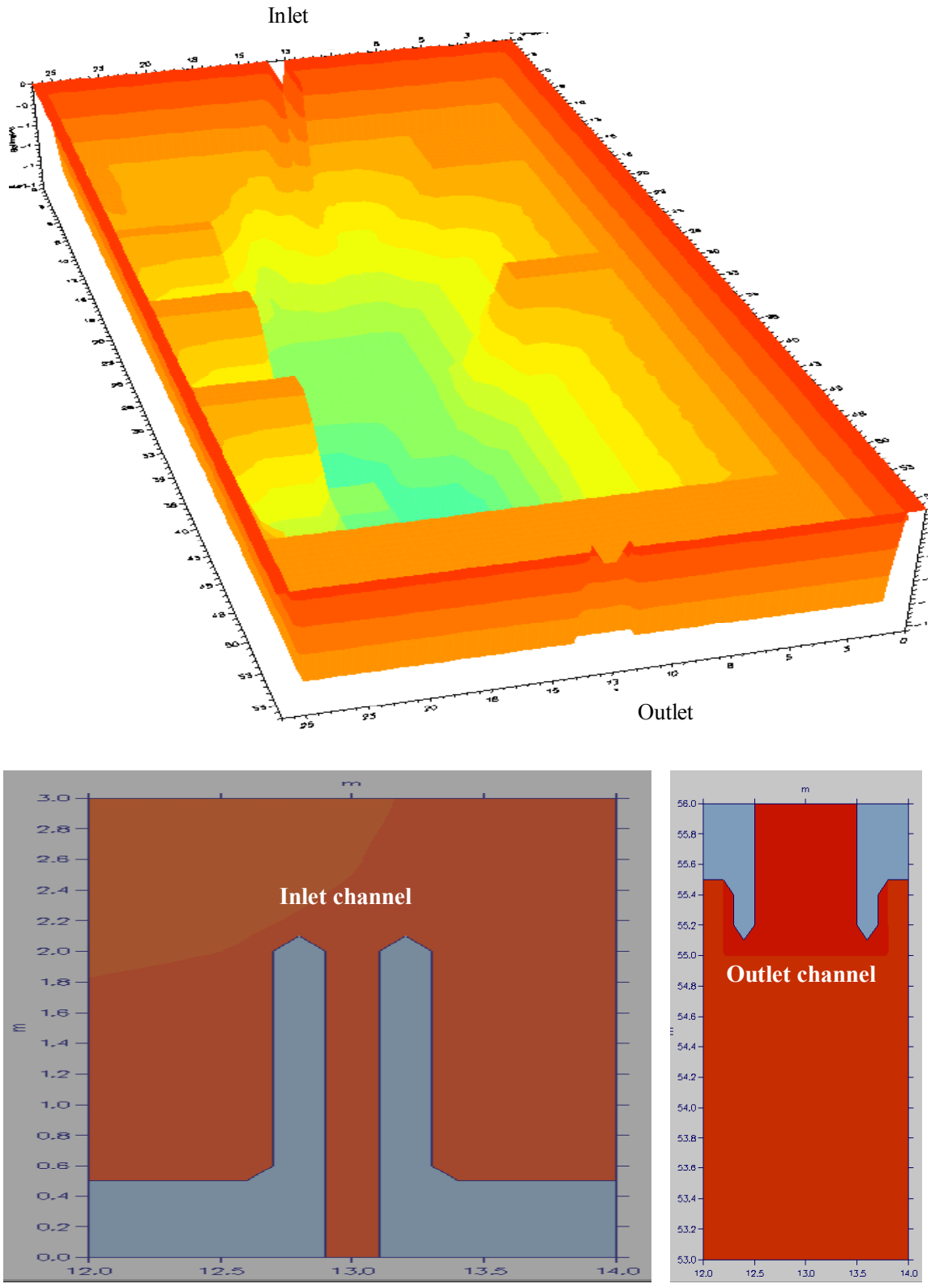

* All units in the above figures are given in metres.

Figure 4.10 3D-view of sludge profile and inlet-outlet boundary conditions.

As pointed out in Section 3.3.2, the existing inlet pipe that feeds the AP at half depth was simulated by means of a rectangular channel. The dimensions of this channel

were calculated based on records of the flow rates and the velocities expected within the pipe. The outlet channel was simulated exactly as it was.

Figure 4.11 shows the experimental (*C vs. T*) values used to calibrate the Advection-Dispersion (AD) module, and Figure 4.12 displays the RTD curves simulated for a constant dispersion number ($\delta = 0.02$) and also for proportionally variable δ values in both the *x* and *y* directions. Experimental dimensionless data are also plotted within the same figure for comparison.

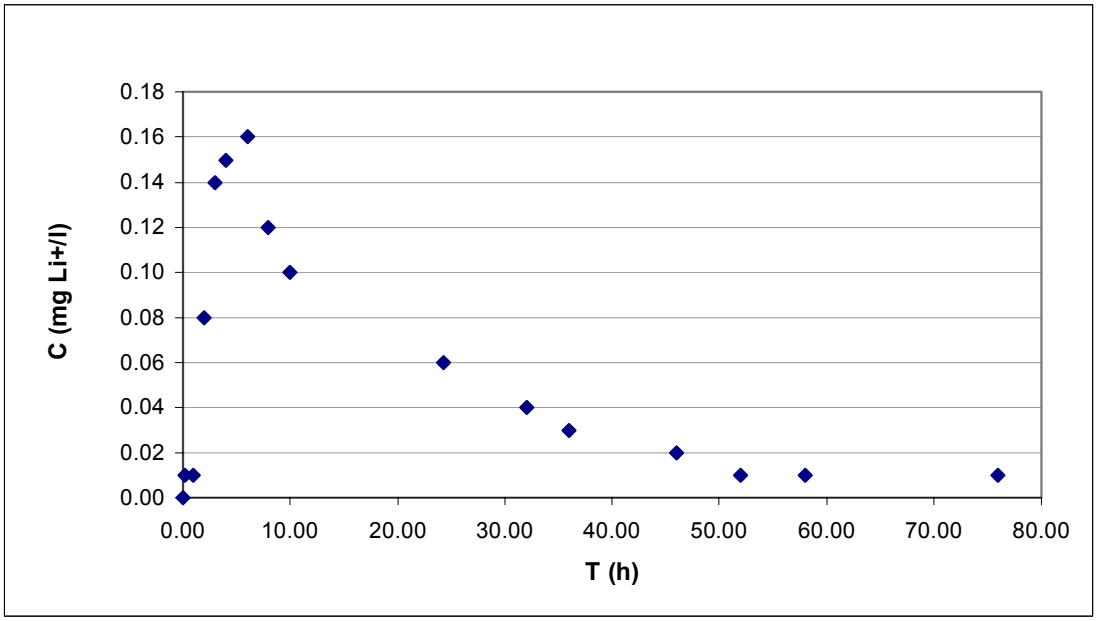

Figure 4.11 Experimental *C vs. T* data set used for the calibration of the model.

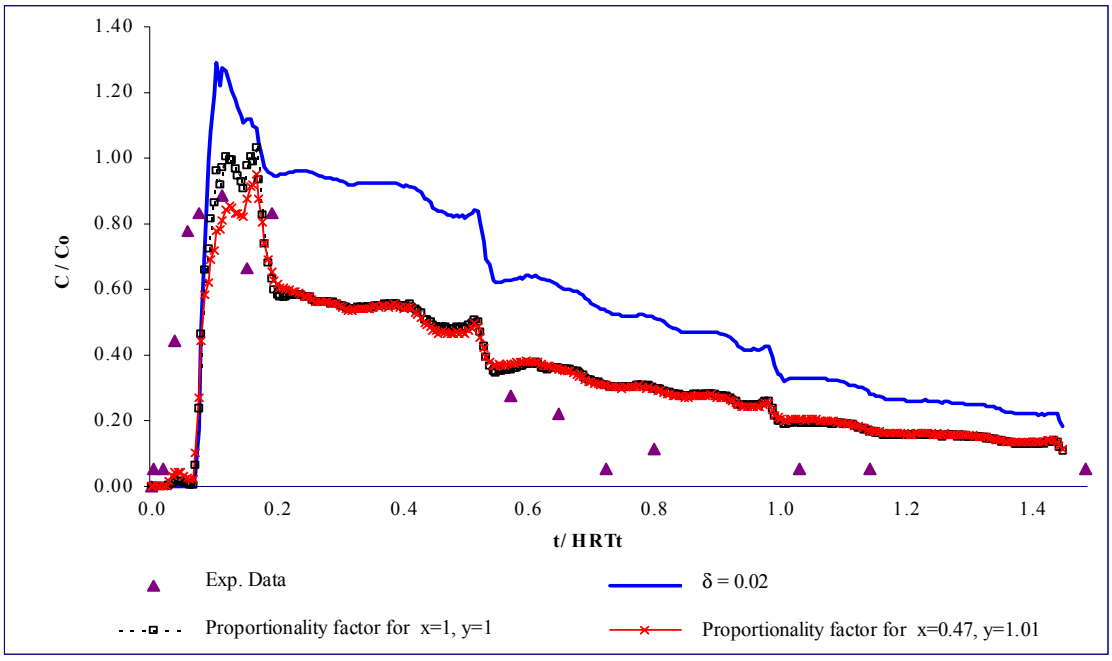

Figure 4.12 Simulated dimensionless RTD curves and experimental data.

The calibration parameters that produced good numerical stability were: average influent flow rate of 18 l/s, maximum water level difference 1 mm, Manning-Strickler roughness coefficient values of 16 – 48 $m^{1/3}/s$, wind speed 1.5 m/s, wind friction coefficient 0.0026 and a predominant wind direction blowing against the inlet-outlet line with a frequency of 80%. A sensitivity analysis of the HD module showed that model outcomes were highly sensitive to influent flow rate and roughness coefficient, whereas wind speed and friction only had a moderate influence on the results. The small velocity field values found for the experimental water level difference between inlet and outlet (0.1 cm) had no effect on model results.

The AD module outcomes showed a high sensitivity to dispersion number (δ) values. Good results were obtained when δ values were estimated as proportional to the velocities in both the *x* and *y* directions. This makes physical sense since flow velocities are a function of influent flow rate and dispersion occurs consequently both in the axial and lateral directions. The proportionality constants were calculated based on an experimental δ value of 0.018 multiplied by the *x* and *y* lengths (26 and 52 m respectively). This proportional variation of δ values was entered into the AD module and produced the lower lines shown in Figure 4.12, which are closer to the experimental values. The blue line, obtained with a constant δ value of 0.02, is well above the experimental figures and does not adequately represent the tracer response.

Temperature variations were also studied, and it was found that RTD curves and δ values were sensitive to high and low temperature values. However, modelling stability was good for the narrow experimental temperature range of 23-26 °C.

Simulation runs. Simulations of hydrodynamic behaviour (HD) and advection-dispersion (AD) phenomena were carried out on each configuration shown in Figure 3.12. Figures 4.13 and 4.14 display the simulated velocity fields in the existing AP configuration for a 50 percent sludge accumulation and for three different baffling layouts respectively. Figure 4.15 depicts the RTD curves obtained for the configurations already mentioned.

The AD module was fine-tuned with the experimental data shown in Figure 4.11 and by several iterations to adjust water levels, pond base roughness coefficient, wind direction, wind speed and wind friction factor. Hence, the simulated RTD curves can be regarded as a good approximation to the experimental values.

The MIKE 21 package also includes an expression for first order reaction kinetics to estimate the degradation of a non-conservative substance within the pond.

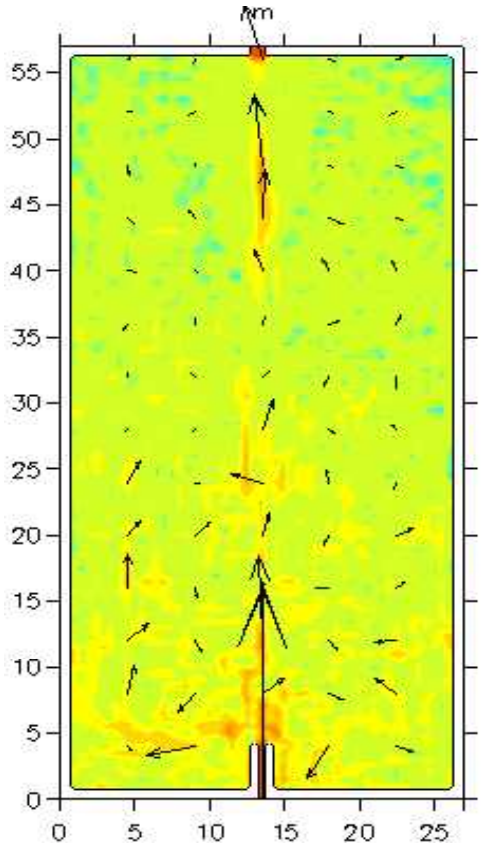

Figure 4.13 Velocity field plot for a 50 percent sludge accumulation.

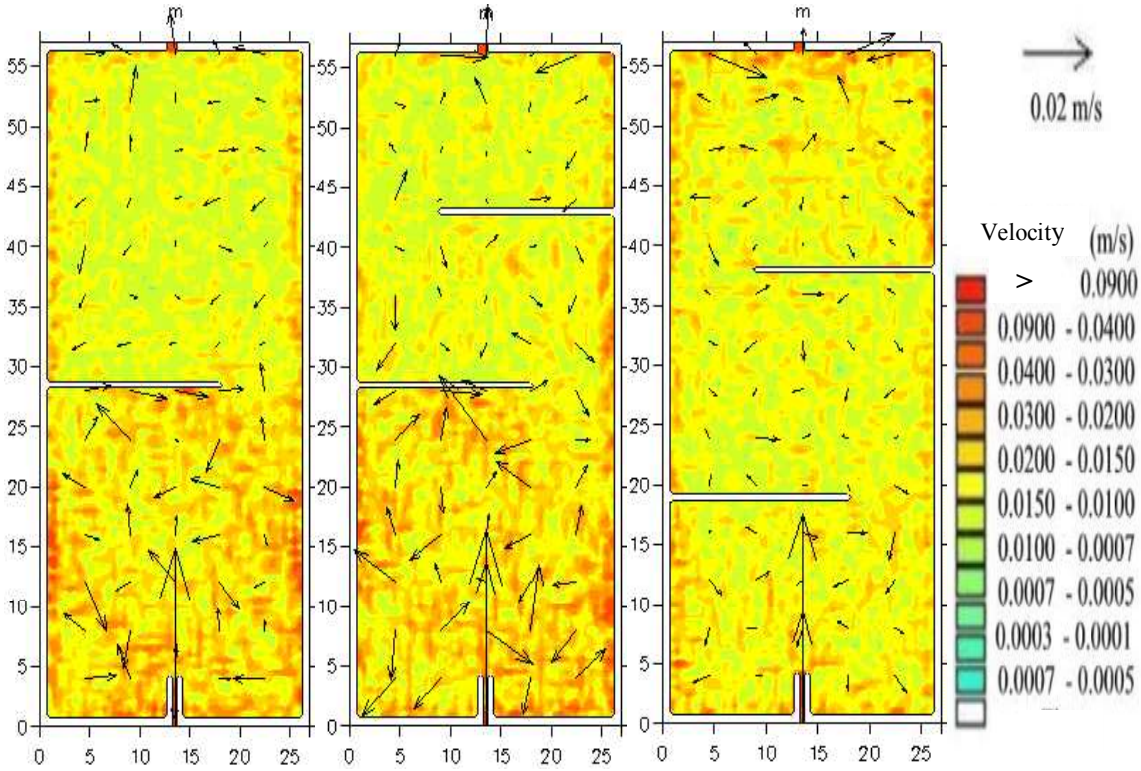

(a) Baffle at L/2 (b) Two baffles (L/2, 3L/4) (c) Two baffles (L/3, 2L/3)

Figure 4.14 Velocity field plots for different baffling arrangements.

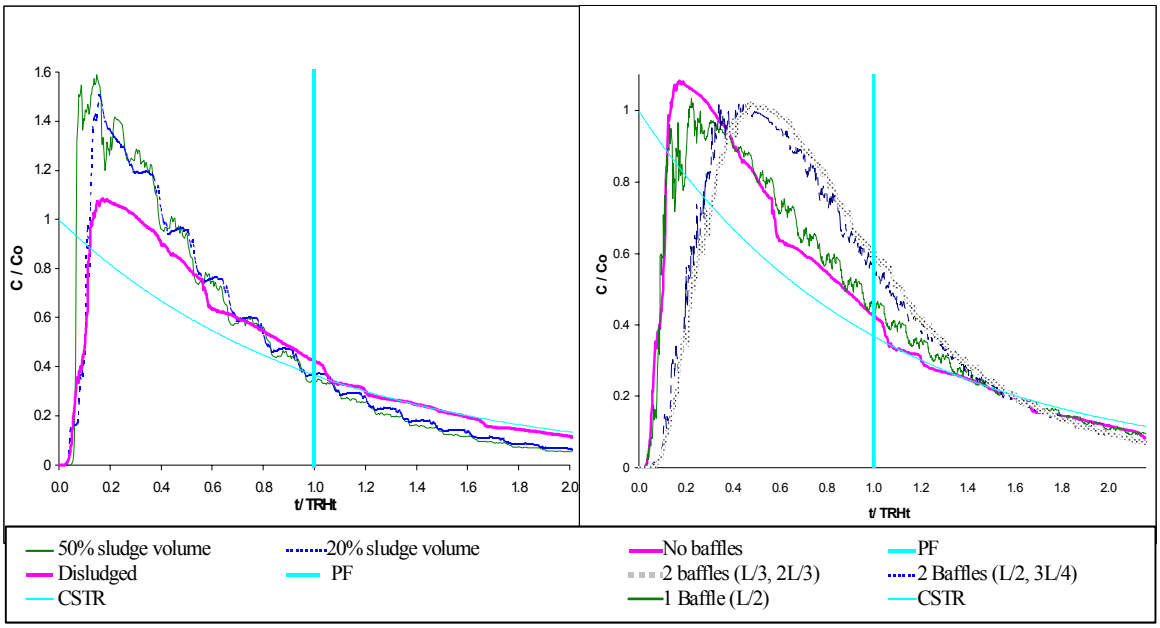

Configurations: A, B, C C, D, E, F
L: W = 2:1 and aligned in-out arrangements; configurations other than A and B are desludged ponds

Figure 4.15 Simulated RTD plots for sludge accumulation and baffled configurations

Figures 4.16 and 4.17 display the velocity field plots for the remaining configurations where positioning of inlet-outlet is changed as well as the geometry of the AP. Figure 4.18 shows the simulated RTD curves for these configurations.

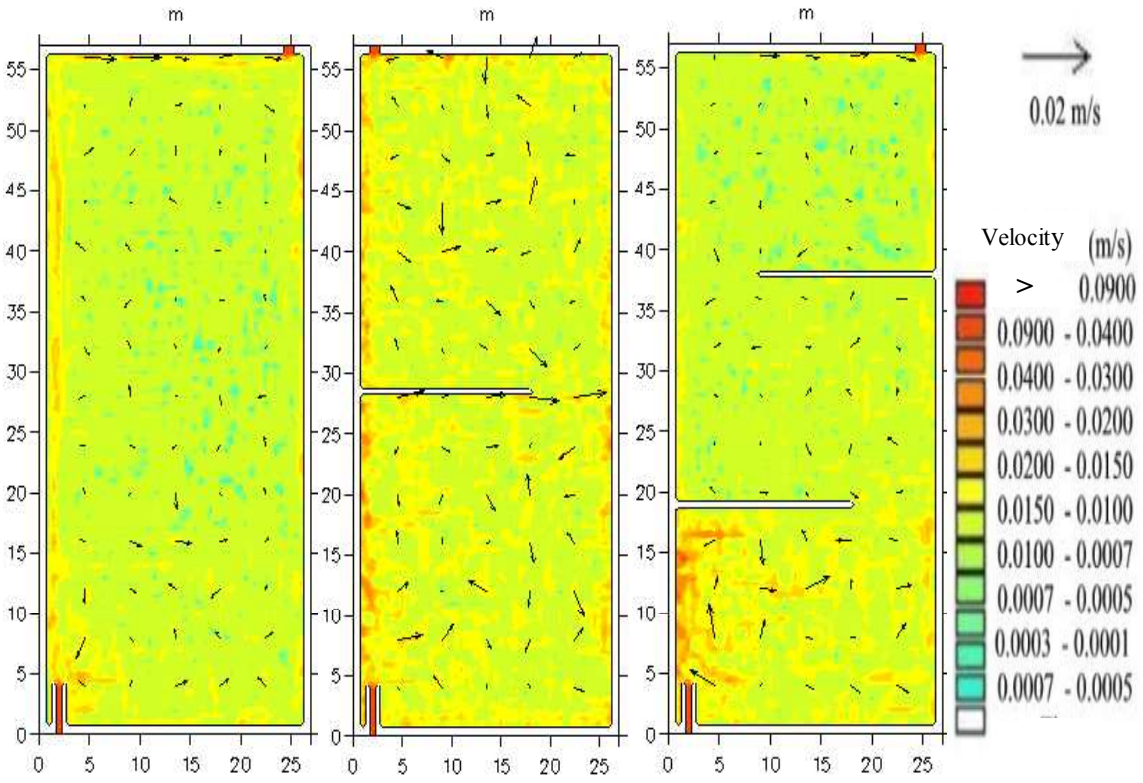

(a) Opposite in-out (b) Opposite in-out (baffle at L/2) (c) Opp. in-out (baffles at L/3, 2L/3)

Figure 4.16 Velocity field plots for varying inlet-outlet positioning plus baffling.

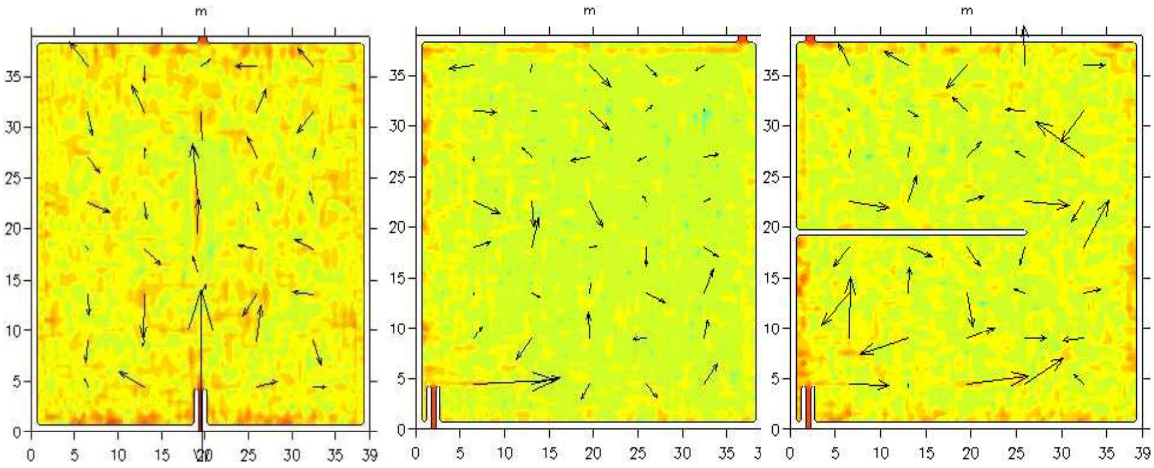

(a) Inlet-outlet aligned (b) Inlet-outlet diagonally opposite (c) One baffle at L/2

Figure 4.17 Velocity field plots for square geometry with change in inlet-outlet positioning and one baffle.

The same scale for velocity values displayed on the right hand side of Figures 4.14 and 4.16 applies in this latter case.

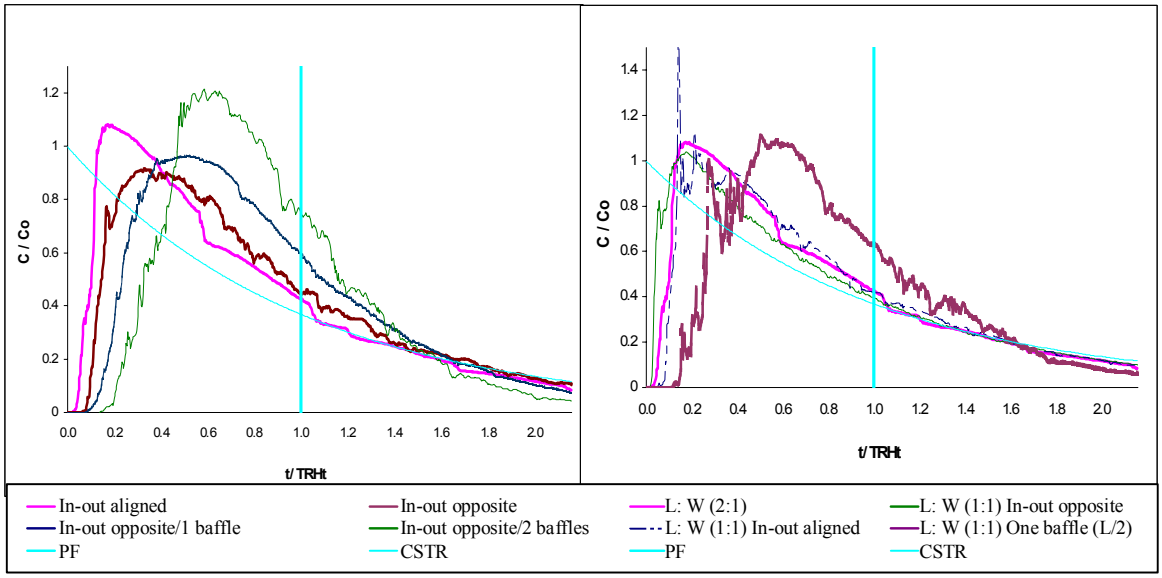

Configurations: C, G, H, I C, J, K, L
Configurations other than A and B were simulated as desludged ponds

Figure 4.18 Simulated RTD plots for inlet-outlet arrangements and square geometry configurations.

The expression (dc/dt = -*k*C) is linked to the AD module and calculates average effluent concentrations by solving the AD and mass balance equations. BOD_5 was used to estimate average removal efficiencies in the configurations simulated. An average influent BOD_5 of 310 mg/l and a temperature of 25 °C were used; these values are

based on experimental records at the Ginebra research station. The first order rate constant value of 0.31 d^{-1} was taken from Metcalf and Eddy (1991).

Table 4.6 summarises the main hydrodynamic parameters obtained from the simulation runs. Dispersion numbers (δ values) and retention factor values ($\beta = t/HRT_t$) were calculated from the RTD curves (Levenspiel, 1999). Average velocity values and estimates of BOD_5 removal were calculated by the CFD package.

Table 4.6 Summary of hydrodynamic parameters and BOD_5 removal estimates.

Configuration	**Average velocity*** (m/s) x 10^{-3}	**δ**	**Retention factor** $\beta = (t/HRT_t)$**	**BOD_5 rem.** (%)
A; 50% sludge volume	2.8^c / 1.8^s	0.06	0.64	39(41***)
B; 30% sludge volume	3.0^c / 2.3^s	0.08	0.69	45(65***)
C; Desludged pond	4.0^c / 4.0^s	0.15	0.74	56
D; One baffle at L/2	12^i / 6.8^m / 5.8^o	0.14	0.77	59
E; Two baffles at L/2 and 3/4L	11.9^i / 8.4^m / 6.1^o	0.11	0.82	62
F; Two baffles at L/3 and 2/3L	8.3^i / 6.2^m / 7.0^o	0.10	0.84	62
G; In-Out opposite	3.2^i / 2.0^m / 2.5^o	0.14	0.82	58
H; In-Out opposite plus baffle at L/2	2.5^i / 2.8^m / 1.2^o	0.11	0.86	62
I; In-Out opposite plus 2 baffles at L/3, 2/3L	3.0^i / 1.8^m / 1.6^o	0.08	0.88	65
J; Square shape and In-Out aligned	10.0^c / 5.8^s	0.16	0.70	56
K; Square shape and In-Out opposite	2.6^c / 2.8^s	0.15	0.76	58
L; Square shape plus baffle at L/2	3.6^i / 2.6^m / 2.3^o	0.10	0.85	64

* Superscripts: c, central zone; s, side zones; i, inlet zone; m, middle zone; o, outlet zone
** t, mean simulated HRT; HRT_t, theoretical HRT
*** Experimental values from full-scale experiments

The δ values from Table 4.6 (obtained for the sludge volume accumulations simulated) were 0.06 and 0.08 respectively. Meanwhile, experimental δ values of 0.060 and 0.079 were obtained for sludge accumulations of 53 and 30 percent in the same AP. Simulated and experimental δ values show a close agreement although there is some difference between the corresponding sludge volumes from which they were calculated. In practical terms, however, these sludge volumes may be regarded as similar given the inherent inaccuracy to estimate the sludge contents out of sludge profile data.

The retention factor (β = ratio of mean simulated HRT to the theoretical HRT) improves with desludging, proper positioning of inlets-outlets and baffling. The latter, however, seems to be the most effective intervention to increase the HRT in the pond according to the results in Table 4.6.

The CFD model applied to the AP at Ginebra was able to predict within reasonable limits its overall hydrodynamic performance. The close agreement between simulated and experimental results (difference less than 10%) provided strong reasons to believe that baffling combined with adequate inlet-outlet positioning are effective engineering measures to improve the hydrodynamic performance of APs. The preferential flow paths shown by unbaffled configurations are controlled through baffling implementation since the velocity fields in baffled configurations are more evenly distributed. Geometric shape of the AP was another important factor, since hydrodynamic performance of square cells was inferior to the existing rectangular configuration. Additionally, hydrodynamic inefficiencies are expected to be high as a result of the wrong geometric shape combined with an inadequate positioning and poor design (i.e. hydraulic and physical) of inlet-outlet devices. The latter situation is shown in Figures 4.17 (a) and 4.18.

Experimental results presented earlier and obtained at Toro showed a massive short-circuiting from inlet to outlet in a square AP with wrong design and positioning of inlet-outlet devices. Thus, the predictions of CFD modelling are confirmed by the experimental results presented in Section 4.1.1. Data obtained from the CFD modelling study are presented in electronic format in Appendix II in the MODELLING-CFD-AP folder. Further discussion of these results compared to the experimental data is presented in Chapter 5.

4.1.3 Start-up of UASB reactor

Wastewater characteristics. Table 4.7 displays the average composition of the domestic wastewater at Ginebra site. Some of the figures in Table 4.7 were taken from other research projects carried out at the same time of this experiment. The strength of the wastewater at Ginebra town is slightly higher than that of an average domestic wastewater. This can be seen from the COD_t and BOD_5 values. It is worth noting that the physicochemical composition of the raw wastewater presented a small variation during the period of study as shown by the *CV* values for most of the parameters.

Local food commerce (restaurants) in the town and the discharge of preliminary treated wastewater from a small slaughterhouse caused the increase in wastewater strength. This wastewater is biodegradable since there is no industrial activity in the municipality. The features already mentioned, the environmental conditions at the site and the possibility of comparing the performance of a low-rate anaerobic reactor (AP)

and a UASB (high-rate anaerobic reactor) treating the same wastewater under the same conditions, gave good reasons to carry out this research work at Ginebra. Furthermore, an adequate start-up phase for the UASB was a prerequisite in order to study its hydrodynamic performance under real operating conditions.

Table 4.7 Wastewater composition at Ginebra.

Parameter	*n*	Average / range	σ	*CV*
pH	50	6.60 – 7.09	0.2	0.03
Temperature (°C)	50	24.0 – 27.0	0.8	0.03
Alkalinity (mg $CaCO_3$/l)	10	185	10.0	0.05
COD_t (mg/l)	27	526	62.9	0.12
COD_f (mg/l)	18	202	35.7	0.18
BOD_5 (mg/l)	14	342	39.4	0.12
COD/BOD_5	14	1.6	-	-
TSS (mg/l)	25	225	46.9	0.21
Settleable solids 1-h (ml/l)	25	2.4	1.2	0.50
Fats (mg/l) *	5	110	10.0	0.09
TKN (mg/l) *	5	42.3	17.1	0.40
P-Org (mg/l) *	5	5.1	2.6	0.51
FC (UFC/100 ml) *	5	1.15×10^6 **	-	-

* Data taken from other experiments.
** Geometric mean.
t, total; f, filtered

Reactor inoculation. Table 4.8 shows the characteristics of the sludge used as inoculum. The parameters were measured in sludge samples taken from the reactor once seeded, after a 24 hour period under maximum inflow rate, after the period of rising up-flow velocities (i.e. selective pressure procedure) and prior to the continuous feeding of the UASB.

Table 4.8 Characteristics of the sludge used as inoculum.

Parameter	Raw seed	After maximum inflow rate *	After selective pressure **	Prior to continuous feeding
SMA ($gCOD\text{-}CH_4/gVS\text{-}d$)	0.14	N.D	0.19	0.19
VS (g/l)	59.0	32.9	15.7	39.5
TS (g/l)	122.0	69.6	34.5	88.0
Settling velocity (m/h)	N.D	3.7	N.D	3.2
VS/TS	0.48	0.47	0.46	0.45

* This period lasted 24 hours
** This period lasted eight days
N.D Not determined

The 55 cubic meters of sludge pumped into the reactor accounted for about 6700 kg TS and 3245 kg VS. These amounts, however, were reduced by the application of the selective pressure procedure prior to the continuous feeding of the reactor.

Operational conditions during start-up. The inoculation stage lasted two weeks and was aimed at improving the characteristics of a poor quality seed in order to shorten the start-up period of the reactor. The long periods and some degree of uncertainty during the start-up phase are probably the main drawbacks of full-scale UASB reactors used in domestic wastewater treatment. In this sense, van Haandel and Lettinga (1994) point out that operational conditions as well as quality and quantity of seed sludge are key factors that have a strong influence on the duration of start-up. These authors quote the experiences of Kampur (India) where a UASB reactor was started-up in three months. In contrast, the UASB reactor at Bucaramanga (Colombia) did not achieve steady state conditions until after four months of operation. In another experience, in Sao Paulo (Brazil) a 120 m^3 UASB was started-up in four weeks at an initial HRT of 16 hours but using a granular sludge inoculum. Thus, it seems that quality of the seed sludge, organic loading rates and operational conditions together determine the duration of the start-up phase of UASBs treating domestic wastewaters in tropical regions.

Table 4.9 outlines the operational conditions for the start-up phase of the UASB at Ginebra site.

Table 4.9 Operational conditions of start-up phase.

Stage	Time (days)	HRT (h)	λ_v (Kg COD/m^3-d)	V_{up} (m/h)
I	6	25.0	0.52	0.17
II	8	16.0	0.69	0.27
III	13	14.3	0.88	0.30
IV	8	9.8	1.28	0.43
V	13	8.3	1.50	0.52
VI	65*	6.7	1.81	0.64

* The last 49 days of this stage corresponded to steady state conditions.

Process performance. Figures 4.19 to 4.25 present the variation of the physicochemical parameters monitored in the influent and effluent (points 5 and 6 in Figure 3.8) throughout the six stages of the start-up period. Table 4.10 summarises the descriptive statistics of the physicochemical parameters for each stage of the start-up.

Figures 4.26 and 4.27 display the evolution of TS and VS throughout the start-up on the basis of sludge samples taken at different depths in the reactor. This was possible due to sludge sampling valves located at 0.3, 1.0, 1.6 and 2.2 m above the

reactor base. Meanwhile, Figure 4.28 shows the sludge profile at day 87 of operation when the UASB was already operating in steady state condition. In general terms, most of the parameters monitored during the start-up phase showed a stable behaviour and there were no overloading warnings throughout the period.

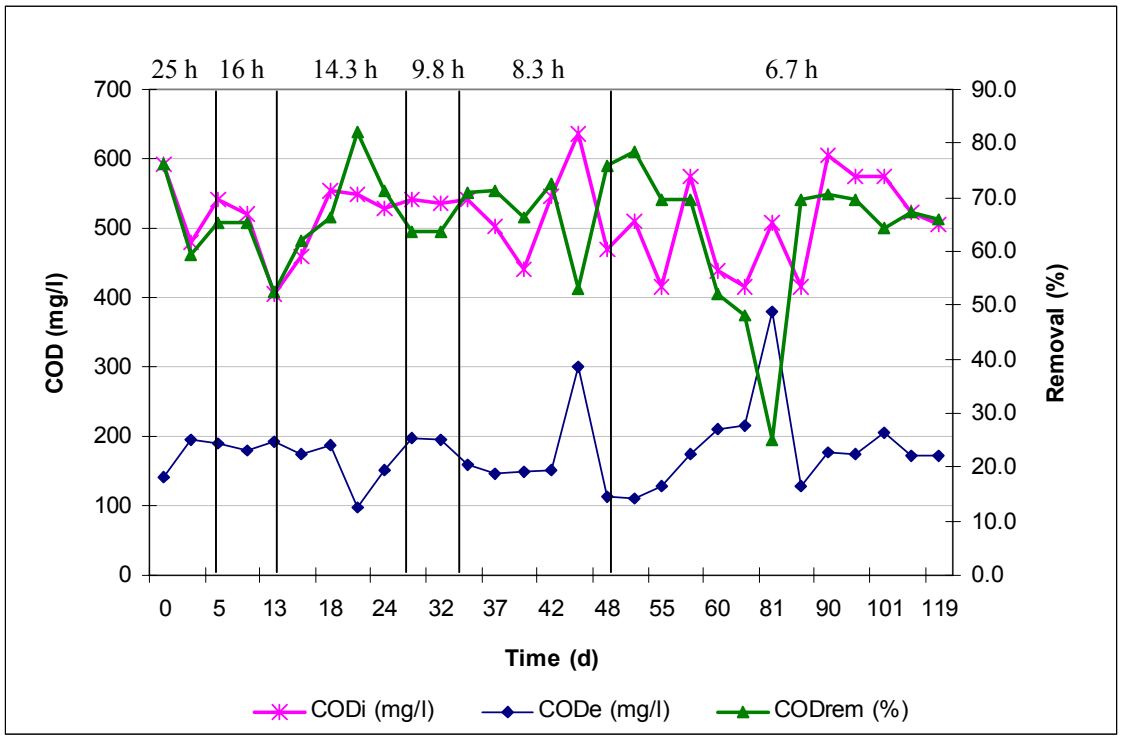

Figure 4.19 Variation of the total COD plus removal efficiency.

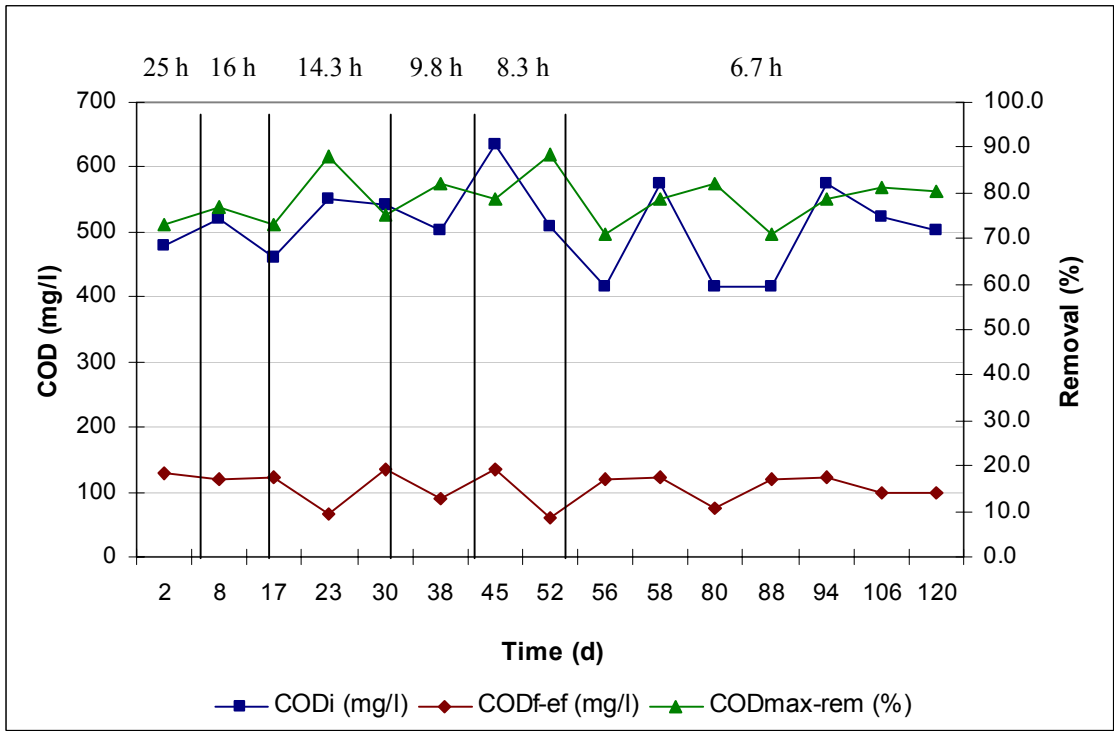

Figure 4.20 Variation of total influent and filtered effluent COD plus maximum COD removal.

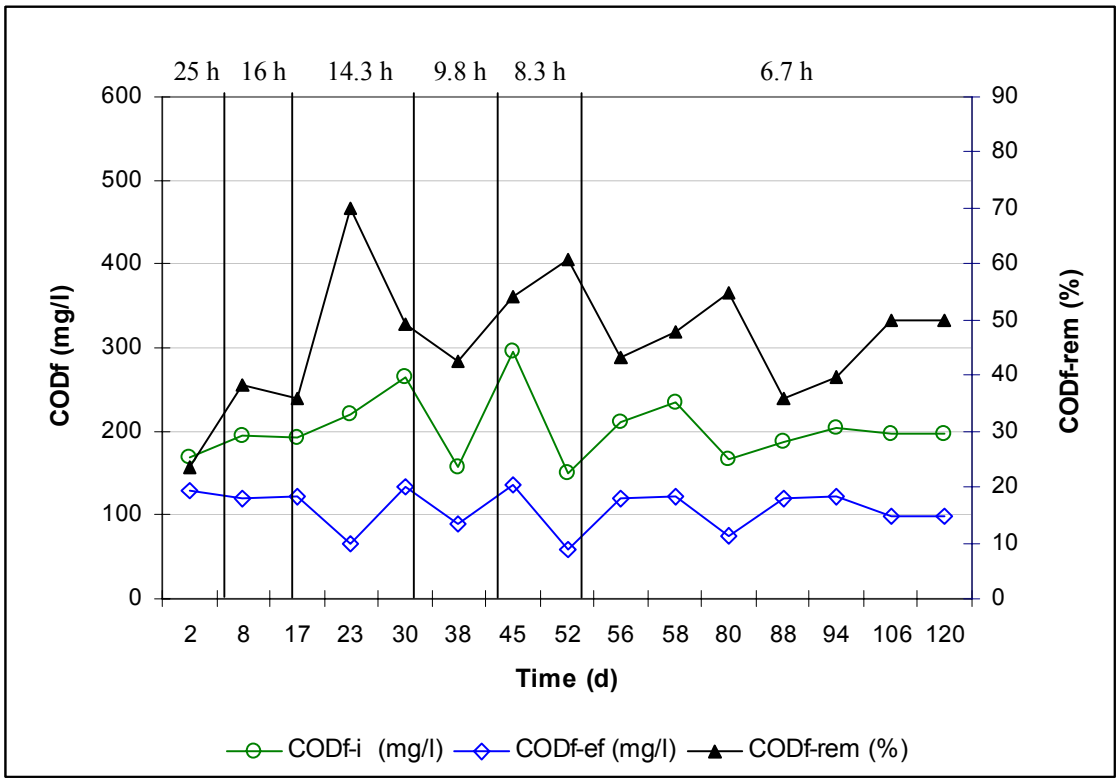

Figure 4.21 Variation of filtered influent and effluent COD plus removal efficiency.

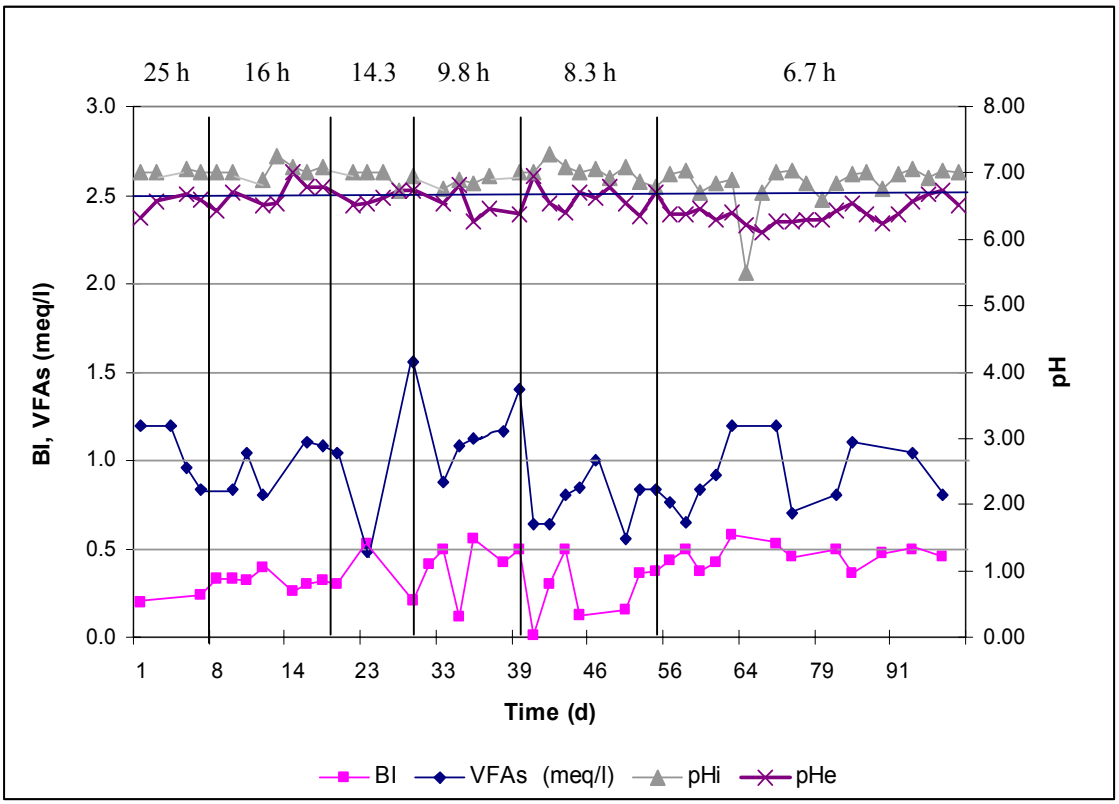

* Buffer index (BI) is a parameter used to evaluate pH stability in anaerobic reactors; it is defined as the strong acid or base concentration needed to produce a unit pH change (van Haandel and Lettinga, 1994). It is determined experimentally by subsequent titration of a wastewater sample at pH 5.75 and 4.30. Details of this test are given in Rojas (1994).

Figure 4.22 Evolution of BI, VFAs and pH along the start-up.

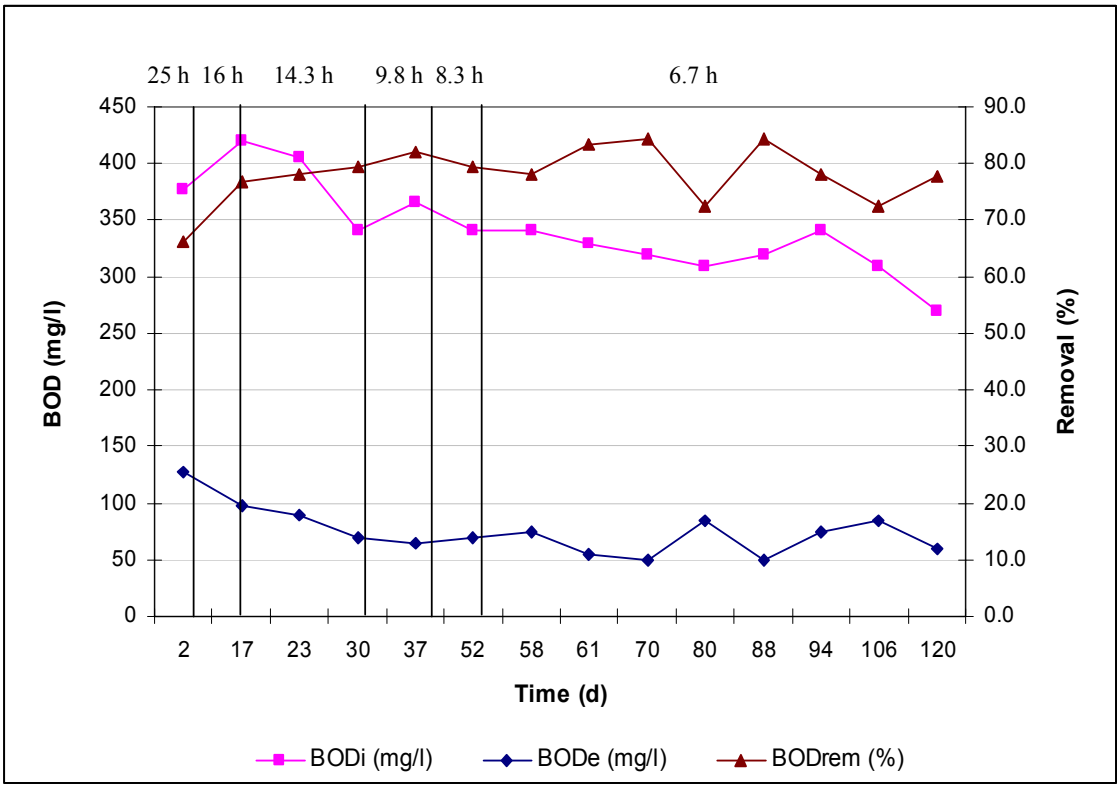

Figure 4.23 Variation of influent and effluent BOD_5 throughout the start-up period.

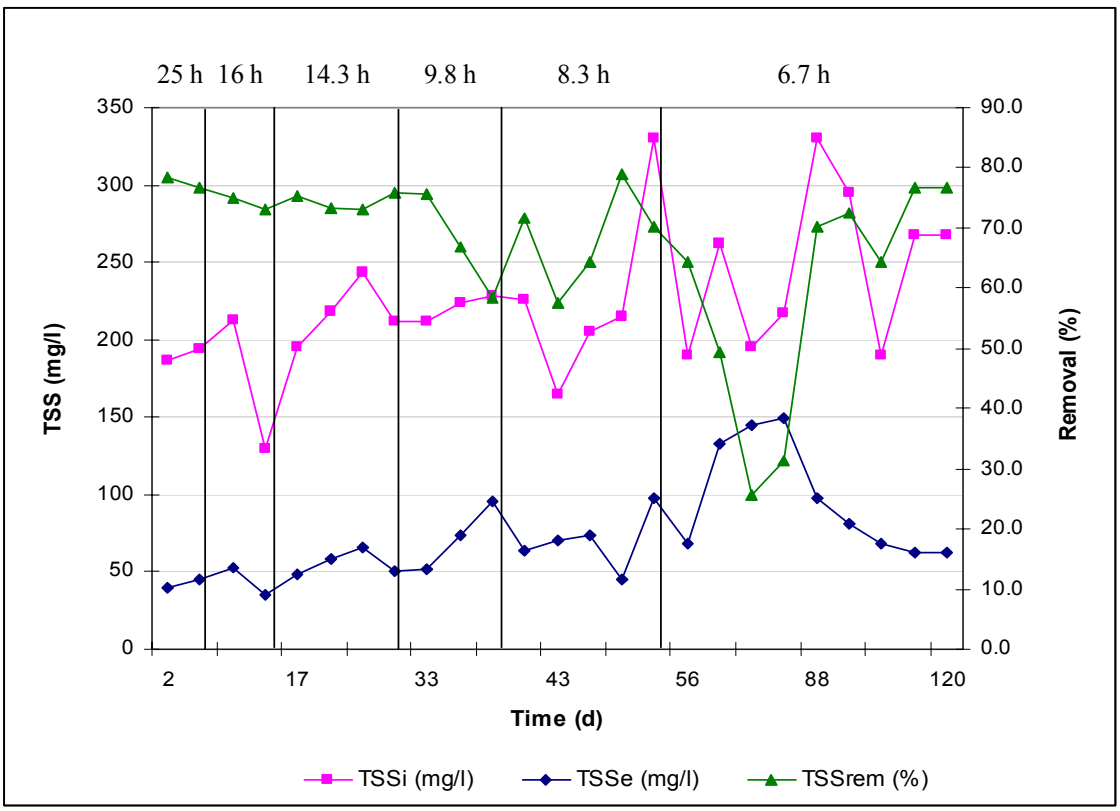

Figure 4.24 Variation of influent and effluent TSS throughout the start-up period.

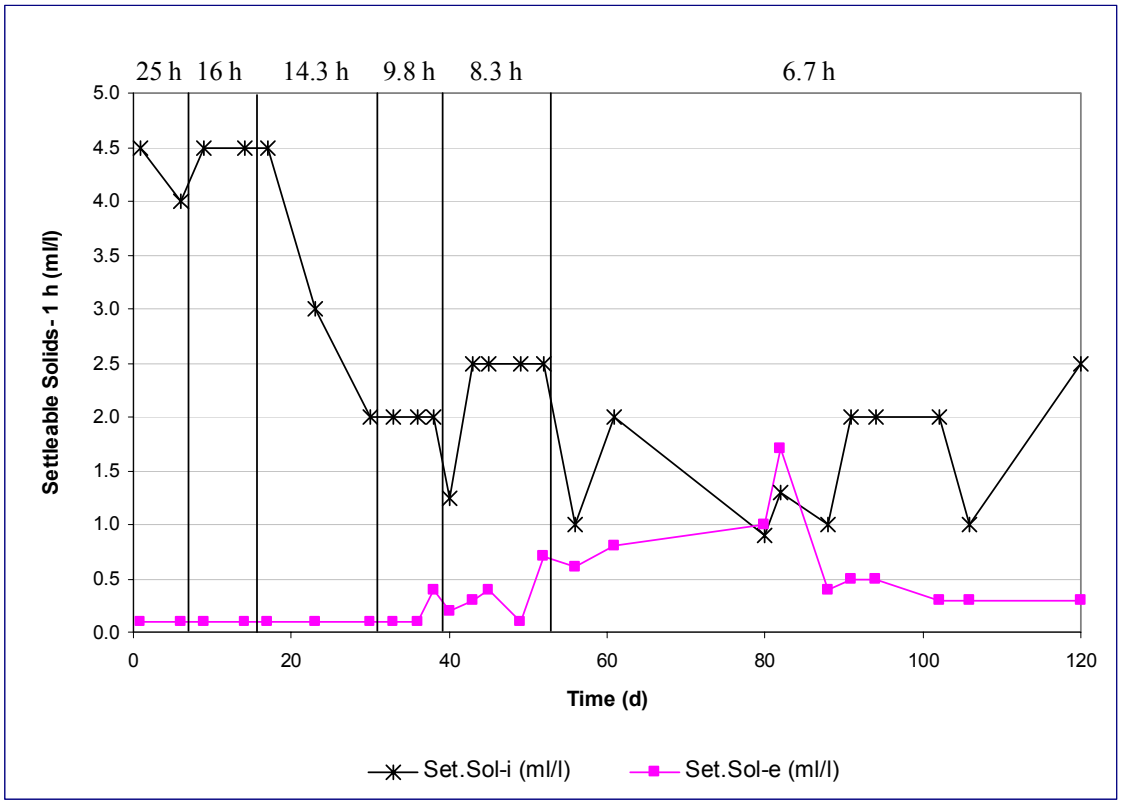

Figure 4.25 Variation of Settleable solids (1-h) throughout the start-up period.

Table 4.10 Descriptive statistics of the main physicochemical parameters.

Parameter		Stages (HRT)					
		I (25 h)	II (16 h)	III (14.3 h)	IV (9.8 h)	V (8.3 h)	VI (6.7 h)
CODi (mg/l)	n	3	2	5	3	5	11
	$\bar{y}$	538	463	527	527	520	504
	σ / CV	56.1/0.1	81.3/0.2	38.5/0.1	20.6/0.04	76.0/0.1	73.3/0.1
CODe (mg/l)	n	3	2	5	3	5	11
	$\bar{y}$	175	187	162	166	164	194
	σ / CV	29.6/0.2	9.2/0.1	39.6/0.2	25.9/0.2	78/0.5	68.1/0.3
CODf-i (mg/l)	n	1	1	3	1	2	7
	$\bar{y}$	169	195	226	157	223	200
	σ / CV	-	-	36.2/0.2	-	102/0.5	21.2/0.1
CODf-e (mg/l)	n	1	1	3	1	2	7
	$\bar{y}$	129	120	108	90	97	108
	σ / CV	-	-	36/0.3	-	54/0.5	18.2/0.17
BODi (mg/l)	n	1	-	3	1	1	8
	$\bar{y}$	377	N.D	388	365	340	317
	σ / CV	-	-	42/0.1	-		22.5/0.1
BODe (mg/l)	n	1	-	3	1	1	8
	$\bar{y}$	128	N.D	86	65	70	67
	σ / CV	-	-	14/0.2	-	-	14.9/0.2

This table continues on the next page. N.D = Not determined.

Continuation of Table 4.10

BI	n	1	7	3	6	7	12
	$\bar{y}$	0.24	0.32	0.35	0.42	0.26	0.46
	σ / CV	-	0.04/0.12	0.17/0.48	0.16/0.38	0.17/0.65	0.06/0.13
VFAs (meq/l)	n	4	5	3	5	8	11
	$\bar{y}$	1.05	0.97	1.03	1.13	0.77	0.91
	σ / CV	0.18/0.17	0.14/0.14	0.54/0.52	0.19/0.17	0.14/0.18	0.19/0.20
pHi	n	4	7	5	5	9	20
	(range)	7.00-7.07	6.90-7.25	6.74-7.00	6.77-7.00	6.78-7.28	5.50-7.06
PHe	n	4	7	5	5	9	20
	(range)	6.33-6.68	6.44-7.02	6.52-6.74	6.28-6.83	6.36-6.95	6.10-6.73
TSSi (mg/l)	n	2	2	4	3	5	9
	$\bar{y}$	190	172	217	221	228	246
	σ / CV	5.7/0.03	58.7/0.34	20.3/0.09	8.3/0.04	61.4/0.27	50.5/0.21
TSSe (mg/l)	n	2	2	4	3	5	9
	$\bar{y}$	42.5	44.0	55.8	73.7	70.0	96.2
	σ / CV	3.5/0.08	12.7/0.29	8.0/0.14	21.5/0.29	19.1/0.27	36.5/0.38
S.sol-i (ml/l)	n	2	2	3	3	5	10
	$\bar{y}$	4.3	4.5	3.2	2.0	2.3	1.6
	σ / CV	0.35/0.08	-	1.26/0.39	-	0.56/0.24	0.59/0.37
S.sol-e (ml/l)	n	2	2	3	3	5	10
	$\bar{y}$	0.1	0.1	0.1	0.2	0.3	0.6
	σ / CV	-	-	-	0.17/0.85	0.23/0.76	0.44/0.73

i, influent; e, effluent.

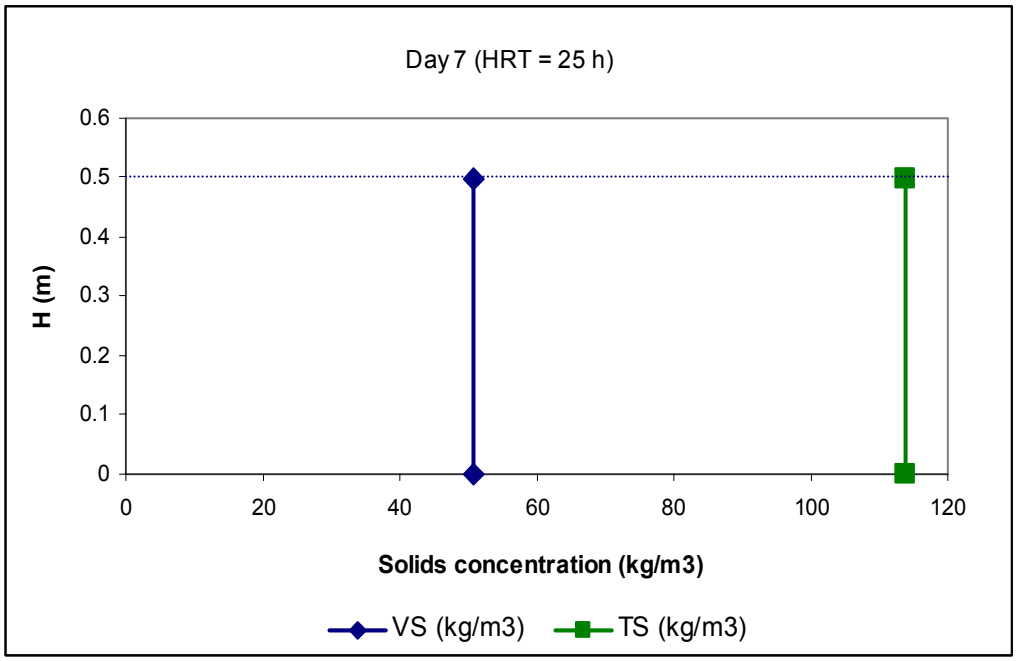

Figure 4.26 Sludge profile after seven days of start-up.

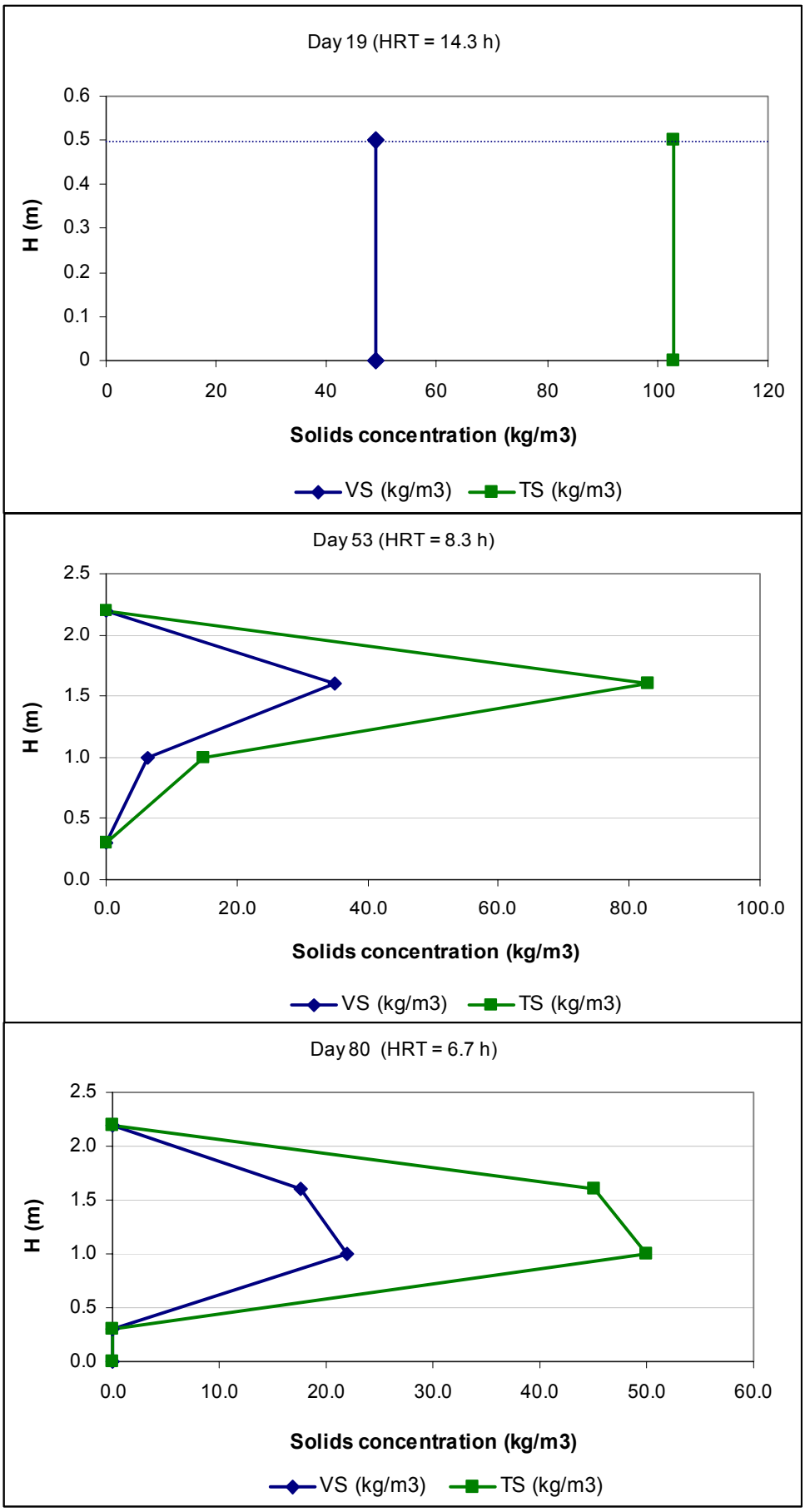

Figure 4.27 Sludge profiles after 19, 53 and 80 days of start-up.

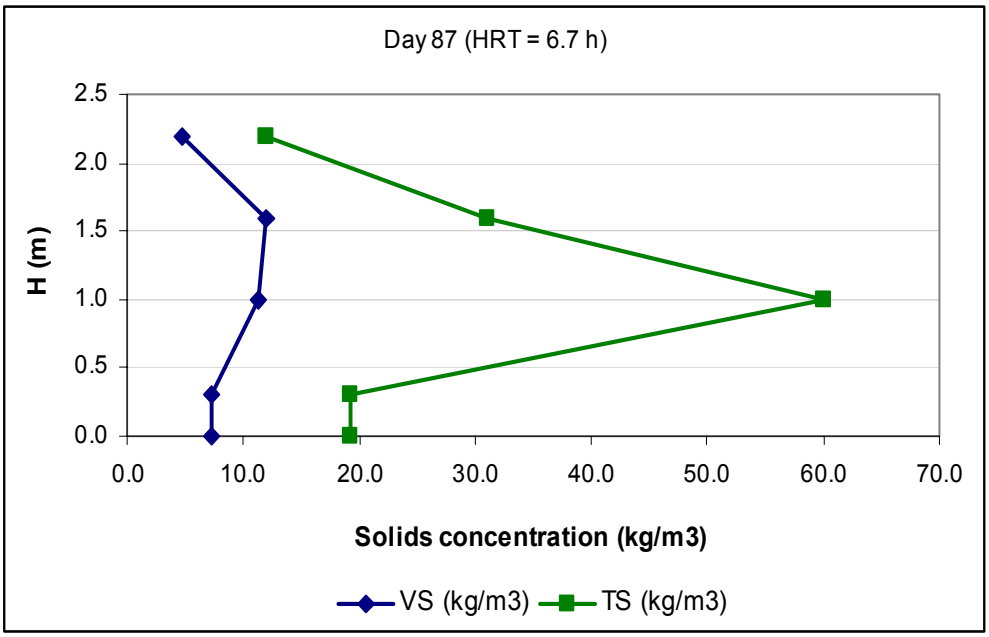

Figure 4.28 Sludge profile in steady state operation after 87 days.

Figure 4.29 shows an estimate of the variation of average sludge contents within the reactor based on the sludge profile data. Figure 4.30 depicts the biogas production and maximum COD removal efficiency (CDO_i-COD_{fe}) as a function of decreasing HRT, that is, as the hydraulic and organic loading rates increased.

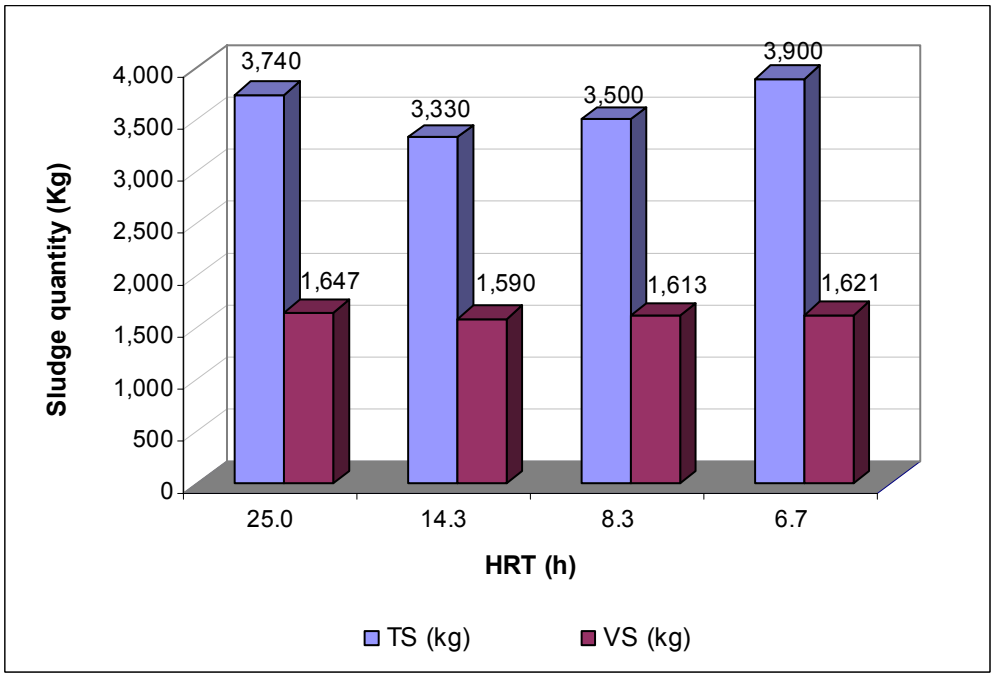

Figure 4.29 Variation of average sludge contents during start-up.

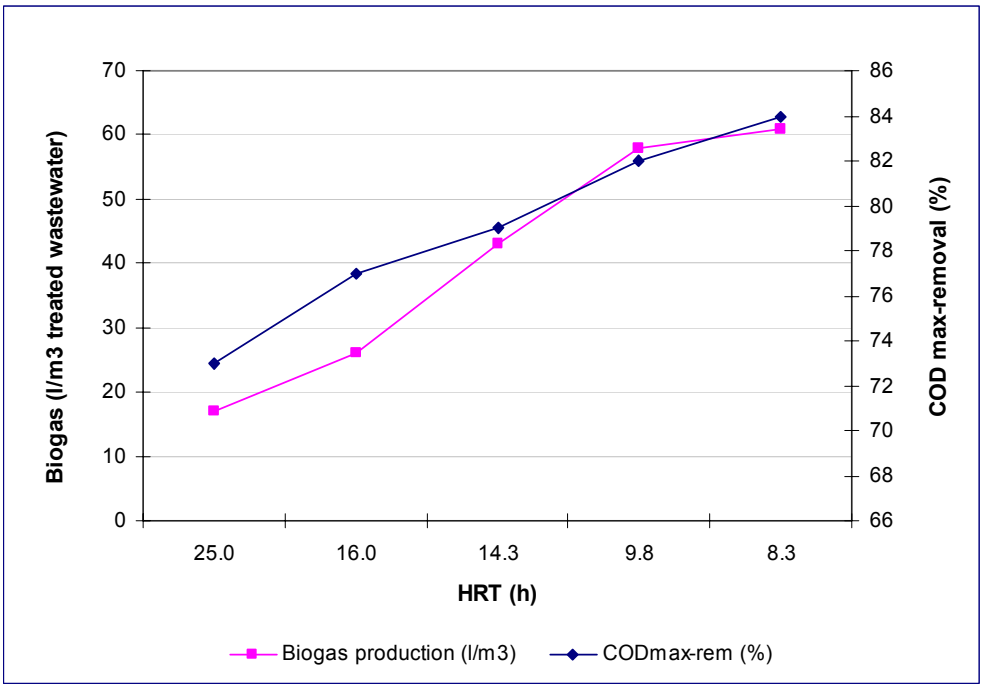

Figure 4.30 Biogas production and COD maximum removal along start-up.

These results suggest that UASB reactors treating domestic sewage under tropical conditions can be started up with low quality seed sludge provided that an appropriate start-up phase is carried out. Moreover, the start-up period can be shortened to 9-10 weeks if the settling properties and activity of sludge particles are improved via the selective pressure method. The discussion of these results based on removal efficiencies and correlations between parameters is presented in the next chapter. The raw data are given in Appendix II in the FULL-SCALE-EXP\UASB-START-UP folder.

4.1.4 Hydrodynamic study of UASB reactor

The UASB was left in continuous operation for seven months (after start-up) before undertaking the hydrodynamic study. As mentioned in Chapter 3, tracer samples were taken at the reactor outlet and also at four internal points located at a depth of 1.50 m. Hence, the dispersion results allowed the analysis of the hydrodynamic behaviour of the reactor in two main parts: the reaction volume (sludge bed plus blanket) and the settling compartment. Each of the four tracer runs was carried out in duplicate.

Flow, pH and temperature. Table 4.11 summarises temperature and pH data taken at the influent and effluent of the UASB during the four tracer runs, and Table 4.12 shows hydraulic loading rate data for each run.

Table 4.11 Temperature and pH data along tracer runs.

Stage	Run	Influent				Effluent			
		Temperature °C		pH		Temperature °C		pH	
		n	Range	*n*	Range	*n*	Range	*n*	Range
1	1	91	23.0-24.9	91	6.46-7.06	91	23.0-25.1	91	6.14-6.65
	2	91	22.1-23.9	91	6.21-7.37	91	23.1-23.9	91	6.21-6.58
2	1	47	22.5-23.9	47	6.63-8.82	47	22.2-23.9	47	6.48-6.84
	2	46	21.5-24.0	46	6.62-7.19	46	22.7-24.1	46	6.44-6.85
3	1	33	23.5-25.0	33	6.71-7.19	33	23.5-26.0	33	6.40-6.62
	2	32	22.7-24.7	32	6.64-7.20	32	23.4-24.4	32	6.35-6.98
4	1	30	23.0-25.0	30	6.40-7.12	30	23.0-25.0	30	6.37-6.62
	2	30	23.0-25.1	30	6.68-7.10	30	23.4-24.7	30	6.33-6.62

Table 4.12 Hydraulic loading rate data.

Stage	Run	Flow (l/s)			
		n	**Mean**	σ	***CV***
1	1	91	7.2	2.0	0.29
	2	91	7.7	0.1	0.01
2	1	47	9.8	0.1	0.01
	2	47	9.6	0.2	0.03
3	1	33	13.3	0.1	0.01
	2	33	13.4	0.5	0.04
4	1	30	15.7	0.3	0.02
	2	30	14.9	0.6	0.04

Retention time distribution curves (RTD). Dimensionless RTD curves were obtained for each of the runs listed in Table 4.11 in the effluent and also at the four internal points shown in Figure 3.8. The RTD curves determined in the effluent showed the overall hydrodynamic behaviour of the UASB reactor for each of the hydraulic loading rates evaluated. Figure 4.31 summarises these RTD curves.

The RTD curves generated at the internal points (1.50 m depth) provided information on the hydrodynamic behaviour of the sludge bed and blanket volumes (i.e. the active reaction zone) of the reactor. The RTD curves from internal points are shown in Figures 4.32 to 4.35. The depth chosen for the internal points was based on the maximum sludge blanket height expected at the design stage. Experimental observations confirmed that a depth of 1.50 m from the water surface allowed sampling just above the blanket interface. Thus, the RTD curves obtained in these points may be regarded as a good representation of the hydrodynamics of the sludge bed and blanket volumes. Positioning of internal points 1, 2, 3 and 4 is shown in Figure 3.8.

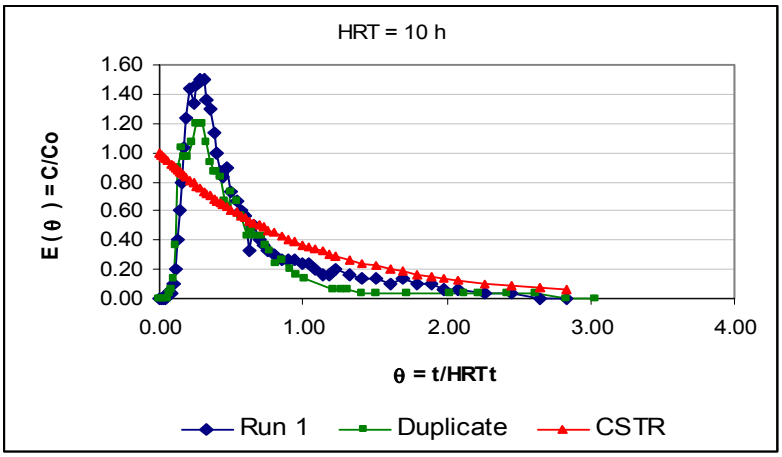

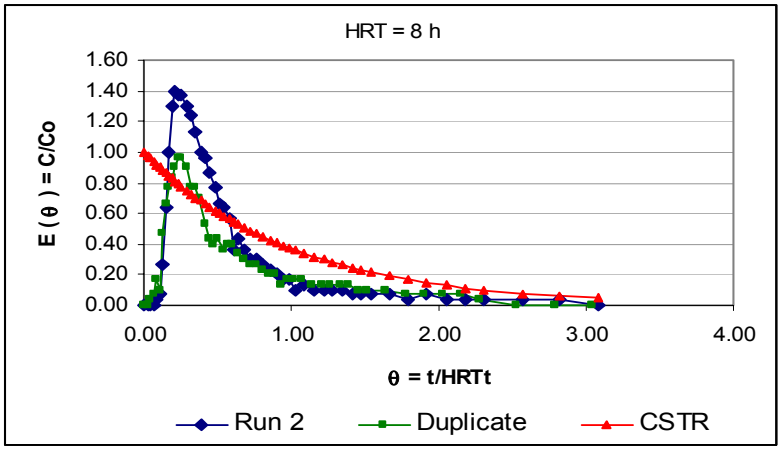

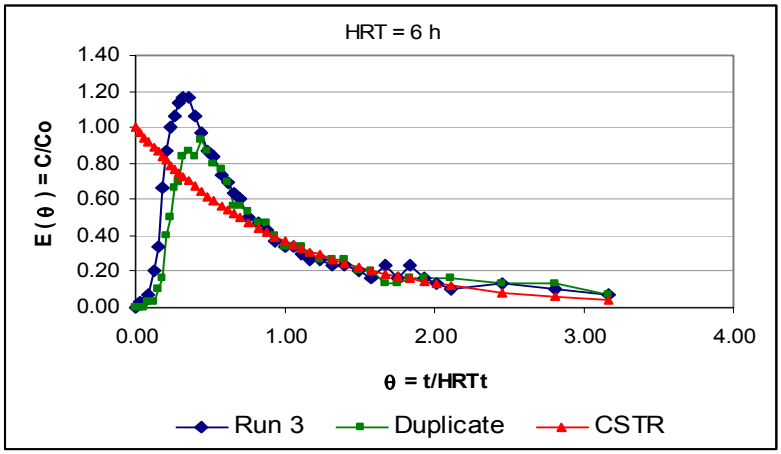

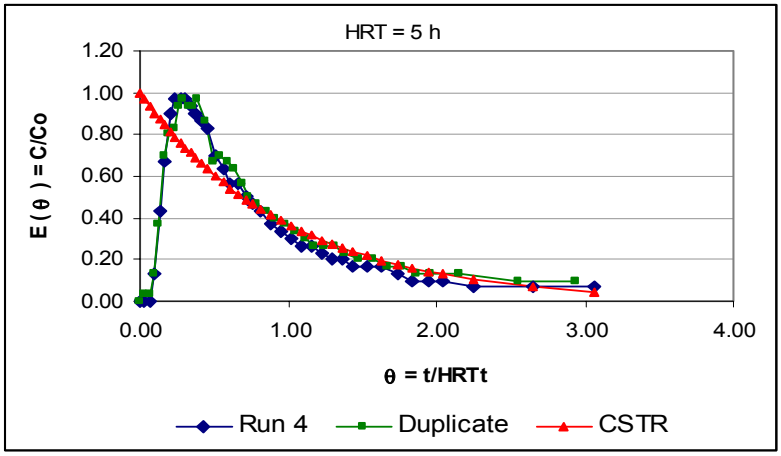

Figure 4.31 RTD curves obtained in the effluent of the UASB.

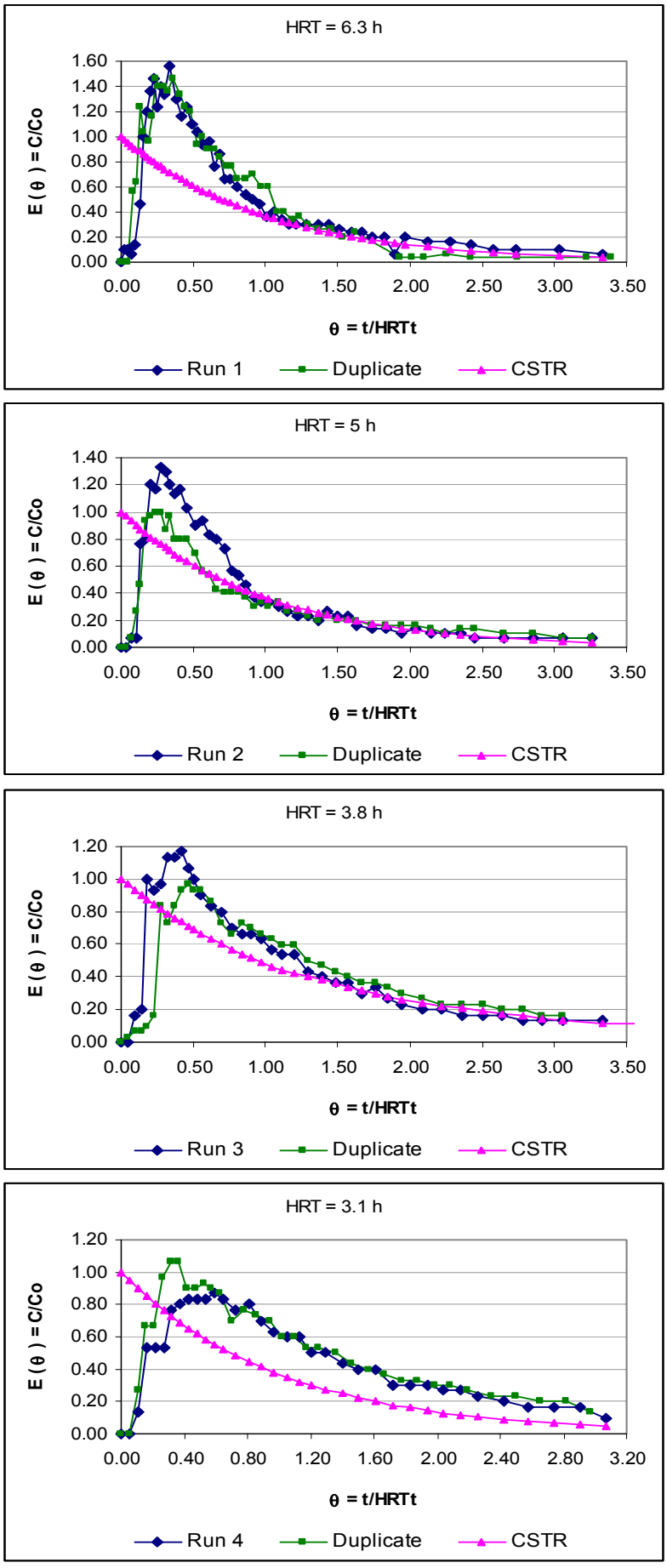

Figure 4.32 RTD curves obtained at internal point 1.

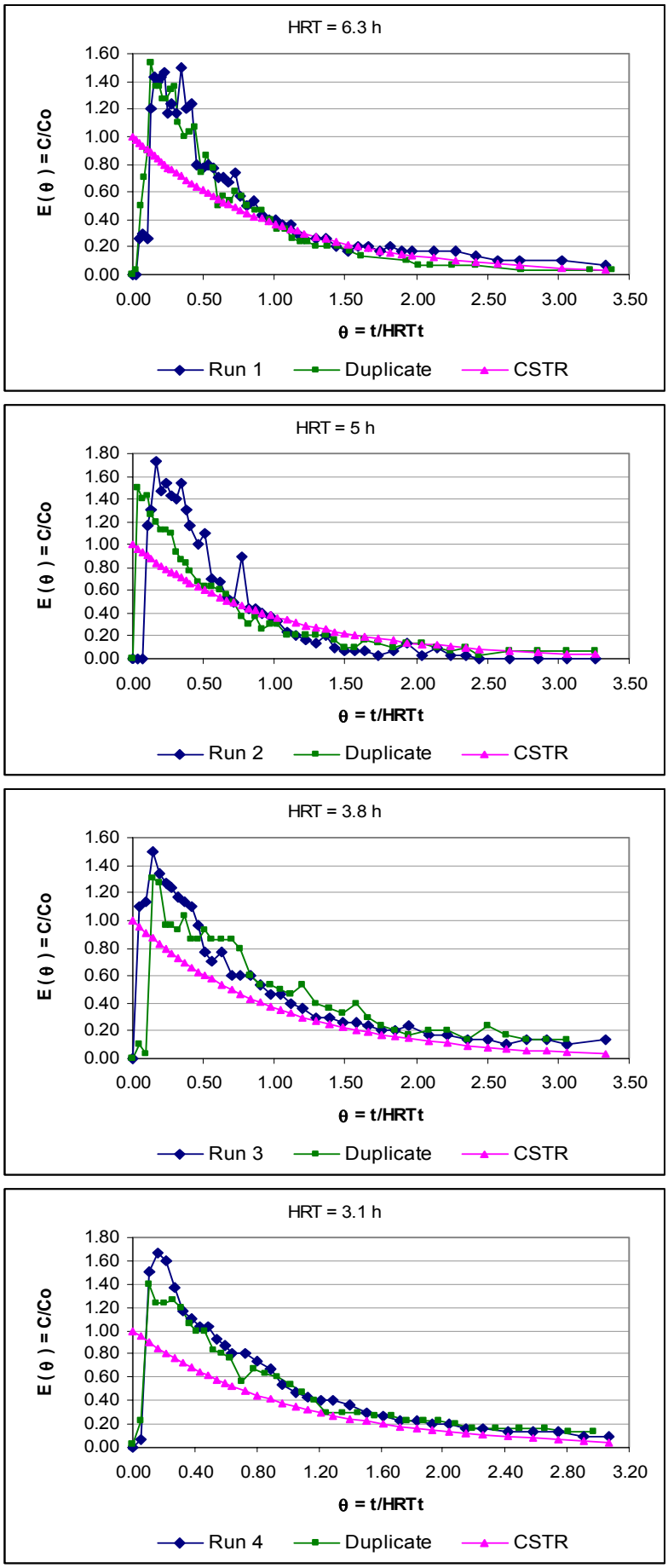

Figure 4.33 RTD curves obtained at internal point 2.

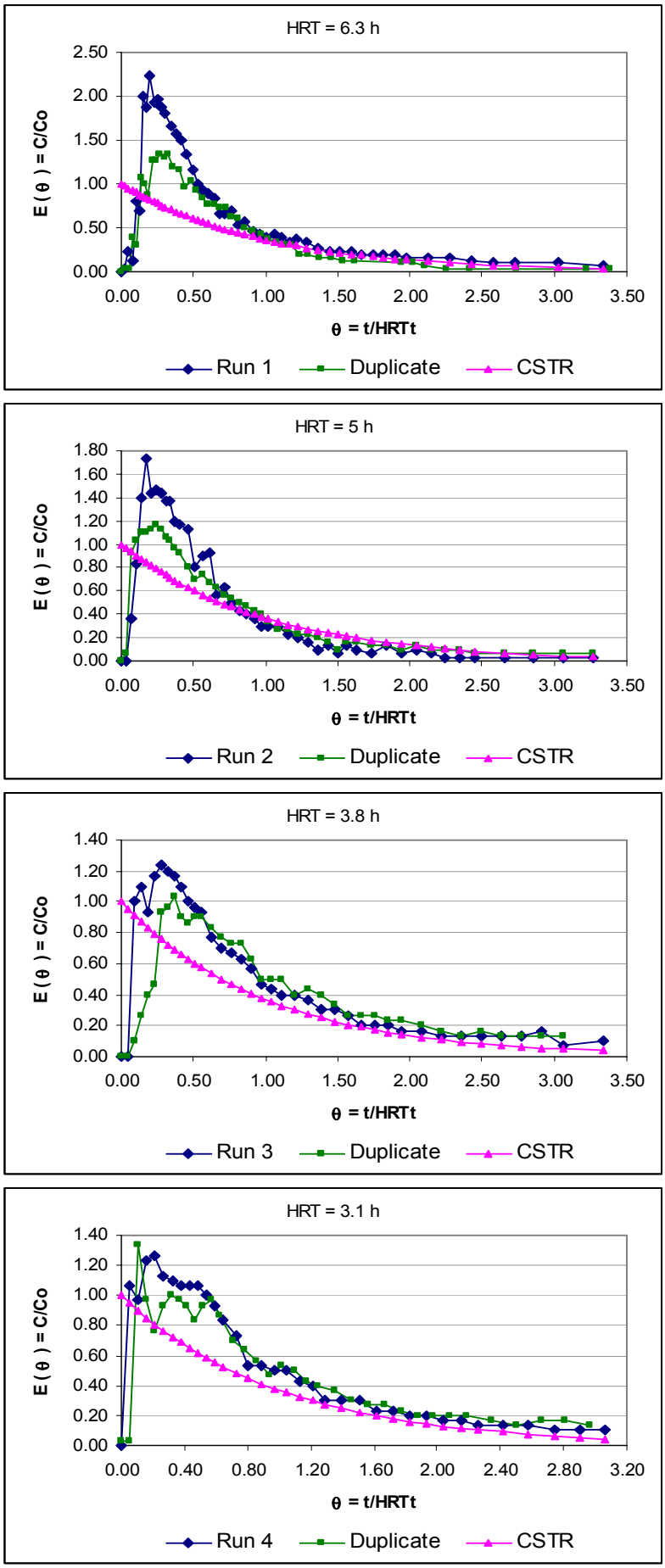

Figure 4.34 RTD curves obtained at internal point 3.

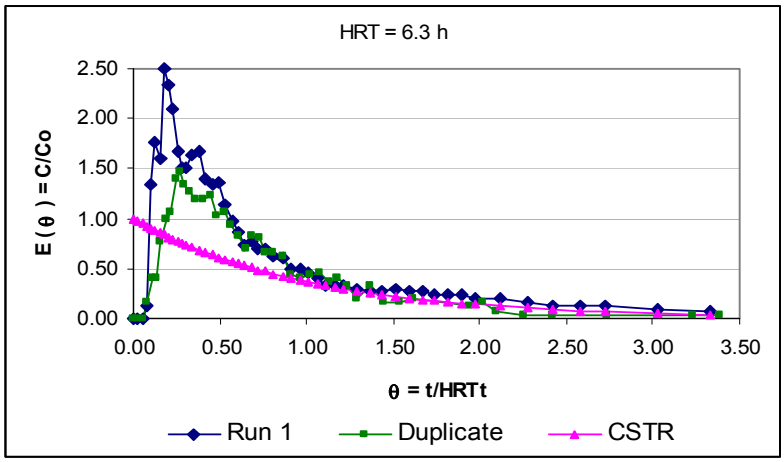

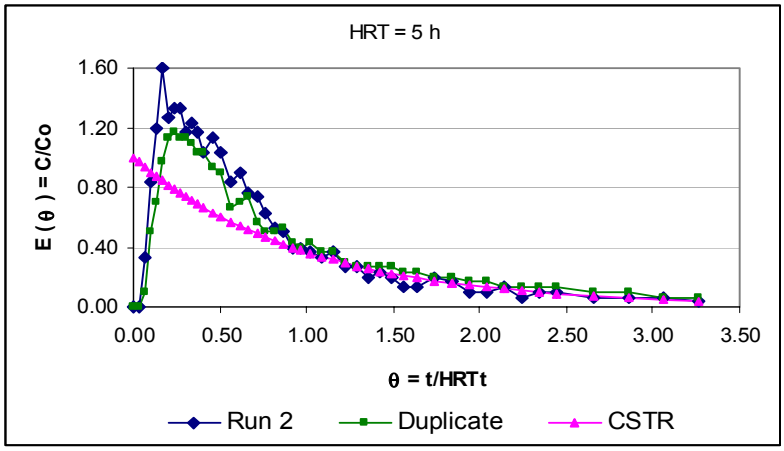

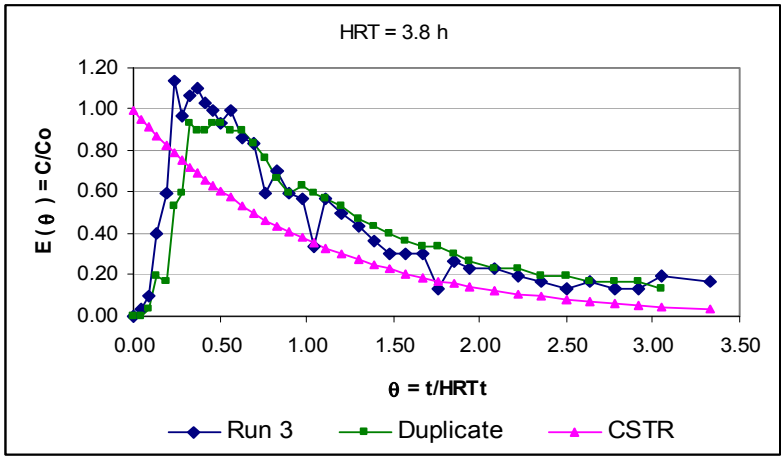

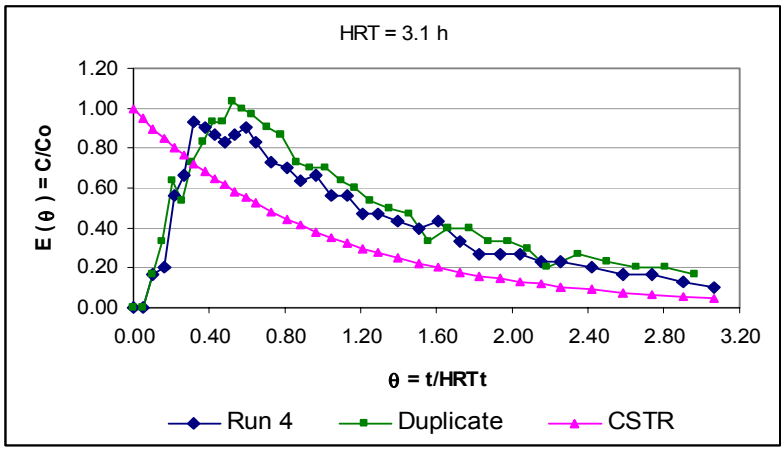

Figure 4.35 RTD curves obtained at internal point 4.

Hydrodynamic parameters. The experimental HRT (HRTe) figures, dispersion number (δ) values and variances of the RTD curves (σ^2) were calculated on the basis of the data series plotted in Figures 4.31 to 4.35. The raw experimental data are given in electronic format in Appendix II in the FULL-SCALE-EXP\UASB-TRACER-DISPERSION folder. Tables 4.13 and 4.14 summarise the experimental values of the hydrodynamic parameters. The data were analysed by the dispersion model applied to discrete data series as described in Levenspiel (1999). The volume occupied by the sludge bed and blanket was estimated and experimentally checked as 172 m^3. This figure corresponds to the height of the sludge bed and blanket (2.5 m) multiplied by the reactor surface area (9.6 m x 7.2 m).

The RTD curves and parameters obtained at the four internal sampling points were assumed to represent the hydrodynamic behaviour of four equal volumes of the sludge bed and blanket zone. Thus, each internal point accounted for a volume of 43 m^3 ($172m^3/4$). This assumption was supported by the even distribution of raw sewage at the reactor's base. Hence, similar hydrodynamic features were likely to occur throughout the UASB cross sectional area.

Table 4.13 Summary of hydrodynamic parameters obtained at the reactor outlet.

Stage	Run	HRT* (h)	HRT_t (h)	HRTe (h)	σ^2	δ
1	1	10	10.6	7.0	0.2724	0.163
	2	10	9.9	5.8	0.2475	0.145
2	1	8	7.8	4.9	0.3163	0.197
	2	8	7.9	5.4	0.3014	0.185
3	1	6	5.7	5.8	0.6619	0.720
	2	6	5.7	6.3	0.6122	0.591
4	1	5	4.9	4.3	0.4726	0.355
	2	5	5.1	4.8	0.5101	0.406

HRT* = Values chosen to run the experiments. HRTe = Experimental HRT values.
HRT_t = Theoretical HRT values based on hydraulic loading rates applied (see Table 4.12).

Table 4.14 Summary of hydrodynamic parameters obtained at internal points.

Stage and run		1		2		3		4	
		1	2	1	2	1	2	1	2
HRT_t (h)		**6.6**	**6.2**	**4.9**	**4.9**	**3.6**	**3.6**	**3.1**	**3.2**
Point 1	HRTe (h)	6.2	4.7	4.2	4.9	4.0	4.4	3.6	3.6
	σ^2	0.5948	0.3481	0.5043	0.6496	0.6443	0.5520	0.5452	0.5540
	δ	0.553	0.223	0.397	0.685	0.671	0.472	0.461	0.475
Point 2	HRTe (h)	6.1	4.6	2.9	3.7	3.3	3.7	2.8	3.0
	σ^2	0.6360	0.4365	0.2108	0.5712	0.6834	0.5687	0.5288	0.5603
	δ	0.649	0.311	0.120	0.507	0.789	0.502	0.434	0.487

Continuation of Table 4.14

Point 3	HRTe (h)	5.6	4.6	3.2	4.0	3.5	3.9	2.7	3.1
	σ^2	0.5778	0.3810	0.3566	0.5426	0.6342	0.5316	0.5299	0.5584
	δ	0.519	0.254	0.231	0.456	0.644	0.438	0.435	0.483
Point 4	HRTe (h)	5.7	5.0	4.0	4.7	4.1	4.2	3.6	3.7
	σ^2	0.6032	0.3797	0.4878	0.5864	0.7119	0.5447	0.5379	0.5288
	δ	0.571	0.252	0.374	0.536	0.894	0.460	0.448	0.434

Process performance. Table 4.15 shows the average composition of the raw wastewater during the whole period of the experiment discriminated per stage.

Table 4.15 Average composition of the raw wastewater throughout the experiment.

Parameter		**HRT_t = 10.2 h**	**HRT_t = 7.9 h**	**HRT_t = 5.7 h**	**HRT_t = 5 h**
COD_t (mg/l)	n	12	12	10	10
	$\bar{y}$	398	396	509	559
	σ / CV	152 / 0.38	182 / 0.46	189 / 0.37	82 / 0.15
COD_f (mg/l)	n	12	12	10	10
	$\bar{y}$	143	120	162	167
	σ / CV	55.2 / 0.38	79.7 /0.66	35 / 0.22	74 / 0.44
TSS (mg/l)	n	12	12	10	10
	$\bar{y}$	148	218	235	272
	σ / CV	57.5 / 0.39	57.6 / 0.26	87 / 0.37	56 / 0.20
Sett. solids ml/l (1-h)	n	12	12	10	10
	$\bar{y}$	1.5	2.3	2.6	3.7
	σ / CV	1.1 / 0.73	1.6 / 0.69	1.2 / 0.46	1.0 / 0.27

HRT_t = the average of the two HRT_t values shown in Table 4.13 per stage.

The composition of the raw wastewater showed a relatively higher variation during this experiment as shown by the CV values of the parameters. This variation may be related to heavy rains registered during the first runs of the experiment. The combined sewerage that conveys the wastewater to the treatment site dilutes the sewage during rain events and modifies its original composition. Nonetheless, the strength of the wastewater recovered its normal values in the last two stages of the experiment. These latter figures were similar to the ones obtained previously during the start-up phase.

Figures 4.36 to 4.39 show the mean variation of total COD, filtered COD, TSS and settleable solids (1-h) throughout the four stages of the experiment. Each of the two points per stage represents the average of six composite samples taken at the effluent in the respective run.

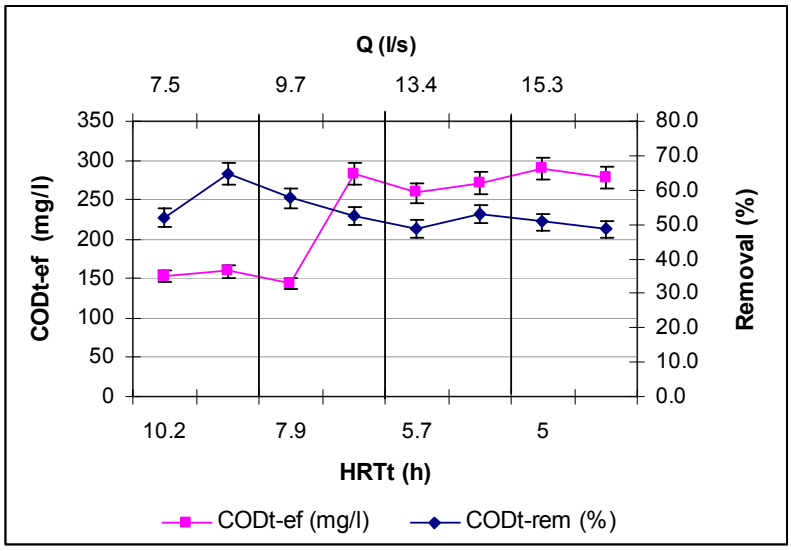

Figure 4.36 Total effluent COD concentration and removal along the experiment.

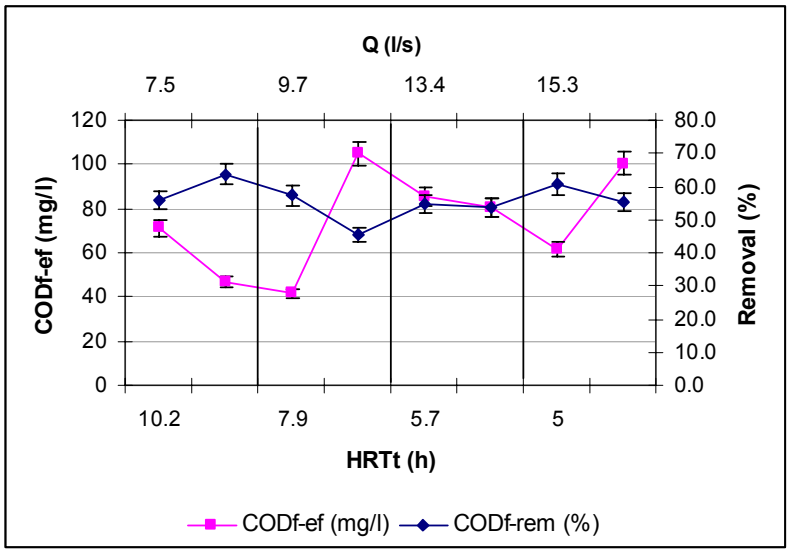

Figure 4.37 Filtered effluent COD concentration and removal along the experiment.

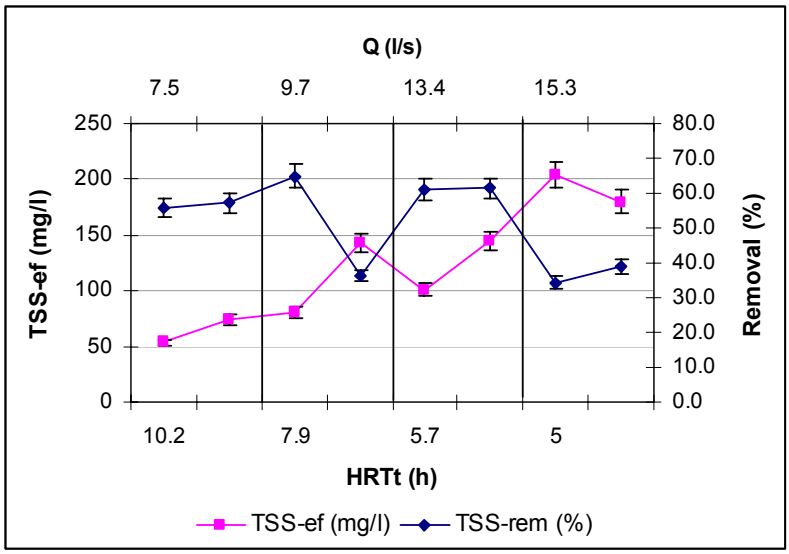

Figure 4.38 Effluent TSS concentration and removal along the experiment.

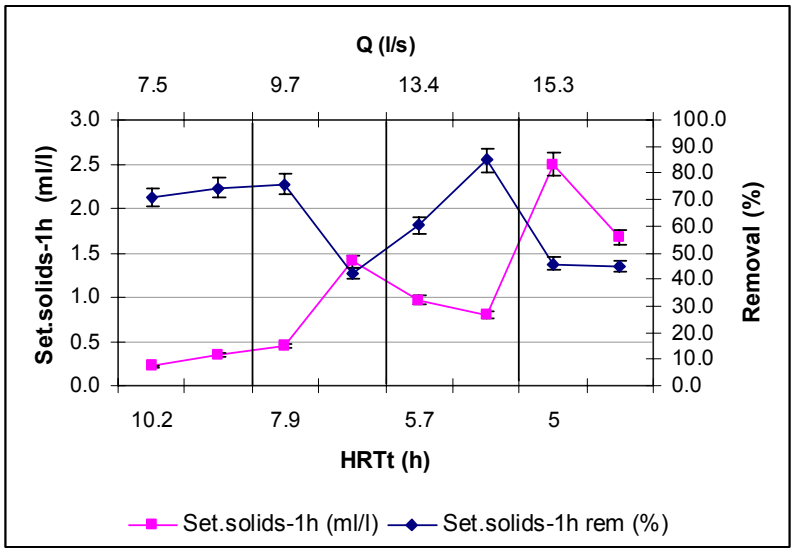

Figure 4.39 Effluent Settleable solids (1h) and removal along the experiment.

Statistical analysis of data. Table 4.16 presents the results of the ANOVA and Tukey's tests performed on the effluent data series for total COD, filtered COD and TSS.

Table 4.16 Summary of ANOVA and Tukey tests results.

Parameter	*F-value*	*F-critical*	*p*	α	Decision rule	Equal means*
CODt-ef	6.351	2.817	0.001	0.05	Reject Ho	(10.2, 7.9) (5.7,5.0)
CODf-ef	5.003	2.901	0.006	0.05	Reject Ho	(10.2, 7.9) (5.7,5.0)
TSS-ef	6.971	2.817	0.001	0.05	Reject Ho	(10.2) (7.9, 5.7, 5.0)

* Values in brackets are the HRT_t figures to which statistically similar means of the parameter were obtained.

The ANOVA test confirmed that there was significant statistical difference between the means of the parameters related to the different HRT_t or applied flow rate values. The F-statistic values were higher than F-critical for all the parameters, and the p-values were always smaller than α for all cases. These features lead to the rejection of the null hypothesis (stated in the equation 3.9) at a 95 percent confidence level and according to the decision rule (Kvanli *et al.,* 2000). In other words, the variation of applied hydraulic loading rate does affect the mixing pattern and consequently the performance of the treatment process. Figure 4.31 shows how, by decreasing HRT_t values (i.e. increasing the hydraulic loading rate), the overall hydrodynamic pattern of the UASB approaches closely the CSTR model at the highest flow value.

Tukey's test yielded the statistically equal means for each parameter, as shown in Table 4.16. This statistic also showed that some of the mean values were different

and the HRT_t figures (i.e. hydraulic loading rates) were related to their variation. The ANOVA and Tukey's tests calculation sheets are given in Appendix II in the FULL-SCALE-EXP\UASB-TRACER-DISPERSION folder. Linear correlations between different process performance and hydrodynamic variables are presented and discussed in Chapter 5.

Removal of microbiological indicators. Table 4.17 displays the figures for concentrations and removal efficiencies of faecal coliforms and helminth eggs. Samples for microbiological analyses were not taken during the second stage of the experiment.

Table 4.17 Removal of microbiological indicators.

Stage/HRTt (h)	Faecal coliforms (CFU/100 ml)			Helminth eggs (No/L)		
	Influent	Effluent	Removal (%)	Influent	Effluent	Removal (%)
1 / 10.2	7.6×10^6	6.0×10^6	21.0	1226	80	93.5
	4.0×10^6	2.9×10^6	27.5	N.D	N.D	N.D
3 / 5.7	7.0×10^6	5.0×10^6	28.6	2727	274	90.0
	10×10^6	2.1×10^6	79.0	N.D	N.D	N.D
4 / 5.0	6.0×10^6	3.0×10^6	50.0	467	48	89.7

N.D. Sample not taken during the run.

Few data are available in the literature on the removal of microbiological indicators in UASB reactors. The evaluation of an UASB treating domestic sewage in Pedregal, Brazil reported 80 percent removal of *E. coli* and 82 percent removal of helminth eggs during a 30 week operational period (van Haandel and Lettinga, 1994). Data from Table 4.17 show a good removal of helminth eggs, but a very low removal of faecal coliforms in the reactor evaluated in this experiment. However, the removal efficiency of helminth eggs deteriorated when the HRT value decreased below 5.7 h. These results are in agreement with findings reported by Haskoning (1989) who confirmed the inability of UASB reactors to remove faecal indicators in a pilot-scale unit operating under tropical conditions. This author argued that the shorter HRT values of UASBs might be the main cause for the low removals. Nonetheless, the propensity of full-scale reactors to release sludge aggregates in the effluent might also explain the poor microbiological removal of these systems. The latter was frequently observed during the tracer runs carried out in this experiment regardless the upflow velocity (i.e. HRT) applied to the reactor.

Further analyses and discussion of the results obtained in this experiment are presented in Chapter 5.

4.2 Pilot-scale experiments

4.2.1 Hydrodynamic studies on the pilot-scale APs

The results obtained in the full-scale experiments provided the basis to design, build, commission and carry out the evaluation of four different pilot-scale AP configurations as described in Section 3.2.2. The modified AP configurations tested in this experiment introduced physical changes aimed at improving the intensity of mixing and contact patterns compared with the conventional AP. The latter was run as a control unit throughout the experiment. Tracer samples were taken at the outlet of each pilot AP. The whole experiment was carried out in two stages as shown in Table 3.17 in Chapter 3.

Flow, pH and temperature. Table 4.18 shows temperature and pH data taken at the influent and effluent of each pilot AP during the two stages of the experiment, and Table 4.19 presents the hydraulic loading rate data.

Table 4.18 Summary of temperature and pH data.

Experiment	Run	Parameter	*n**	Influent	Effluents		
					VBAP	PNFAP	AP
Experiment I	1	T (°C)	42	23.0-25.9	23.2-25.9	23.0-25.5	23.2-25.3
		pH	42	6.34-7.17	6.06-6.62	6.13-6.67	6.14-6.66
	2	T (°C)	42	23.3-25.8	23.7-26.0	23.9-25.6	23.8-25.9
		pH	42	6.38-7.19	6.12-6.60	6.11-6.69	6.12-6.85
	3	T (°C)	42	23.3-25.7	23.7-26.1	23.7-26.1	23.6-26.2
		pH	42	6.45-7.05	6.32-6.60	6.34-6.57	6.33-6.61
	4	T (°C)	42	22.8-25.4	22.7-26.1	22.7-25.8	22.8-26.0
		pH	42	6.29-7.12	6.35-6.64	6.36-6.64	6.34-6.58
	Run	**Parameter**	**n**	**Influent**	**HBAP**	**MPAP**	**AP**
Experiment II	1	T (°C)	42	24.2-26.7	23.7-27.2	23.8-25.8	23.9-26.0
		pH	42	6.55-7.20	6.41-6.77	6.45-6.89	6.46-6.82
	2	T (°C)	42	23.7-26.2	23.7-26.6	23.8-25.6	23.8-26.3
		pH	42	6.40-7.19	6.48-7.00	6.53-6.89	6.45-6.85
	3	T (°C)	42	24.2-26.7	24.6-26.5	24.7-26.1	24.7-26.3
		pH	42	6.53-7.57	6.17-6.95	6.29-7.01	6.33-6.96
	4	T (°C)	42	24.1-26.6	24.4-27.1	24.6-26.5	24.5-26.5
		pH	42	6.63-7.44	6.40-6.76	6.28-6.65	6.22-6.68

* *n* values refer to the number of data taken at each sampling point.

Sections 3.2.2 and 3.3.5 explain the details on how both experiments were operated in the three APs shown in Figure 3.6.

Table 4.19 Hydraulic loading rate data.

Experiment	Run	Parameter	Hydraulic loading rates applied (l/s)		
			VBAP	**PNFAP**	**AP**
Experiment I	1	n = 60	1.20	2.10	0.95
		σ / CV	0.10 / 0.08	0.20 / 0.09	0.06 / 0.06
	2	n = 60	1.90	1.00	1.40
		σ / CV	0.14 / 0.07	0.07 / 0.07	0.17 / 0.12
	3	n = 60	1.00	1.20	2.00
		σ / CV	0.02 / 0.02	0.04 / 0.03	0.06 / 0.03
	4	n = 60	1.50	1.50	1.10
		σ / CV	0.10 / 0.07	0.04 / 0.03	0.10 / 0.09
	Run	**Parameter**	**HBAP**	**MPAP**	**AP**
Experiment II	1	n = 60	1.20	1.20	1.50
		σ / CV	0.09 / 0.08	0.05 / 0.04	0.09 / 0.06
	2	n = 60	2.00	1.00	1.00
		σ / CV	0.09 / 0.05	0.06 / 0.06	0.07 / 0.07
	3	n = 60	1.00	1.50	1.20
		σ / CV	0.02 / 0.02	0.03 / 0.02	0.09 / 0.08
	4	n = 60	1.50	2.00	2.00
		σ / CV	0.09 / 0.06	0.10 / 0.05	0.05 / 0.03

* n values refer to the number of data recorded at each AP inlet.

Tracer response curves (RTD). Dimensionless RTD curves were obtained at the outlet of each pilot AP for each of the runs shown in Table 4.19. The pilot AP did not operate simultaneously with the same hydraulic flow rates since these values were randomly assigned at each run. The latter procedure was aimed at reducing external error sources as noted in Section 3.3.5. Figures 4.40 to 4.43 show the experimental RTD curves obtained from experiments I and II, respectively. The dimensionless curves allowed direct comparison of results within and across both experiments.

Equations 3.4, 3.5 and 3.6, given by Levenspiel (1999), were used to normalize the *C vs. t* data sets obtained in each run at every AP configuration. The normalized RTD concentration values were calculated based on the Co figures shown in Table 3.18. The theoretical hydraulic retention time (HRTt) was calculated as the AP volume divided by the respective average hydraulic loading rate figure, as shown in Table 4.19. The first and second moments of the RTD curves were calculated in order to determine the experimental hydraulic residence time (HRTe) values and the corresponding dispersion numbers (δ).

Hydraulic loading rates applied: 1.0 and 1.2 l/s

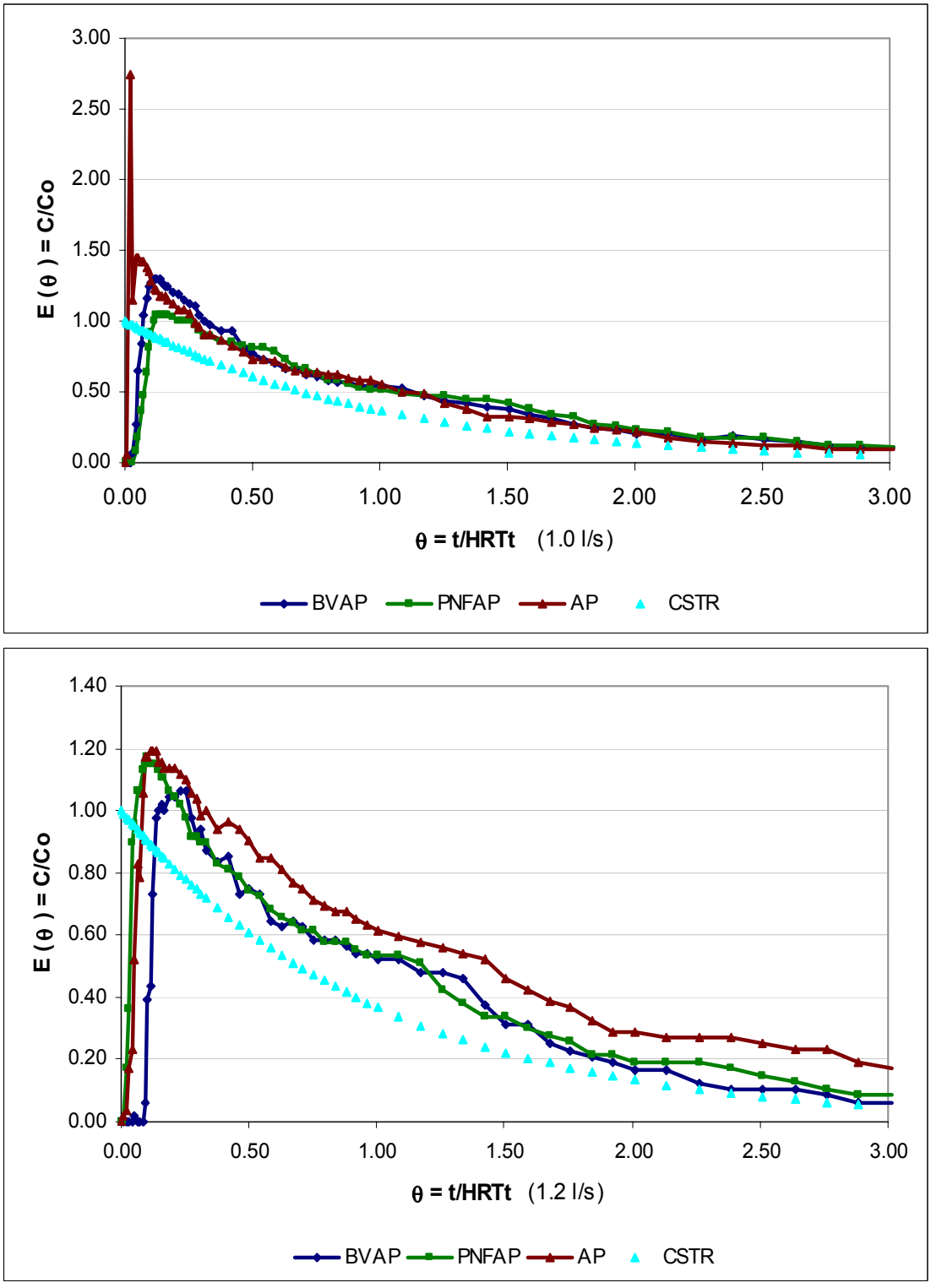

Figure 4.40 Dimensionless experimental RTD curves from experiment I.

Hydraulic loading rates applied: 1.5 and 2.0 l/s

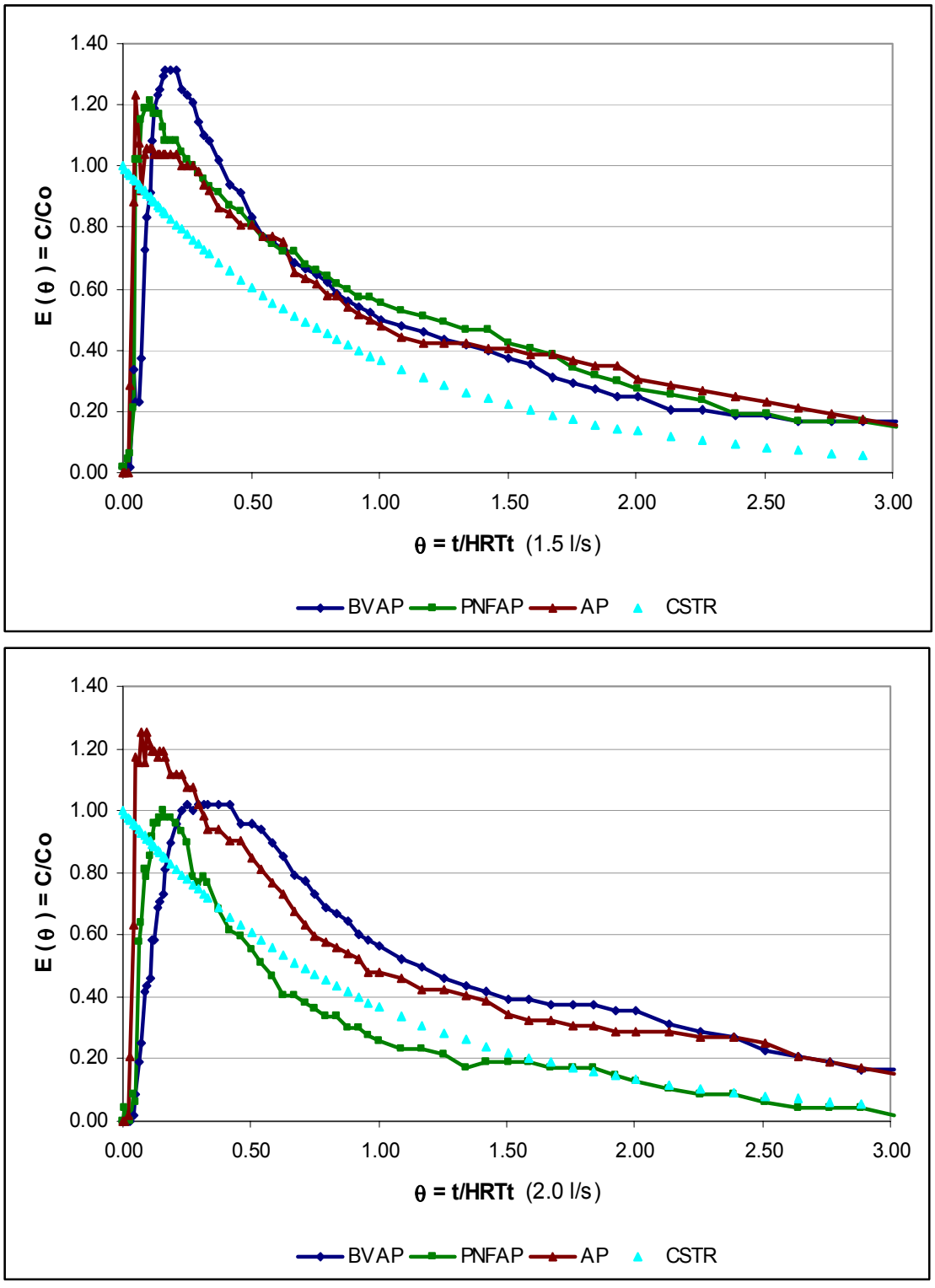

Figure 4.41 Dimensionless experimental RTD curves from experiment I.

Hydraulic loading rates applied: 1.0 and 1.2 l/s

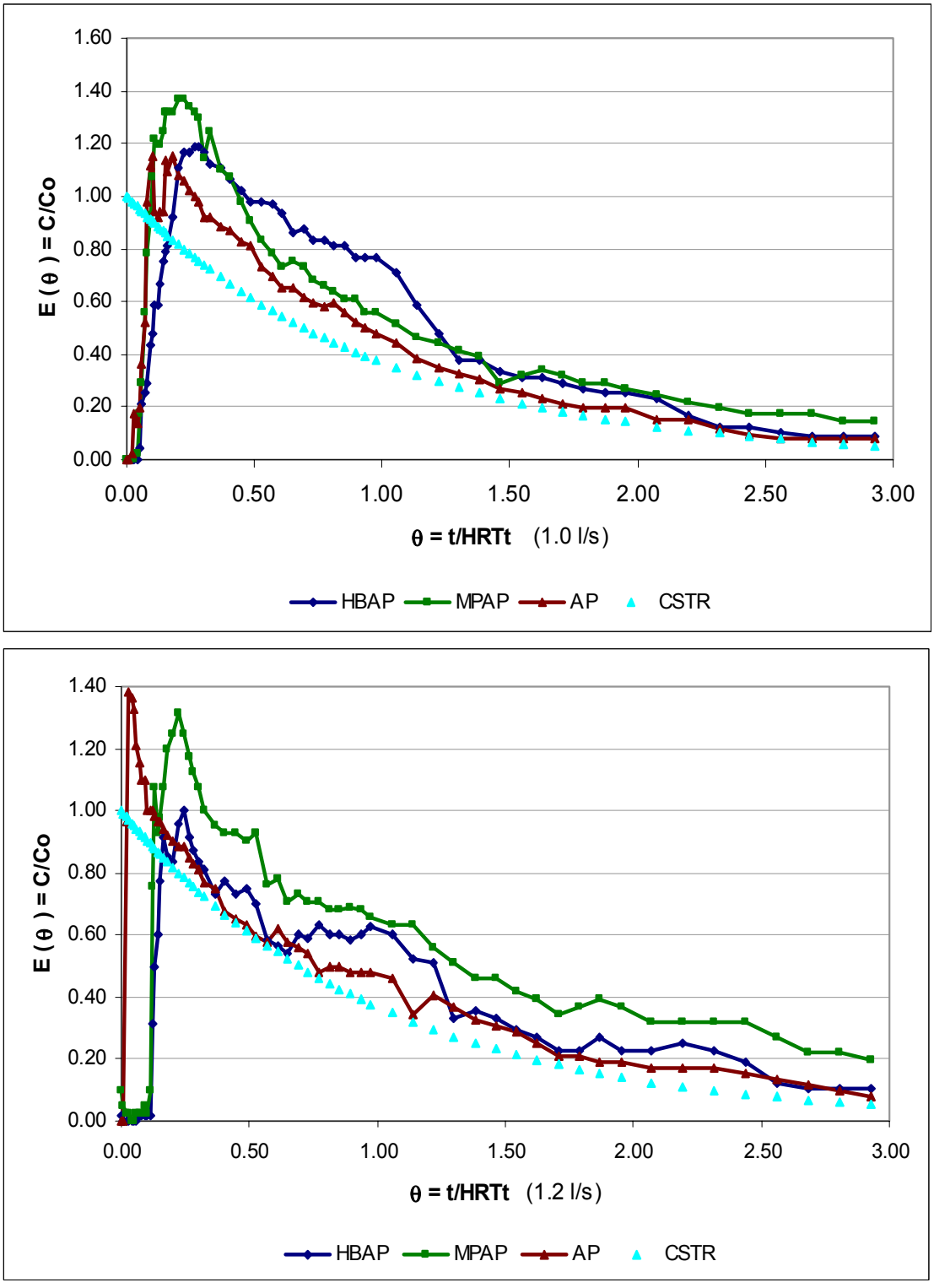

Figure 4.42 Dimensionless experimental RTD curves from experiment II.

Hydraulic loading rates applied: 1.5 and 2.0 l/s

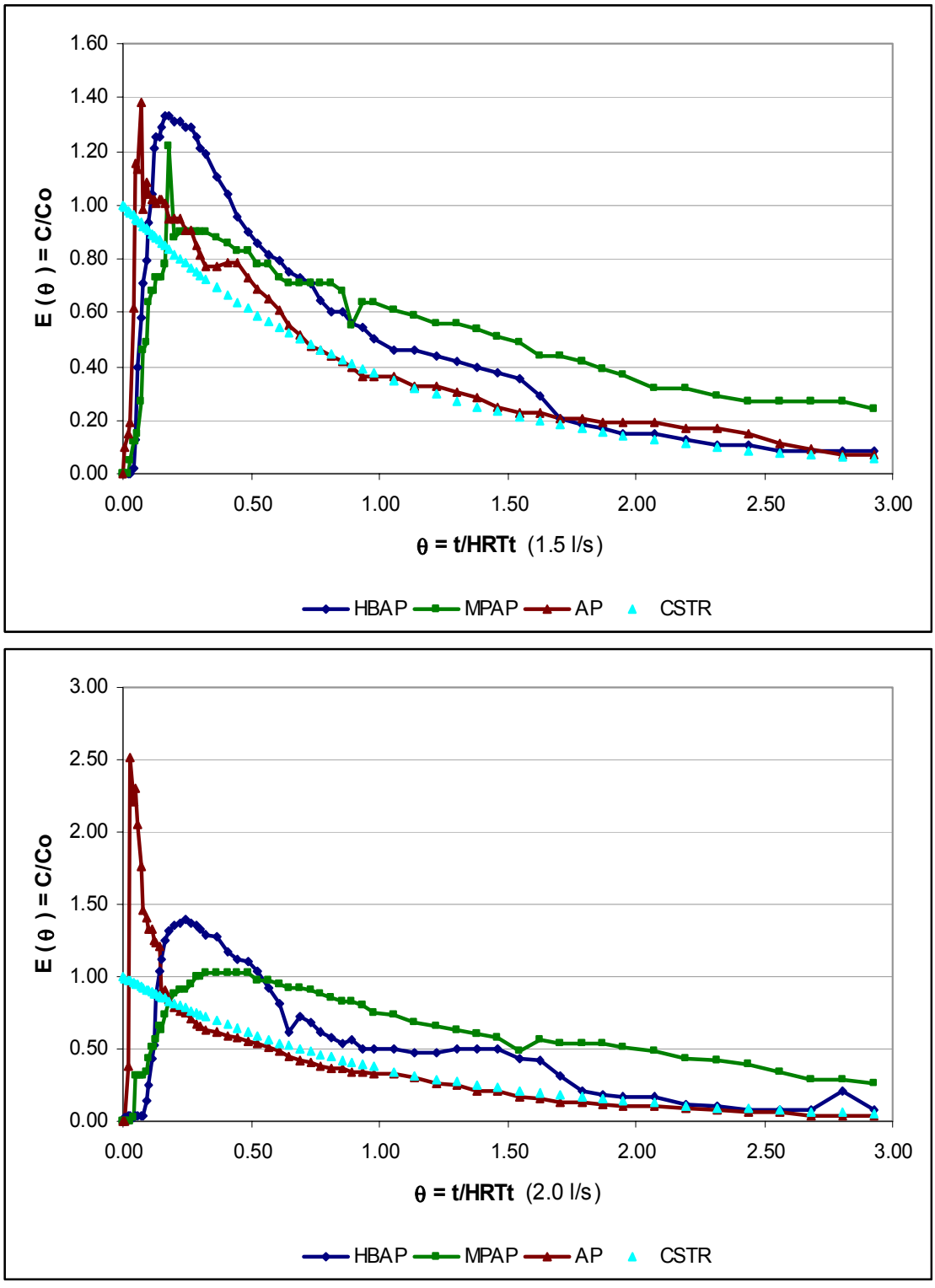

Figure 4.43 Dimensionless experimental RTD curves from experiment II.

Hydrodynamic parameters. The experimental (HRTe) figures, dispersion number (δ) values and variances of the RTD curves (σ^2) were calculated from the curves shown in Figures 4.40 - 4.43. The corresponding raw experimental data are given in electronic format in Appendix II in the PILOT-SCALE-EXP file. Tables 4.20 and 4.21 display the average values of operational variables and the figures for hydrodynamic parameters obtained from each run.

Table 4.20 Average flows, HRT_t and λ_v values applied to each AP.

	VBAP				**PNFAP**			**AP**		
Experiment I	Qd (l/s)*	Qr (l/s)	HRT_t (h)	λ_v**	Qr (l/s)	HRT_t (h)	λ_v**	Qr (l/s)	HRT_t (h)	λ_v**
	1.0	1.0	25	613	1.0	25	501	1.0	24	372
	1.2	1.2	21	425	1.2	21	730	1.1	21	665
	1.5	1.5	16	873	1.5	17	822	1.4	16	783
	2.0	1.9	13	963	2.1	12	745	2.0	11	1394
	HBAP				**MPAP**			**AP**		
Experiment II	1.0	1.0	25	570	1.0	29	373	1.0	23	470
	1.2	1.2	21	601	1.2	24	526	1.2	19	751
	1.5	1.5	16	847	1.5	19	751	1.5	15	842
	2.0	2.0	12	902	2.0	14	968	2.0	11	1232

* Qd = Flow rate defined in the experimental design; Qr = Hydraulic flow rates applied
** λ_v expressed in g COD/m^3 d

Table 4.21 Summary of hydrodynamic parameters obtained at the APs outlet.

	VBAP			**PNFAP**			**AP**		
Experiment I	HRTe (h)	σ^2	δ	HRTe (h)	σ^2	δ	HRTe (h)	σ^2	δ
	22	0.5288	0.434	23	0.4959	0.385	21	0.5362	0.446
	19	0.4389	0.314	18	0.4856	0.371	21	0.5750	0.514
	14	0.5678	0.500	15	0.5347	0.443	16	0.6245	0.620
	13	0.5161	0.414	10	0.4832	0.368	12	0.7286	0.967
	HBAP			**MPAP**			**AP**		
Experiment II	22	0.4298	0.304	23	0.4005	0.273	21	0.5412	0.454
	21	0.5047	0.398	22	0.4257	0.299	17	0.6446	0.672
	13	0.4333	0.308	17	0.4352	0.309	13	0.6344	0.645
	11	0.4563	0.334	14	0.4304	0.304	8	0.5294	0.435

The RTD curves and hydrodynamic parameters obtained at each AP are meant to represent the mixing patterns due mostly to the interaction between pond configuration and hydraulic loading rates. In other words, the data from these

experiments described essentially the hydrodynamic behaviour of the pilot AP due to the interaction between water movement and in-pond mixing device.

Sludge seeding at the beginning of each experiment accounted for only five percent of the AP volume, and each experiment lasted a maximum of three months. Therefore, the likely contribution of biosolids growth and contents to the overall hydrodynamic behaviour of the pilot APs was expected to be minimum. This assumption seemed to be true as none of the RTD curves showed large deviations from the ideal CSTR model. Furthermore, there were no extreme early peaks such as those recorded in the full-scale AP with significant sludge accumulation.

Process performance. Table 4.22 shows the average composition of the raw wastewater during both experiments for each run.

Table 4.22 Average composition of the raw wastewater throughout the experiments.

Experiment	Parameter		Run 1	Run 2	Run 3	Run 4
Experiment I	COD (mg/l)	n	21	21	21	21
		$\bar{y}$	372	522	639	582
		σ / CV	100 / 0.27	132 / 0.25	157 / 0.25	146 / 0.25
	TSS (mg/l)	n	12	12	12	12
		$\bar{y}$	185	259	277	221
		σ / CV	45 / 0.24	115 / 0.44	87 / 0.31	59 / 0.27
	Set. sol. (ml/l)	n	12	12	12	12
		$\bar{y}$	0.9	2.5	2.3	1.9
		σ / CV	0.7 / 0.78	1.4 / 0.56	1.0 / 0.43	1.5 / 0.79
Experiment II	COD (mg/l)	n	21	21	21	21
		$\bar{y}$	526	451	594	565
		σ / CV	110 / 0.21	133 / 0.29	113 / 0.19	109 / 0.19
	TSS (mg/l)	n	12	12	12	12
		$\bar{y}$	190	137	270	247
		σ / CV	38 / 0.20	47 / 0.34	65 / 0.24	54 / 0.22
	Set. sol. (ml/l)	n	12	12	12	12
		$\bar{y}$	2.3	1.4	3.0	2.4
		σ / CV	1.2 / 0.52	1.5 / 1.07	2.0 / 0.67	1.5 / 0.63

Table 4.22 shows a stable composition of the raw wastewater along the experiments. This can be seen from the *CV* figures, which varied only in a narrow range within each experiment. On the other hand, variations across the experiments showed that total COD was the more stable parameter followed by TSS and settleable (1-h) solids. Figures 4.44 and 4.45 depict the average variation of total COD, TSS and

settleable (1-h) solids throughout each experiment. Average values of total COD, TSS and settleable solids in the plots are the mean of 21, 12 and 12 figures respectively.

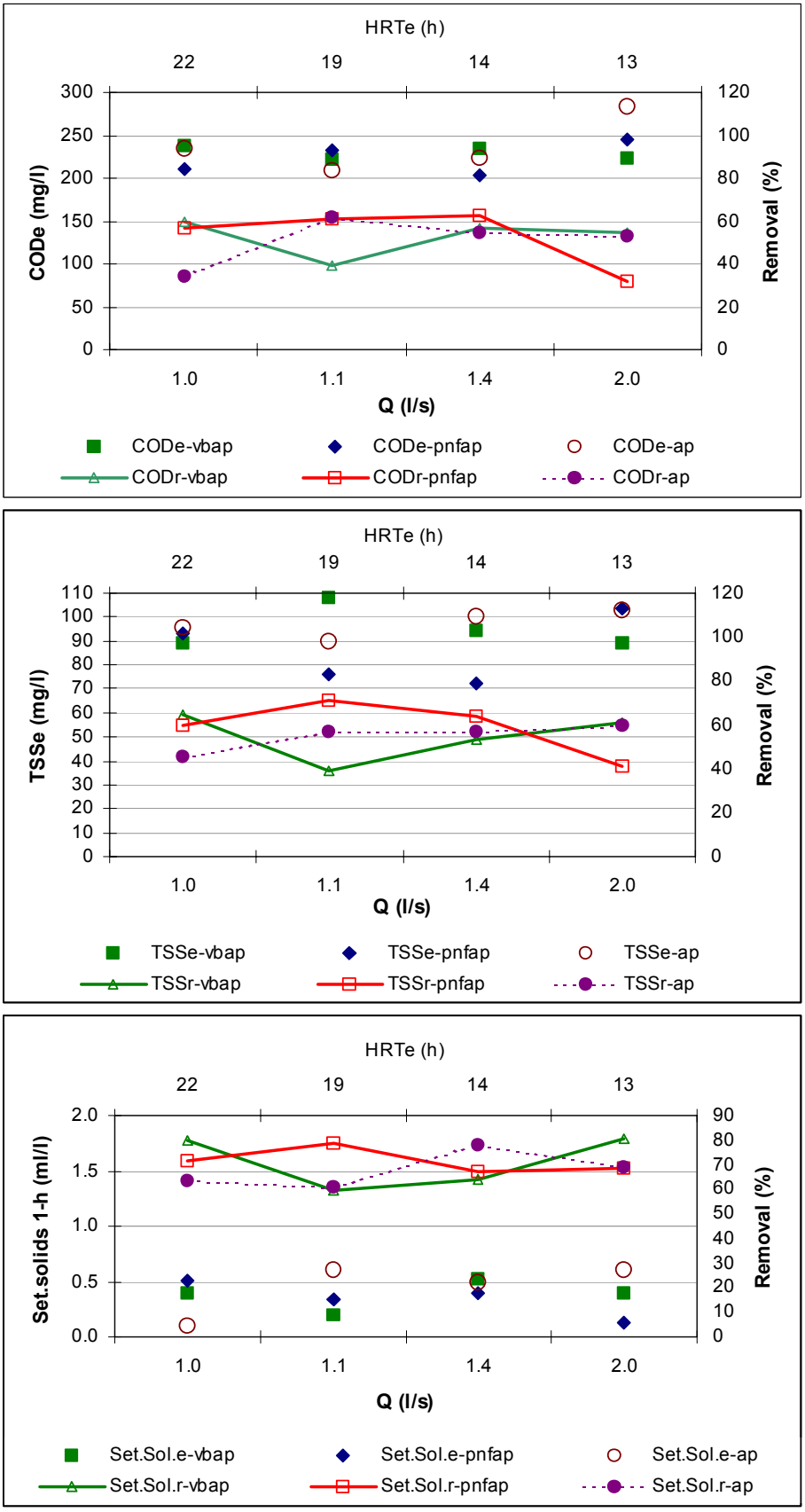

e, effluent concentration of the parameter. r, removal efficiency of the parameter.

Figure 4.44 Variation of effluent COD, TSS and settleable (1-h) solids in Exp I.

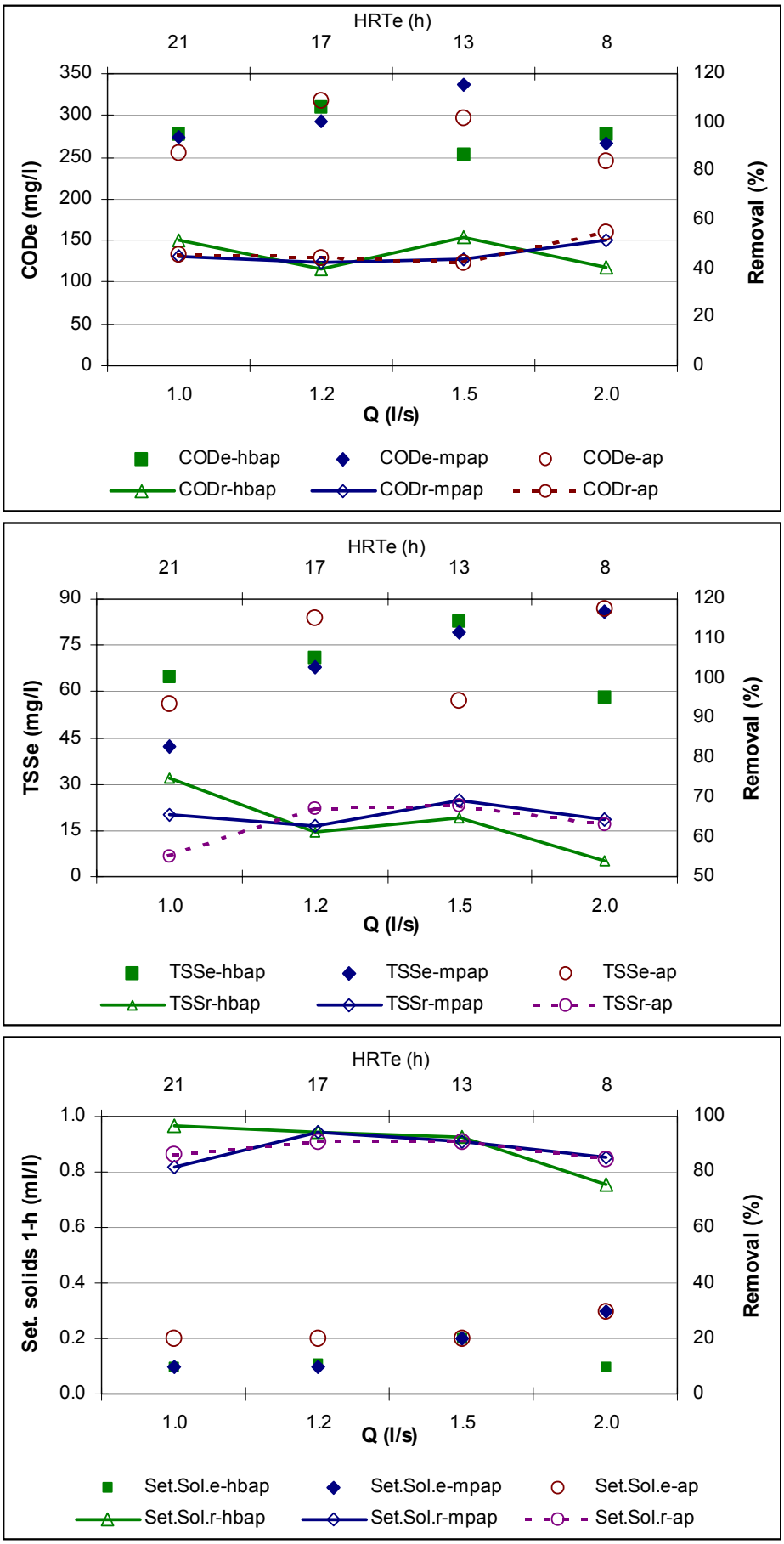

e, effluent concentration of the parameter. r, removal efficiency of the parameter.

Figure 4.45 Variation of effluent COD, TSS and settleable (1-h) solids in Exp II.

Statistical analysis of data. Table 4.23 summarises the results of the two-factor ANOVA and Tukey's tests performed on the effluent data series of COD, TSS and settleable solids from each experiment.

Table 4.23 Summary of two-factor ANOVA and Tukey tests results.

Combination	Parameter	*F-value*	*F-critical*	*p*	α	Decision rule*
VBAP-PNFAP	CODe	3.712	2.661	0.0129	0.05	Reject Ho
	TSSe	9.745	2.708	0.0000	0.05	
	Set.solids-e	6.840	2.708	0.0003	0.05	
VBAP-AP	CODe	5.574	2.661	0.0012	0.05	Reject Ho
	TSSe	4.297	2.708	0.0071	0.05	
	Set.solids-e	20.780	2.708	0.0000	0.05	
PNFAP-AP	CODe	3.626	2.661	0.0144	0.05	Reject Ho
	TSSe	4.143	2.708	0.0085	0.05	
	Set.solids-e	23.870	2.708	0.0000	0.05	
HBAP-MPAP	CODe	6.733	2.661	0.0003	0.05	Reject Ho
	TSSe	10.776	2.708	0.0000	0.05	
	Set.solids-e	2.863	2.708	0.0413	0.05	
HBAP-AP	CODe	3.430	2.661	0.0185	0.05	Reject Ho
	TSSe	28.650	2.708	0.0000	0.05	
	Set.solids-e	12.201	3.949	0.0007	0.05	
MPAP-AP	CODe	9.225	2.661	0.0000	0.05	Reject Ho
	TSSe	10.967	2.708	0.0000	0.05	
	Set.solids-e	4.749	2.708	0.0041	0.05	

* Decision rule for the statistical hypothesis stated in Section 3.3.5 by Equation 3.11.

The two-factor ANOVA test confirmed that there were significant statistical differences (> 10%) amongst the means of the parameters related to the interaction between different configurations (mixing device) and the applied hydraulic loading rates. The F-statistic values were higher than F-critical for all the parameters, and the p-values were always smaller than α-values in all cases. Therefore, the decision rule is to reject the null hypothesis as stated in equation 3.11 with a confidence level of 95 percent. In other words, the combined effect of AP configuration (mixing device) and hydraulic loading rate variation do affect the mixing pattern and consequently the performance of the pilot AP. The experimental results showed earlier point out to the same conclusion but the statistical hypothesis test reassured this feature.

Likewise, the Tukey's test yielded the statistically equal means for each parameter. These figures are given in Appendix II in the PILOT-SCALE-EXP folder under Experiment I and Experiment II subfolders. This statistic also showed that several

mean values differed by at least 10% from one another, which confirmed the two-factor ANOVA test results. Further discussion of these data is presented in Chapter 5.

4.2.2 Process performance of the pilot-scale AP

Results from the previous experiment supported by the statistical tests showed that in general the modified AP configurations performed better than the conventional AP particularly at HRT values below 19 h. Additionally, the hydrodynamic stability of these modified configurations seemed to be superior (under hydraulic loading rate increases) since the variance (σ^2) and (δ) values obtained from their RTD curves showed a narrower variation compared to the conventional AP.

The baffled configurations (VBAP, HBAP) and the AP fitted with the mixing pit (MPAP) demonstrated a good potential for improved removal of organic matter provided that they reach proper steady state conditions. Therefore, the HBAP and the MPAP were monitored for a further 5-month period after the hydrodynamic study, so as to evaluate their process performance and removal efficiencies under steady-state conditions. The conventional AP was also run in parallel as a control unit for this experiment. The details of this experiment are given in Tables 3.20 and 3.21 of Chapter 3. The three hydraulic loading rates applied during this experiment were chosen based on the results from the hydrodynamic study.

Flow, pH and temperature. Tables 4.24 and 4.25 present the hydraulic loading rates applied, and the influent and effluent data taken during this last experiment.

Table 4.24 Hydraulic loading rates applied and related HRT theoretical values.

Stage	Parameter	Hydraulic loading rates applied (l/s) / HRTt (h)		
		HBAP	MPAP	AP
1	n = 119	1.0 / 24.5	1.1 / 26.0	0.9 / 25.3
	σ / CV	0.08 / 0.08	0.08 / 0.08	0.07 / 0.08
2	n = 139	1.3 / 18.2	1.5 / 19.0	1.3 / 17.9
	σ / CV	0.02 / 0.01	0.03 / 0.02	0.03 / 0.02
3	n = 139	2.0 / 12.3	2.3 / 12.6	1.8 / 12.6
	σ / CV	0.04 / 0.02	0.04 / 0.02	0.06 / 0.03

* n values refer to the number of data recorded at each AP inlet.

The pH values of the raw wastewater showed a narrow variation around neutrality throughout the monitoring period. The effluents from the three APs showed slightly lower pH values compared to the influent raw wastewater; this is expected in anaerobic reactors due to acidogenesis.

Table 4.25 Temperature and pH data recorded throughout the experiment.

Stage	Parameter	*n**	Influent	Effluents		
				HBAP	MPAP	AP
1	T (°C)	72	23.1-27.5	23.3-27.8	23.5-27.9	23.4-27.9
	pH	72	6.50-7.16	6.39-6.68	6.36-6.68	6.37-6.70
2	T (°C)	72	23.6-28.6	23.5-29.6	23.7-29.7	23.6-29.6
	pH	72	6.50-7.34	6.24-6.69	6.28-6.75	6.29-6.79
3	T (°C)	72	23.2-26.3	23.3-26.8	23.4-26.6	23.4-26.9
	pH	72	6.63-7.28	6.34-6.83	6.40-7.02	6.43-6.83

* *n* values refer to the number of data taken at each sampling point.

Maximum and minimum temperature figures differed by 3 to 5 °C in the raw wastewater. Meanwhile, in all of the effluents these figures differed by 3 to 6 °C. The lower temperature values were always obtained in the early morning (0600-0800), whilst the higher values were always recorded at noon (1200-1400) in both raw wastewater and APs effluent.

Process performance. Table 4.25 shows a very stable behaviour of temperature and pH values in the raw wastewater. Meanwhile, Table 4.26 presents the average composition of the raw wastewater throughout the three stages of the experiment.

Table 4.26 Average composition of the raw wastewater.

Parameter	Stages											
	1				2				3			
	n	$\bar{y}$	σ	CV	*n*	$\bar{y}$	σ	CV	*n*	$\bar{y}$	σ	CV
COD_t	6	597	70.7	0.12	6	600	36.5	0.06	6	590	221	0.37
COD_f	6	163	40.6	0.25	6	172	89.5	0.52	6	199	55.9	0.28
TSS	6	267	36.2	0.14	6	274	25.5	0.09	6	321	119	0.37
VSS	6	194	29.4	0.15	6	179	26.6	0.15	6	223	53.9	0.24
VFA	6	1.4	0.8	0.58	6	1.5	0.3	0.20	6	1.7	0.8	0.48
SO_4^{2-}	6	105	46.4	0.44	6	94	36.5	0.39	6	95	38.9	0.41
ORP (mV)	6	-38	34	0.89	6	-30	38	1.26	6	+15	50	3.33
Alkalinity*	6	209	11.1	0.05	6	224	12.9	0.06	6	223	14.7	0.07

* Alkalinity expressed as mg $CaCO_3$/l t, total; f, filtered
All the parameters are expressed in (mg/l) with the exception of ORP.

The strength of the raw wastewater measured in terms of total COD showed a good stability although the CV value from stage three revealed a wider variation compared to the previous stages. All the other parameters seemed to vary similarly along the stages with the exception of ORP. This parameter usually had positive values early in the morning, but changed to negative figures as day went on and sewage became more concentrated and abundant.

Figures 4.46 to 4.52 display the average variation of the parameters monitored in the effluents of the three pilot-scale AP. Six 12-h composite samples were taken during every stage and analysed for each parameter. Hence, each point in Figures 4.46 and 4.47 is the mean of six values determined per stage. Meanwhile, ORP was determined in grab samples hourly during each sampling day.

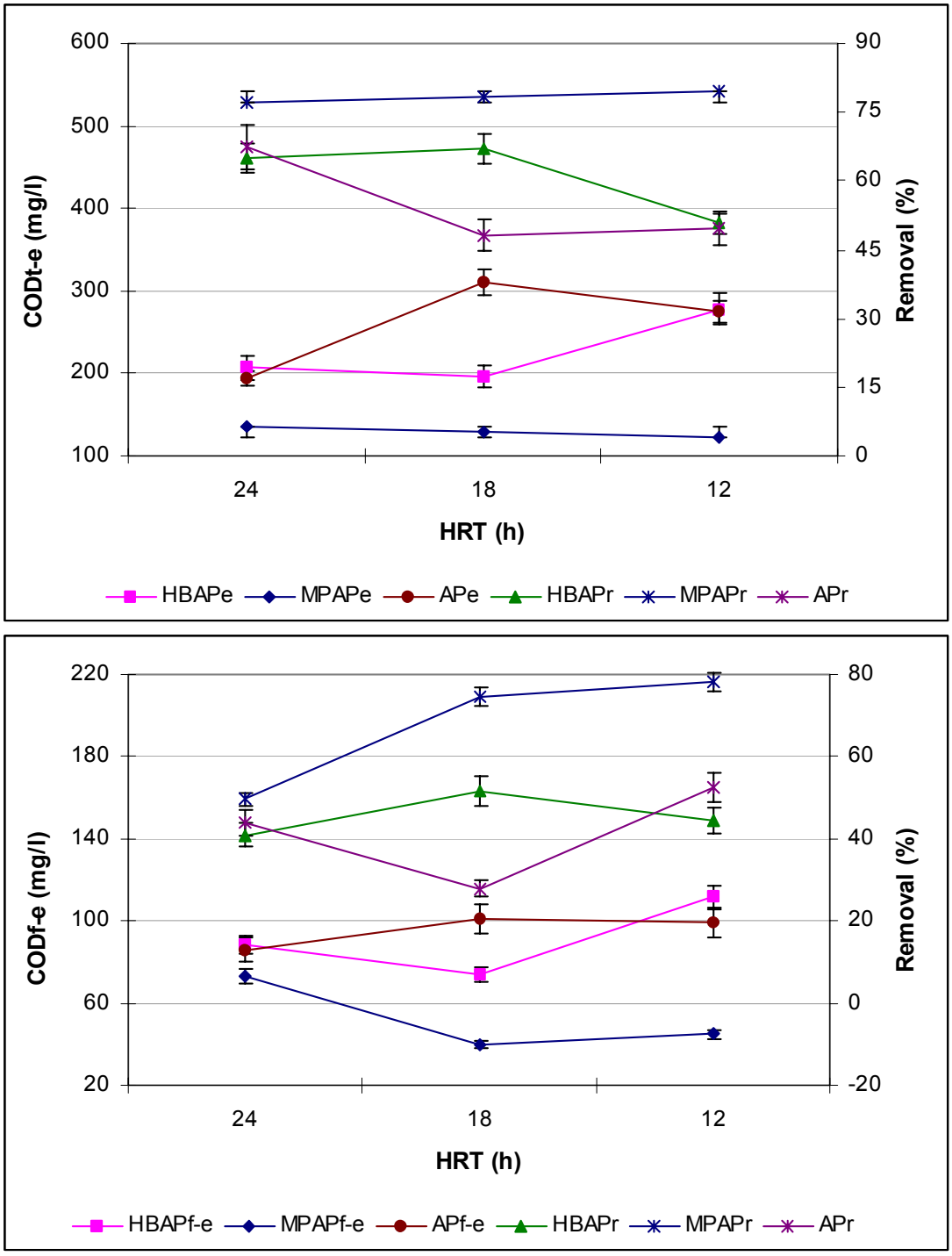

* e, effluent; r, removal; t-e, total effluent; f-e, filtered effluent.

Figure 4.46 Average total and filtered COD effluent concentrations and removals in the pilot-scale AP.

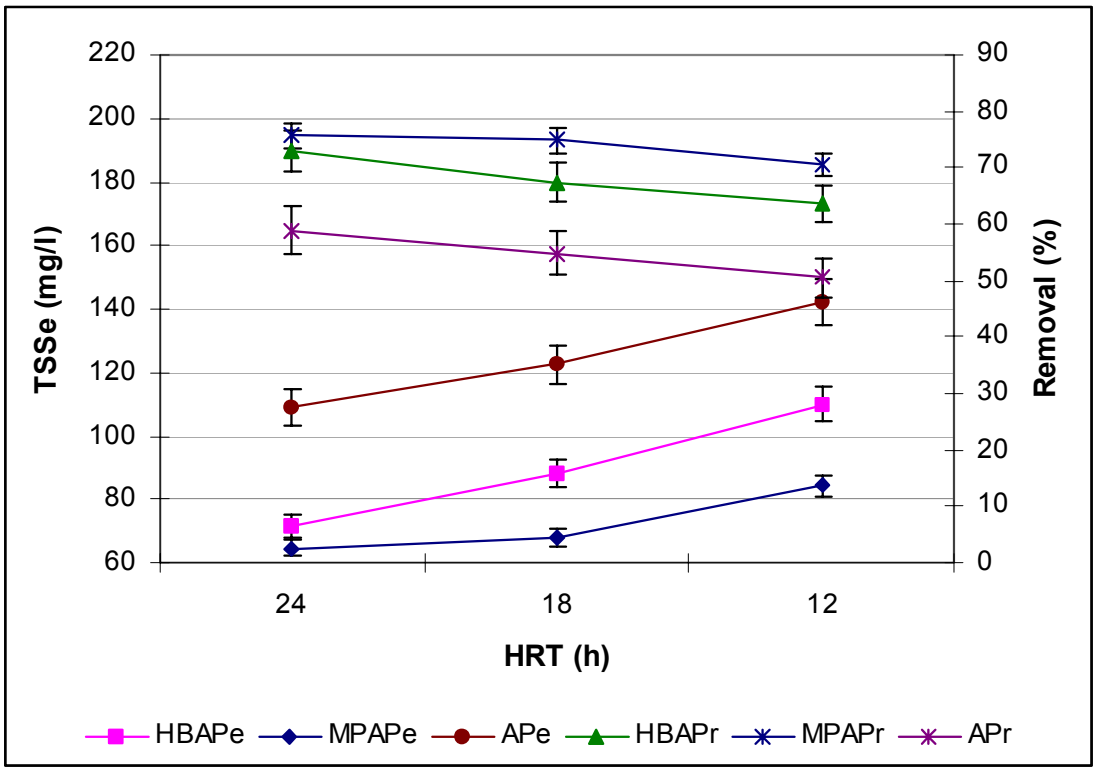

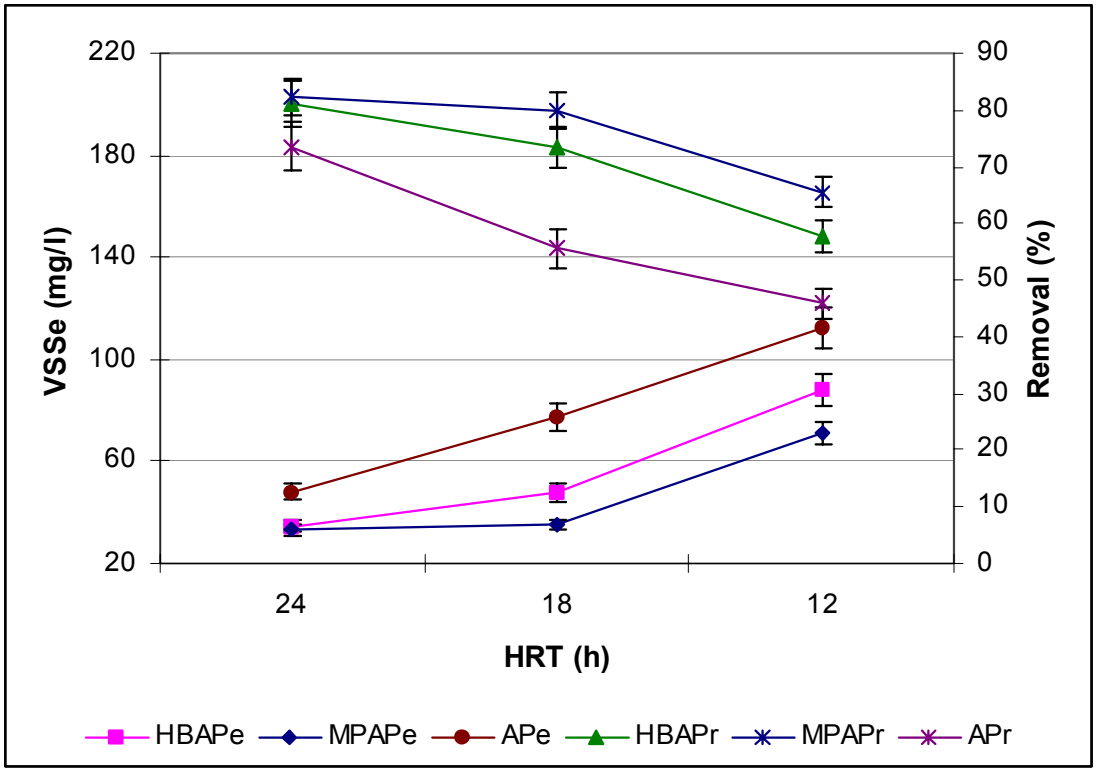

* e, effluent; r, removal.

Figure 4.47 Average TSS and VSS effluent concentrations and removals in the pilot-scale AP.

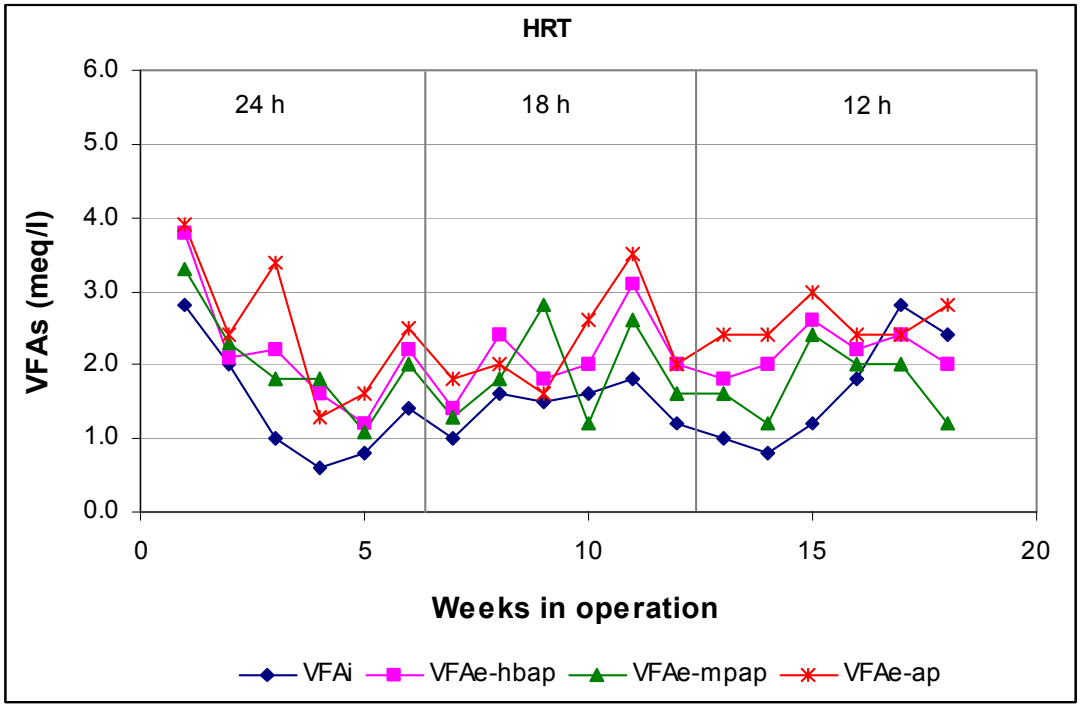

* i, influent; e, effluent.

Figure 4.48 Variation of VFA in the influent and effluent of the pilot-scale AP.

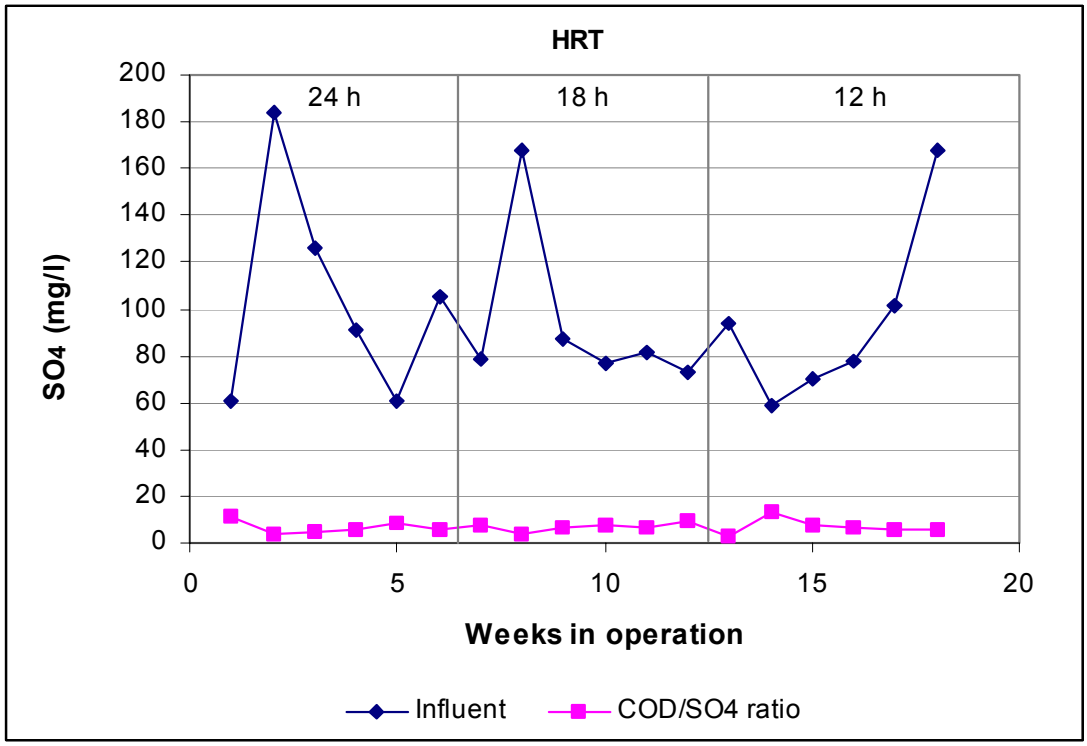

Figure 4.49 Variation of SO_4^{2-} and COD/ SO_4^{2-} ratio in the raw wastewater.

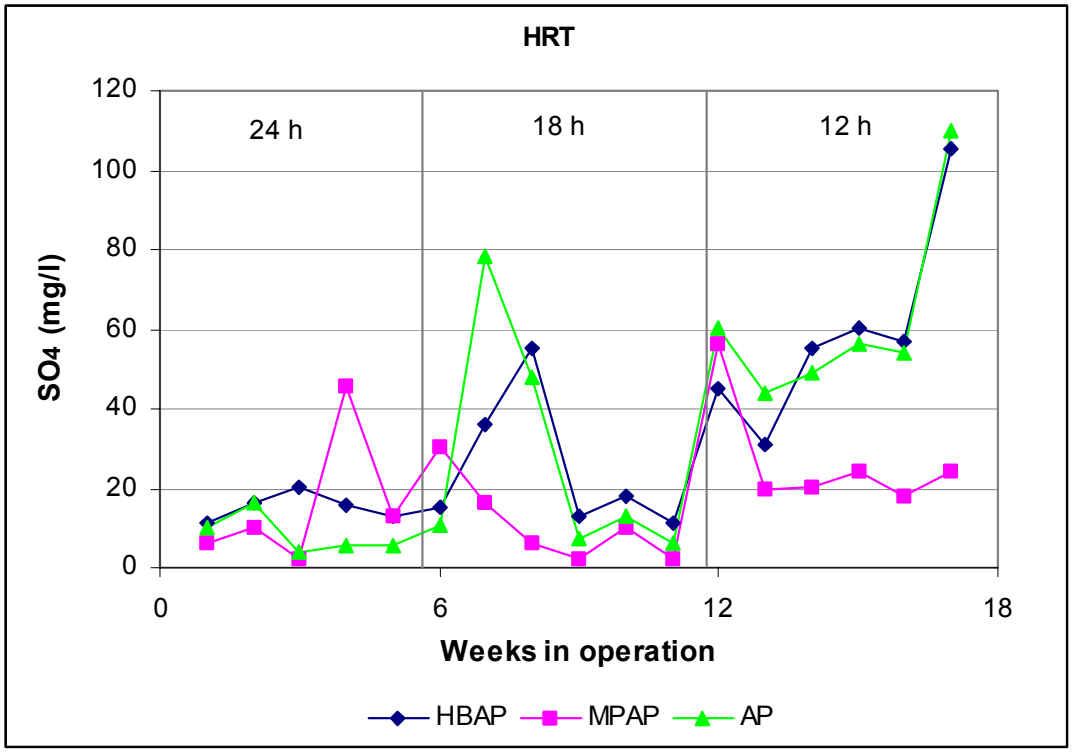

Figure 4.50 Variation of SO_4^{2-} concentration in effluents of the pilot-scale AP.

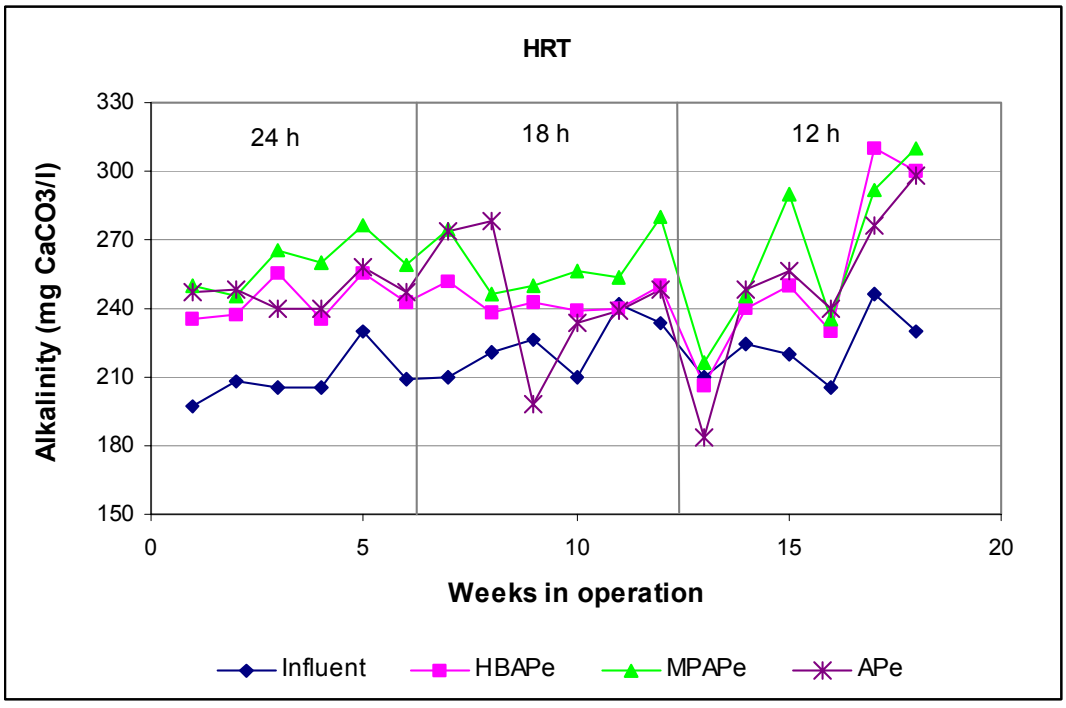

Figure 4.51 Variation of alkalinity in the influent and effluent of the pilot-scale AP.

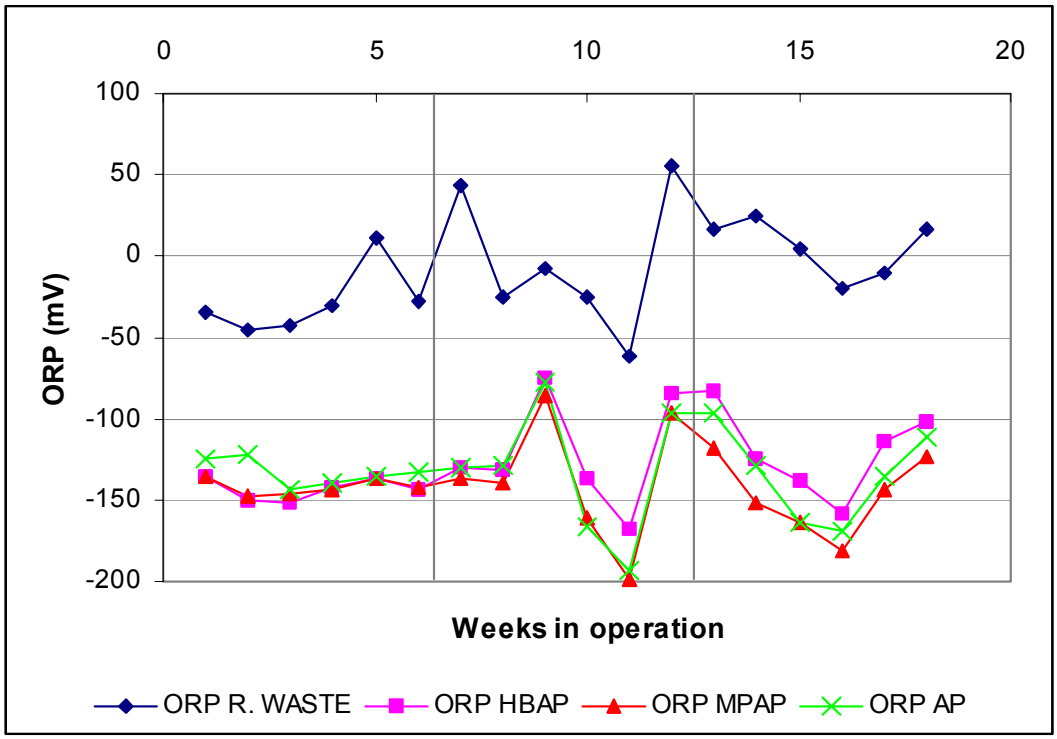

Figure 4.52 Variation of ORP in the influent and effluent of the pilot-scale AP.

Table 4.27 displays the average values of operational parameters in the pilot-scale AP and Table 4.28 shows additional physico-chemical parameters determined during the last stage corresponding to a HRT of 12 h. The few figures obtained for the latter parameters do not permit an in-depth analysis, but they complement the results presented earlier.

Table 4.27 Average flows, HRT_t and λ_v values applied to each pilot-scale AP.

HBAP				MPAP			AP		
Qd (l/s)*	Qr (l/s)	HRT_t (h)	λ_v**	Qr (l/s)	HRT_t (h)	λ_v**	Qr (l/s)	HRT_t (h)	λ_v**
1.0	1.0	24.5	584	1.1	26.0	551	0.9	25.3	566
1.5	1.3	18.2	791	1.5	19.0	758	1.3	17.9	800
2.0	2.0	12.3	1151	2.3	12.6	1124	1.8	12.6	1124

* Qd = Flow rate defined in the experimental design; Qr = Hydraulic flow rate applied
** λ_v expressed in g COD/m^3 d

Based on figures from Table 4.28, the estimated BOD_5 volumetric organic loading rates (λv) applied to each pilot-scale AP in the last stage were 780, 762 and 762 g BOD_5/m^3 d for HBAP, MPAP and AP respectively.

Table 4.28 Values of influent and effluent total BOD_5, TKN, $N\text{-}NH_3$ and H_2S determined at the highest loading rates.

Parameter	Influent	HBAP	MPAP	AP
BOD_5 (mg/l)	400	239	98	243
TKN	14	10.8	9.3	13.5
$N\text{-}NH_3$ (mg/l)	5.5	8.0	9.0	5.6
H_2S (mg S/l)	2.2	3.5	2.1	1.7
Dissolved $S^{=}$ (mg/l)	3.3	4.0	3.0	2.0

Values shown in the table are the mean of three fortnightly 12 h composite samples.

The MPAP presented the highest BOD_5 removal (75%), followed by the HBAP (40%) and then the conventional AP (39%). TKN and $N\text{-}NH_3$ values showed a normal variation range for anaerobic reactors. TKN effluent concentrations decreased slightly whilst $N\text{-}NH_3$ effluent concentrations increased in comparison to influent values.

The H_2S effluent concentrations seemed unexpectedly low given the amount of in-pond sulphate reduction suggested by Figures 4.49 and 4.50. These results are further discussed in Chapter 5.

Sludge monitoring. The samples taken from the biosolids layer were analysed for TS and VS contents during each stage of the monitoring period. The ratio VS/TS was calculated for each sludge sample and plotted as shown in Figures 4.53 and 4.54.

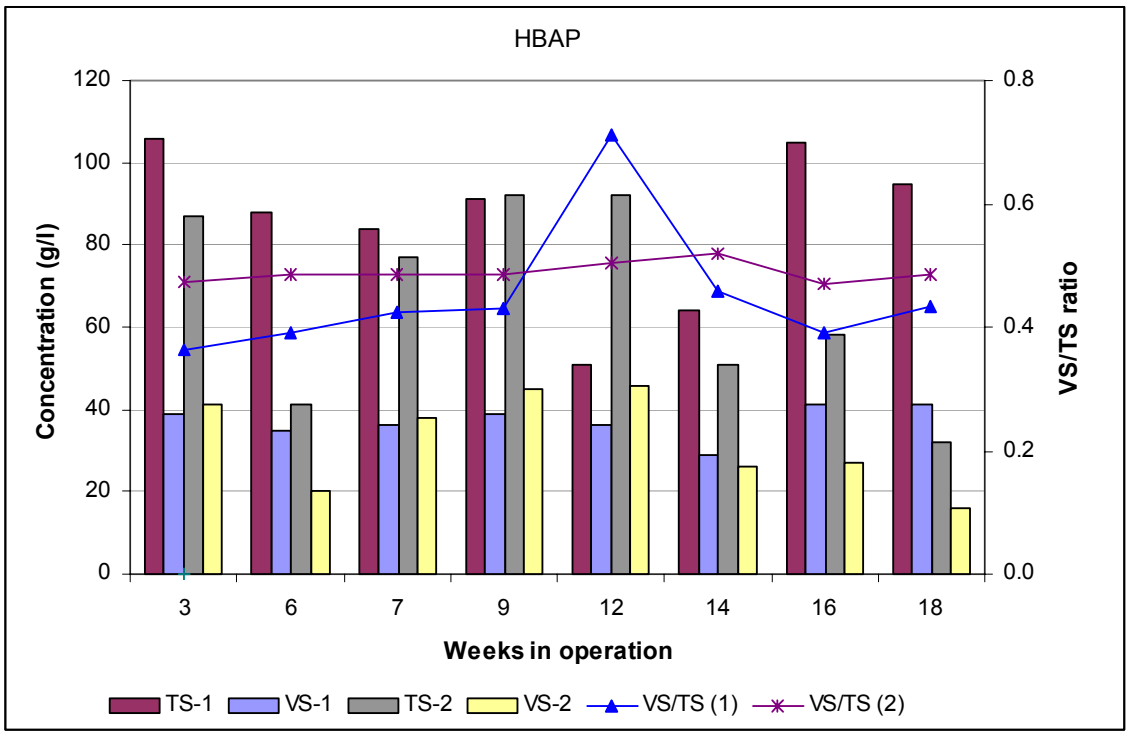

* The sampling points (1 and 2) for biosolids were located at L/3 and 2/3L in each AP.

Figure 4.53 Variation of TS, VS and VS/TS ratio in the HBAP.

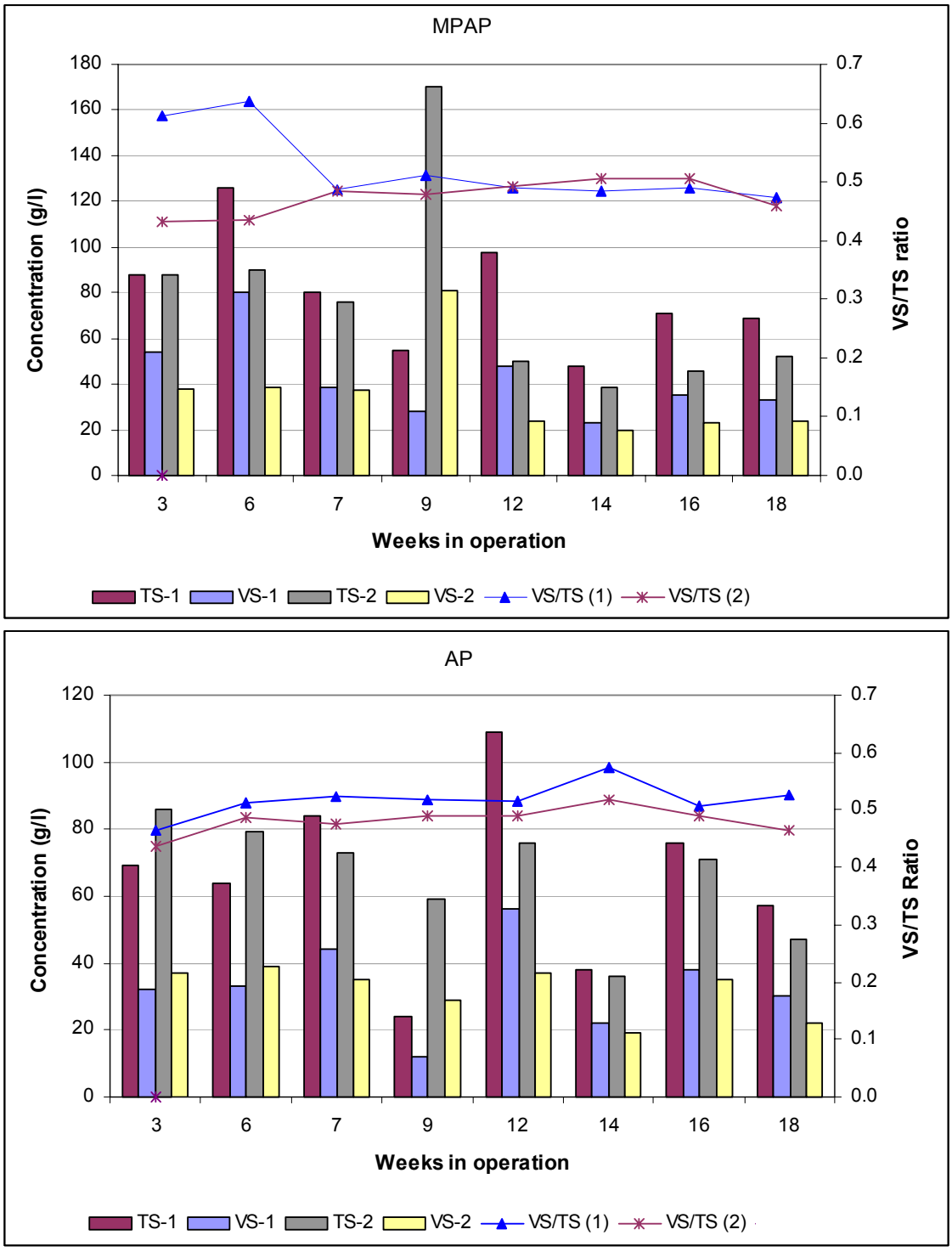

* The sampling points (1 and 2) for biosolids were located at L/3 and 2/3L in each AP.

Figure 4.54 Variation of TS, VS and VS/TS ratio in MPAP and AP.

The samples taken at each internal point were integrated by four aliquots in an attempt to obtain a representative sample of the sludge settled at the particular sampling point. However, in the MPAP point 1 was located in the mixing chamber and so the aliquots were taken every 0.20 m over the entire chamber depth (1.50 m), in order to have an average composition of the sludge bed.

Removal of microbiological indicators. The microbiological quality of the effluents was also investigated by monitoring the densities of faecal coliforms, *E. coli* and helminth eggs. Table 4.29 displays the average influent and effluent concentrations, and Figures 4.55 and 4.56 depict the average removal efficiencies in each pilot AP.

Table 4.29 Average influent and effluent concentrations of microbiological indicators.

Indicator	Stage	Raw waste	HBAP-ef	MPAP-ef	AP-ef
FC * (UFC/100 ml)	1	3.33E+07	1.22E+07	9.74E+06	9.01E+06
	2	2.61E+08	1.47E+07	1.20E+07	1.57E+07
	3	2.42E+07	1.02E+07	4.99E+06	7.89E+06
E. coli ** (UFC/100 ml)	1	3.30E+07	8.90E+06	2.68E+06	1.89E+06
	2	8.03E+07	1.15E+07	1.01E+07	1.21E+07
	3	1.52E+07	7.09E+06	7.47E+06	4.40E+06
Helminth eggs *** (No eggs/l)	1	353	115	85	81
	2	191	102	89	97
	3	111	54	65	104

* Geometric mean of four values at each stage.
** Geometric mean of three values at stages 1 and 3, and five values at stage 2.
*** Arithmetic mean of four values at each stage.

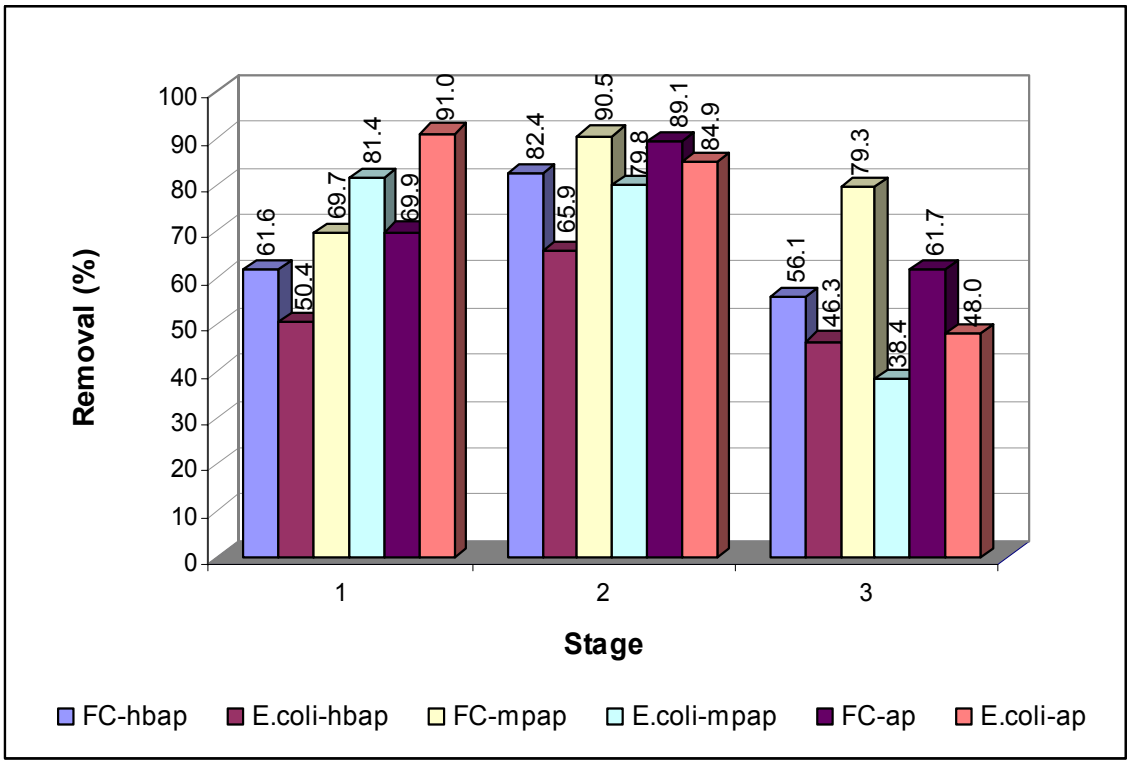

Figure 4.55 Average removal of FC and *E. coli* in the pilot-scale AP.

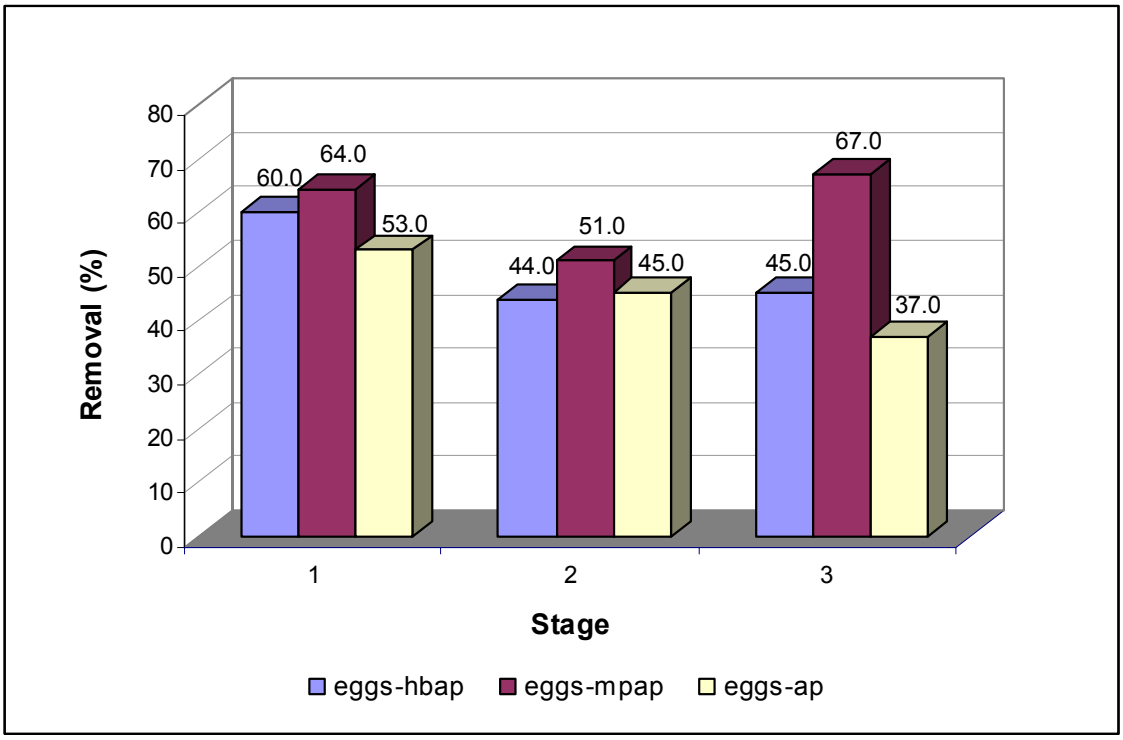

Figure 4.56 Average removal of helminth eggs in the pilot-scale AP.

Statistical tests. A two-factor ANOVA test was performed on the effluent data series of COD_t, COD_f, TSS, VSS, FC, *E. coli* and helminth eggs. This test was aimed at confirming statistically significant differences within and between mean effluent values in the pilot-scale AP. Table 4.30 summarises the results of the ANOVA test.

Table 4.30 Summary of two-factor ANOVA test results.

Ponds	Parameter	*F-value*	*F-critical*	*p*	α
HBAP-MPAP-AP	CODt	35.708	3.204	0.0001	0.05
	CODf	6.219	3.204	0.0041	0.05
	TSS	21.127	3.204	0.0001	0.05
	VSS	10.282	3.204	0.0002	0.05

The two-factor ANOVA test confirmed that there were significant statistical differences (> 10%) between the means of the physico-chemical parameters related to the pond configuration and to the applied hydraulic loading rate or the respective HRT. The F-statistic values were higher than F-critical for all the parameters, and the p-values were always smaller than α-values for all cases. This test was run at a 95 percent confidence level. Hence, a statistically significant difference in pond performance arose from the interaction between AP configuration and increasing hydraulic loading rates or decreasing HRT values. The experimental results showed earlier suggest a superior

performance of the MPAP, followed by the HBAP and the AP with regards to organic matter removal.

On the other hand, the two-factor ANOVA test run on the effluent microbiological indicators showed no statistical difference between the AP means. In other words, the effluent values for FC, *E. coli* and helminth eggs are not related to either AP configuration or hydraulic loading rate variations. Nonetheless, the average removals of microbiological indicators obtained in all the APs compare well with data reported in the literature for high-rate anaerobic reactors such as UASBs (van Haandel and Lettinga, 1994). It has to be said that given the high faecal coliforms densities normally found in domestic wastewater, the significance of the removal values for this parameter in anaerobic reactors is negligible. The data obtained in this research confirm the inability of APs to carry out bacterial disinfection of the influent wastewater.

The compartmentalization of the AP volume either by providing a mixing chamber (MPAP) or baffling arrangements (HBAP) improves its hydrodynamic behaviour and the concomitant degradation rates (higher removals) of organic matter. Cherchinaro and Cardoso (1999) applied this strategy successfully to a single compartment UASB reactor with a large variation of the daily inflow rate. These authors observed that the partitioned UASB reactor (i.e. with three digestion compartments and three GLS separation devices) had an improved distribution of the highly variable inflow rate within and across the digestion compartments. Thus, more stable flow velocities and less occurrence of dead zones produced a better contact pattern between biomass and substrate and this enhanced the overall performance of the reactor. Therefore, the adequate handling of flow variations by a given reactor configuration is particularly useful in the case of domestic wastewater treatment. This feature is another advantage of the modified APs since they had two and three compartments (MPAP and HBAP) respectively.

Further discussion and analyses of these results together with statistical correlations are presented in Chapter 5. The raw data and ANOVA calculation tables for this experiment are given in Appendix II in the PILOT-SCALE-EXP folder in the Experiment III subfolder.